WARSAW UNIVERSITY
OF TECHNOLOGY

Faculty of Electrical Engineering

Ph.D. THESIS

Grzegorz Sarwas, M.Sc.

Modelling and Control of Systems with Ultracapacitors Using Fractional Order Calculus

Supervisor:
Prof. Andrzej Dzieliński

Warsaw, 2012

To my Parents

Abstract

In this thesis modelling and control of the system with ultracapacitor using the fractional order calculus is presented. To introduce the subject of the fractional orders calculus some basic definitions and dependencies are shown. Next, the internal structure of the ultracapacitor is described. Based on this description the appropriateness of using fractional order calculus to ultracapacitors modelling is proofed. Also an analytical derivation of a new ultracapacitor, more precise model based on the anomalous diffusion is presented. Additionally, some other ways of the ultracapacitor dynamics modelling are discussed.

Some of presented models are examined and their properties are discussed. Next, the explanation of the phenomenon of capacity decrease with frequency, based on the fractional order model, is shown. For the Davidson-Cole (Quintana) ultracapacitor model the step response in time domain is derived. Also derivation of the step response for the system with ultracapacitor is shown. Achieved results are validated and compared with the physical devices. In this case two designed and built experimental setups for ultracapacitor examination are shown. It is also highlighted that, although, ultracapacitor dynamics can be described precisely for zero initial conditions in fact they have some non–linearity.

At the end of this thesis a new type of neural network for modelling non–linear fractional order systems is proposed. This network is called: Discrete Fractional Order Neural Network (DFONN), because it is based on the Discrete Fractional Order Space State (DFOSS) system connected with a traditional neural network. Usefulness of this network is presented in the process of the ultracapacitor non–linear modelling. For this experiments another electrical circuit was built. Additionally using this new neural network structure and electrical setup the fractional order neural network controller for control of the process of ultracapacitor charging and discharging is proposed. Results of control of physical systems with ultracapacitor are shown.

Streszczenie

Niniejsza rozprawa traktuje o modelowaniu i sterowaniu układem z ultrakondensatorem przy użyciu rachunku różniczkowego niecałkowitego rzędu. W celu wprowadzenia do tematyki rachunku niecałkowitego rzędu zostały przedstawione niektóre podstawowe definicje oraz zależności. Następnie opisana została wewnętrzna struktura ultrakondesatora, na podstawie której uzasadnione zostało użycie rachunku niecałkowitego do opisu badanego układu. Rozbudowując opis procesów zachodzących wewnątrz ultrakondensatora został wyprowadzony nowy, bardziej precyzyjny model wynikający z równań dyfuzji anomalnej. Dodatkowo zostały zaprezentowane inne metody modelowania ultrakondensatorów.

W niniejszej pracy, niektóre z zaprezentowanych modeli zostały przebadane, a ich właściwości przedyskutowane. Następnie, na podstawie modelu niecałkowitego rzędu zostało wyjaśnione zjawisko spadku pojemności ultrakondensatora wraz ze wzrostem częstotliwości. Dla modelu Davidson-Cole (Quintana) zostały wyprowadzone wzory na odpowiedź skokową w dziedzinie czasu ultrakondensatora oraz czwórnika z ultrakondensatorem. Wszystkie otrzymane rezultaty zostały porównane z danymi otrzymanymi z fizycznego układu. W tym celu zostały zbudowane dwa układy badawcze. W książce tej zostało także podkreślone, że dynamika ultrakondensatorów może zostać precyzyjne opisana przy pomocy zaprezentowanych modeli, jednakże tylko w przypadku zerowych warunków początkowych. W rzeczywistości ultrakondensatory charakteryzują się pewną nieliniowością.

Na końcu tej rozprawy zaproponowany został nowy typ sieci neuronowej do modelowania nieliniowych układów niecałkowitego rzędu. Sieć ta została nazwana Dyskretna Sieć Neuronowa Niecałkowitego Rzędu (ang. Discrete Fractional Order Neural Network (DFONN)), ponieważ opiera się o dyskretny układ różnicowy opisany w przestrzeni stanu w połączeniu z tradycyjną siecią neuronową. Możliwości tej sieci zaprezentowane zostały na podstawie modelowania ultrakondensatora. W celu wykonania eksperymentów został zbudowany kolejny układ elektryczny. Dodatkowo przy użyciu nowego typu sieci neuronowej oraz przygotowanego układu elektrycznego został opracowany i opisany neuronowy sterownik niecałkowitego rzędu, służący do sterowania procesem ładowania i rozładowania ultrakondensatora. W efekcie, zostały również przedstawione rezultaty sterowania fizycznym obiektem przy użyciu otrzymanego sterownika.

Preface

Recent years have been characterized by increased emphasis on renewable forms of energy and their economical and ecological uses. Devices which can support this kind of systems are required to be relatively small in size and weight in comparison to the energy portion which they can store. Also the ability of lossless and fast energy transfer like charging and discharging has become an important factor of new technology. In the industrial applications the common use of ultracapacitors as elements that can support existing energy storage systems like: electrical storage devices for solar and wind farm, electrical-car, elevator etc. [34] has begun in the last decades. To improve the accuracy and to understand the behaviour of ultracapacitors scientists tried to build mathematical and physical models with similar dynamics [13, 91]. It became clear immediately that these devices do not have as simple dynamics as traditional capacitors. It is noticeable that in case of ultracapacitors energy is stored not in the ions polarisation, as in the electrolytic capacitor, but in the ions movement. This feature implies that the behaviour of this kind of systems should be more similar to the dynamics of the diffusion process. In the solution of the diffusion equation [47], which are modelled like heat transfer process [87], there exits Laplace'a complex operator s in the form $\sqrt{s}$, what can be interpreted as derivation of the order 0.5. This is the purpose of use of the fractional order calculus in the diffusion or heat transfer processes description [5, 27, 48, 74, 77, 87, 90] and also in case of ultracapacitors modelling [13, 76, 85, 91] .

Fractional calculus is a generalization of integer order integral and differential calculus to any arbitrary real or even complex order. This generalization extends a traditional definition of integration and differentiation to non integer order and joins them into one definition where operator depends on the order sign. The popularity of this subject has increased during the last decades in several fields of science and engineering. Development of algorithms and methods for solving fractional equations and special functions allows the fractional calculus to become very useful tool for precise description of real-world phenomena.

One believes that the concept of fractional calculus was introduced in the end of 17th century. Gottfried Wilhelm Leibniz (1646–1716) wrote the reply letter to Marquis de L'Hôpital (1661–1704) answering to the question about the notation $\frac{d^n y}{dx^n}$ for $n = \frac{1}{2}$, where he presented the following conclusion "... *This is an apparent paradox from which, one*

day, useful consequences will be drawn. ..."

This letter had become a motivation for future generation of mathematicians, such as: Euler, Lagrange, Laplace, Lacroix, Fourier, Liouville, Riemann, Greer, Holmgren, Grünwald, Letnikov, Sonin, Laurent, Nekrassov and Krug, who, till the end of 19th century, formed the basis of the fractional calculus [35, 50], but the first monograph [63] was published only in 1974. More information on the subject can be found in works [1, 4, 10, 30, 32, 33, 39, 45, 46, 51, 52, 62, 73, 75, 79]. In 1974 was organised first conference on this topic: "International Conference on Fractional Calculus and Its Applications." [78].

At the beginning, the theories of differential, integral and integro-differential equations were the domain of mathematical physics as well as their extensions and generalizations in one and more variables. In the second half of the 20th century, parallel to the development of computers and algorithms, this calculus has spread out to engineering areas and it has become very powerful and useful tool in a lot of application in the fields such as: fluid flow, mechanics, rheology, dynamical processes in self-similar and porous structures, diffusive transport akin to diffusion, electrical networks, probability and statistics, control theory of dynamical systems, viscoelasticity, electrochemistry of corrosion, chemical physics, optics and signal processing and so on.

Utilization of fractional order calculus for modelling the diffusion process suggests that a lot of electrochemical devices which construction or mode of action is based on this phenomenon can be more accurate modelled and controlled using fractional order models and algorithms. In works [13, 76, 85, 91] were shown very efficient ways of ultracapacitor modelling. These works show the different models but some of them are only useful in a small range of frequency. Because for the precise control of ultracapacitors one needs a broad knowledge of its dynamic, a new model was necessary. Also the detailed research about existing models was desired. In the effects of five years of author's works in this field presented in articles and at the international conferences are collected in this thesis [20, 21, 22, 23, 27, 81, 82, 83, 88].

Application of fractional order calculus in Control Theory has forced the generalization of this domain for non–integer order. Definitions and properties of the continuous fractional order systems are described in the following works [2, 3, 36, 44, 49, 55, 59, 60, 64, 68, 69, 70, 71, 72].

Issues concerning fractional system identification can be found in e.g. : [19, 22, 23, 54, 89].

Discrete fractional order systems, their properties, implementation and description in state space are described in e.g. : [26, 41, 42, 43, 53, 65, 66, 67, 85].

This caused my interest in the subject of ultracapacitors, which are applicable in many industrial implementation. Since their mode of action is based on the diffusion phenomenon that is why the following thesis can be concluded:

Fractional order calculus can be a very precise and useful tool for modelling and control of systems with ultracapacitor.

Presented thesis is described in this book in the following organisation. In this work two main parts can be distinguished: theoretical and practical. The first contains mathematical preface and an introduction to the ultracapacitor subject with conclusions of the theoretically obtained results. The second part describes experiments on physical systems with implementation of theory presented in the first part and proposes a practical tool to model and control systems with elements of the nonlinear fractional dynamics. In Chapter 1 mathematical prefaliminaries are presented. This chapter contains introduction to the fractional order calculus with the definitions and the relations helpful for understanding undertaken subject. In Chapter 2 different ways of ultracapacitor modelling are described. First, the internal structure of ultracapacitor is discussed. Based on this description it is explained why ultracapacitors have the noninteger dynamic. Next, through developing assumptions, the traditional normal diffusion, which is used for explanation of the ultracapacitor base of action, is replaced with subdiffusion equation, which leads to the derivation of a new ultracapacitor fractional order model. This model has non constant order in contrast to the half-order model derived through normal diffusion. Than, these two models are compared with other fractional order models. In this chapter also the different methods of ultracapacitor modelling, based on the RC cascade and artificial neural network, are shown. In Chapter 3 properties of theoretical fractional order ultracapacitor models are discussed. In this chapter the differences between presented models are shown. Also the ultracapacitor behaviour, well known by the producers and engineers, like capacity decreasing with the frequency is discussed and explained. This phenomenon confirms the need for use the fractional order model in case of modelling the ultracapacitor dynamics. In this chapter are also derived the relations for step responses of frequency theoretical models in time domain what allows to validate achieved model. The second part of this thesis begins with Chapter 4, where at the beginning experimental setups are described. Next, the results of identification using fractional order ultracapacitor models are shown and discussed. Also validations of achieved parameters through the comparison with ultracapacitors parameters measured directly for the devices are presented. Further confirmation of the correctness of the application and identification of the studied models by the comparison of theoretical and measured step responses is shown. At the and of this chapter the linearity of ultracapacitor has been tested. Achieved results lead to the next chapter where is presented a tool for dealing with nonlinear fractional order systems. In Chapter 5 is described an ultracapacitor control based on the fractional order nonlinear controller. First, a new type of artificial neural network for non–linear fractional order systems modelling is proposed. Next, the adaptation of this system for online work is presented. After that, a configuration of the fractional order artificial neural network for ultracapacitor modelling and control of the process of ultracapacitors

charging and discharging is presented. All theoretical results are tested and validated on a physical systems. In the last chapter all results are summarized and concluded with the highlighting of unsolved and open problems.

Claims of Originality

The following novel contributions are made in this dissertation:

- Derivation of a new linear fractional order model of ultracapacitor based on anomalous diffusion equations.
- Description of fractional order ultracapacitors models properties.
- Explanation of ultracapacitors capacity decrease with frequency phenomenon.
- Derivation of step responses of an ultracapacitor and a system with ultracapacitor for Davidson-Cole's ultracapacitor capacity model.
- Physical devices identification using fractional order models.
- Models validation in frequency and time domain.
- Preposition of Fractional Order Neural Network for modelling non-linear fractional order system.
- Preparation of ultracapacitor non–linear model based on Fractional Order Neural Network.
- Design of an ultracapacitor controller based of the Fractional Order Neural Network invert controller.

Contents

Chapter 1

Mathematical Preliminary

In the following chapter the main definitions and properties of mathematical relation necessary for understanding undertaken subject are presented. Majority definitions are connected with fractional order calculus but this chapter is not a full overview of non integer order calculus but includes only the main elements used in this work.

In the Section 1.1 the definition of Gamma function is presented. This function is the generalisation of factorial function for the integer arguments. Then, the definition of Mittag-Leffler function is presented. In the Section 1.5 the main definitions of the fractional order integral are presented. There are also explained the main differences between definition and properties of fractional order dynamical systems. In the Section 1.6 the definition and properties of fractional discrete order system are presented.

1.1 Gamma Function

The gamma function has a very important role in finding the Laplace transforms of fractional powers of s. It has different, equivalent (under some assumptions), definitions depending on the application in advanced mathematics.

Definition 1.1. *The gamma function by the integral representation is defined as:*

$$\Gamma(x) = \int_0^\infty e^{-u} u^{x-1} du, \tag{1.1}$$

where $Re(x) > 0$.

Figure 1.1 presents the graph of gamma function for the interval from 0 to 5. This function is concave upward with a minimum value of approximately 0.885 at $x = 1.46$.

The main property of gamma function is:

$$\Gamma(x+1) = x\Gamma(x) \tag{1.2}$$

Using recursive relationship we can define the factorial operation for integral values of x,

because $\Gamma(1) = 1$. Hence, we can write $\Gamma(n+1) = n\Gamma(n) = n!$ for $n \in \mathbb{N}$. In addition, the integral representation of the gamma function establishes a direct way of interpolating the factorial operation between its integer values.

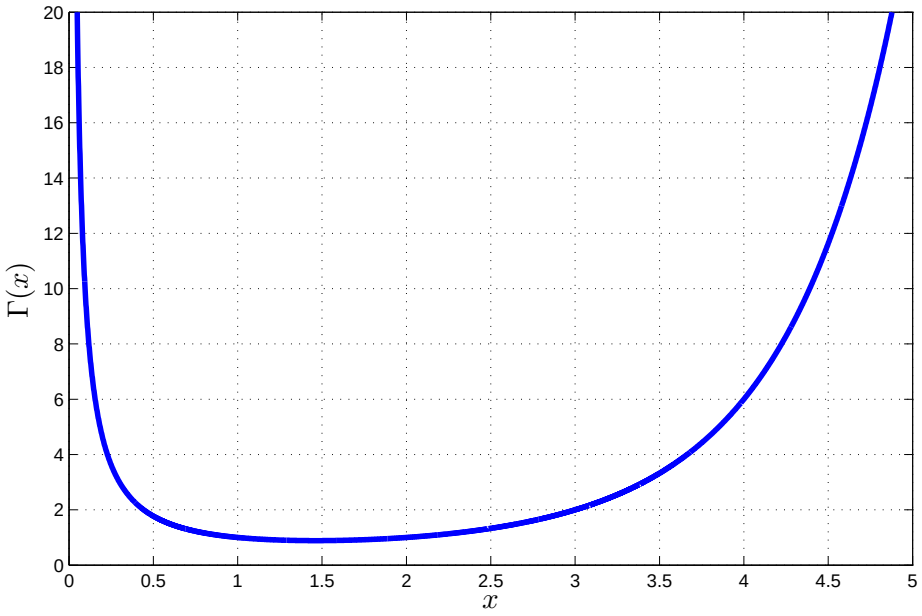

Fig. 1.1. Gamma function for $x > 0$

The alternative definition for the gamma function [72] is:

$$\Gamma(x) = \lim_{n \to 0} \frac{n! n^x}{x(x+1)(x+2)\dots(x+n)} \tag{1.3}$$

which is equivalent to the integral representation for $x > 0$.

This definition permits to use negative value of x. The gamma function for positive and negative values we can see in Fig. 1.2. We can notice that this function for $x \leq 0$ is discontinuous for $x \in \mathbb{Z}_-$.

To explain how important is the gamma function in the calculation of Laplace transform let us calculate the following example.

Example 1.2. *Let the power law function be $f(t) = t^x$, where x is non-integer. Using the definition of the Laplace transform, we obtain*

$$\mathscr{L}\{t^x\} = \int_0^\infty e^{-st} t^x dt$$

If we let $u = st$, then we can write

$$\int_0^\infty e^{-u} \left(\frac{u}{s}\right)^x \frac{du}{s} = \frac{1}{s^{x+1}} \int_0^\infty e^{-u} u^x du$$

$$\mathscr{L}\{t^x\} = \frac{\Gamma(x+1)}{s^{x+1}},\ x > -1$$

If we take $x = -\frac{1}{2}$*, we obtain*

$$\mathscr{L}\left\{\frac{1}{\sqrt{t}}\right\} = \frac{\Gamma\left(\frac{1}{2}\right)}{s^{\frac{1}{2}}} = \frac{\sqrt{\pi}}{\sqrt{s}}$$

and talking the inverse Laplace Transform for $s^{\frac{1}{2}}$ *we have*

$$\mathscr{L}^{-1}\left\{\frac{1}{\sqrt{s}}\right\} = \frac{1}{\sqrt{\pi t}}.$$

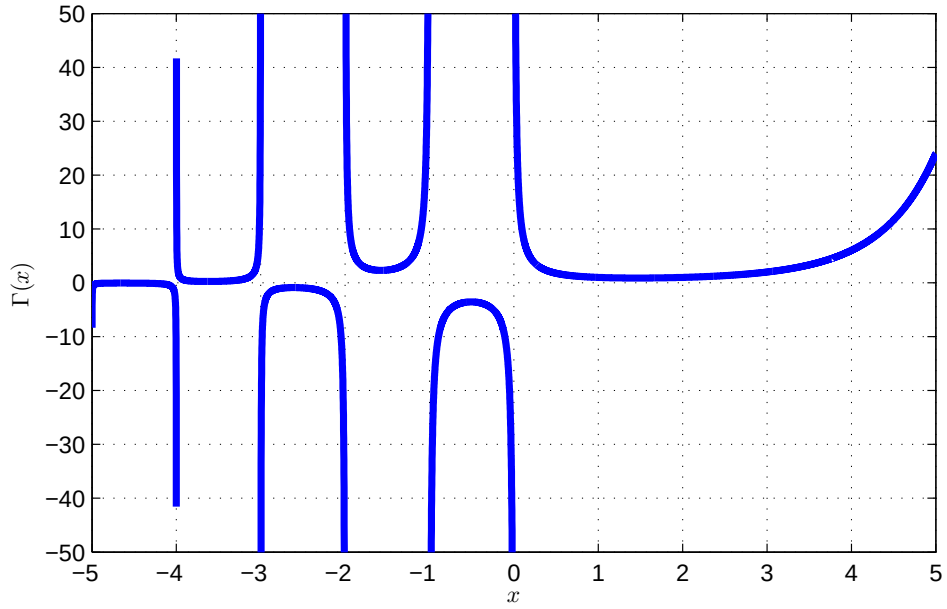

Fig. 1.2. Graph of gamma function, $\Gamma(x)$ for both positive and negative values of x

1.2 Error Function

The error function [56] occurred earlier in the historical discussion of the solution to the one-dimensional heat transfer problem. It is important in probability theory, diffusion and heat transfer. Like the gamma function, the error function is defined by the integral equation.

Definition 1.3. *The error function is defined as:*

$$\operatorname{erf}(x) = \frac{2}{\sqrt{\pi}} \int_0^x e^{-u^2} du \quad -\infty < x < \infty \tag{1.4}$$

The values of the error function at $x = 0$ and at $x = \infty$ can be calculated from the definition as follows:

$$\operatorname{erf}(0) = \frac{2}{\sqrt{\pi}} \int_0^0 e^{-u^2} du = 0,$$

$$\operatorname{erf}(\infty) = \frac{2}{\sqrt{\pi}} \int_0^\infty e^{-u^2} du = \frac{1}{\sqrt{\pi}} \int_0^\infty e^{-v} v^{-\frac{1}{2}} dv = \frac{\Gamma(\frac{1}{2})}{\sqrt{\pi}} = 1.$$

Definition 1.4. *The complementary error function is defined by:*

$$\operatorname{erfc}(x) = \frac{2}{\sqrt{\pi}} \int_x^\infty e^{-u^2} du \tag{1.5}$$

The complementary error can be connected with error function through following equation:

$$\operatorname{erfc}(x) = 1 - \operatorname{erf}(x) \tag{1.6}$$

so that the properties of the $\operatorname{erfc}(x)$ can be expressed in terms of $\operatorname{erf}(x)$. Graphs of $\operatorname{erf}(x)$ and $\operatorname{erfc}(x)$ are shown in Fig. 1.3.

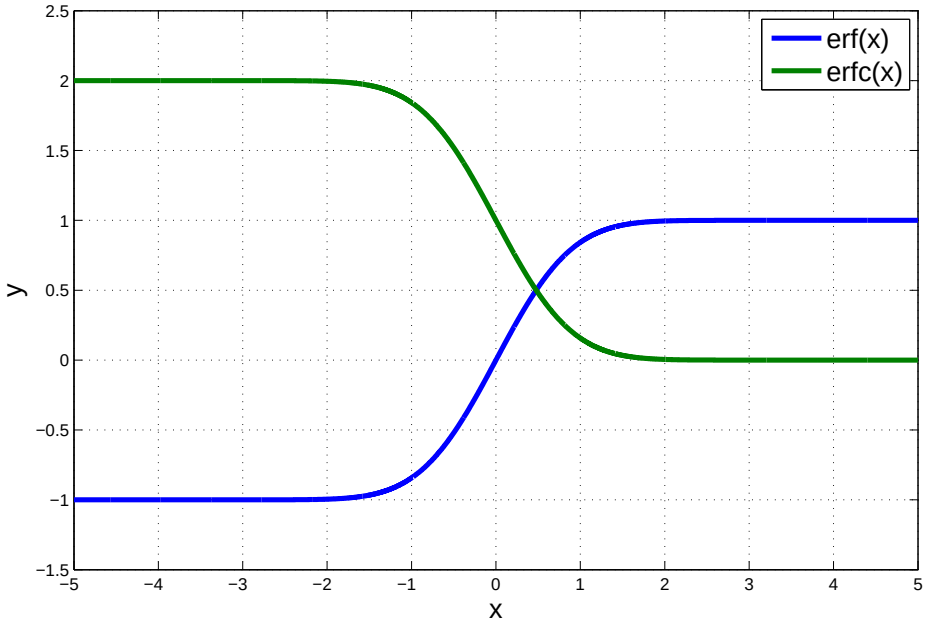

Fig. 1.3. Graphs of the $\operatorname{erf}(x)$ and $\operatorname{erfc}(x)$

We can notice that the error function is an odd function, $\operatorname{erf}(-x) = -\operatorname{erf}(x)$, but that $\operatorname{erfc}(-x) = 2 - \operatorname{erfc}(x)$. The error and the complementary error function are useful in the Laplace transform solutions to the heat or diffusion equation, where one encounters transforms involving $\sqrt{s}$ or $e^{-\sqrt{s}}$.

Example 1.5. *Let us calculate the inverse Laplace transform for the following expression:*

$$\mathscr{L}^{-1}\left\{\frac{1}{s\sqrt{s+a}}\right\},$$

where "a" is a constant.

Using the exponential shift theorem $\mathscr{L}\{e^{at}f(t)\} = F(s-a)$ *and Example 1.2 we have*

$$\mathscr{L}^{-1}\left\{\frac{1}{\sqrt{s+a}}\right\} = \frac{e^{-at}}{\sqrt{\pi t}},$$

and because the Laplace transform of integration the above equation can be considered as

$$\mathscr{L}^{-1}\left\{\frac{1}{s\sqrt{s+a}}\right\} = \int_0^t \frac{e^{-at}}{\sqrt{\pi\tau}}d\tau$$

Let us change variables using $u^2 = a\tau$

$$\mathscr{L}^{-1}\left\{\frac{1}{s\sqrt{s+a}}\right\} = \frac{1}{\sqrt{\pi}}\int_0^{\sqrt{at}} e^{-u^2}\frac{2u}{a\sqrt{\tau}}du = \frac{2}{\sqrt{\pi a}}\int_0^{\sqrt{at}} e^{-u^2}du$$

which can be finally written as

$$\mathscr{L}^{-1}\left\{\frac{1}{s\sqrt{s+a}}\right\} = \frac{1}{\sqrt{a}}\operatorname{erf}\left(\sqrt{at}\right)$$

1.3 Mittag-Leffler Function

The Mittag-Leffler function was developed by the Swedish mathematician G.M.Mittag-Leffler (1846-1927). This function is a generalization of the exponential function that plays an important role in fractional calculus.

1.3.1 Definition and Relation to Other Functions

Definition 1.6. *The two-parameter representation of the Mittag-Leffler function defined in terms of a power series is defined as:*

$$E_{\alpha,\beta}(x) = \sum_{k=0}^{\infty}\frac{x^k}{\Gamma(\alpha k+\beta)} \quad (\alpha>0, \beta>0) \tag{1.7}$$

When the parameter $\beta = 1$ than above function can be rewritten as one-parameter Mittag-Leffler function:

$$E_{\alpha}(x) = E_{\alpha,1}(x) = \sum_{k=0}^{\infty}\frac{x^k}{\Gamma(\alpha k+1)} \quad (\alpha>0) \tag{1.8}$$

Below some special forms of Mittag-Leffler function are presented:

Example 1.7.

$$E_1(x) = \sum_{k=0}^{\infty} \frac{x^k}{\Gamma(\alpha k + 1)} = \sum_{k=0}^{\infty} \frac{x^k}{k!} = e^x$$

$$E_{0.5,1}(x) = \sum_{k=0}^{\infty} \frac{x^k}{\Gamma(\frac{k}{2} + 1)} = e^{x^2} \operatorname{erfc}(-x)$$

$$E_{1,2}(x) = \sum_{k=0}^{\infty} \frac{x^k}{\Gamma(k + 2)} = \frac{1}{x} \sum_{k=0}^{\infty} \frac{x^{k+1}}{(k+1)!} = \frac{e^x - 1}{x}$$

$$E_{2,1}(x^2) = \sum_{k=0}^{\infty} \frac{x^{2k}}{\Gamma(2k + 1)} = \sum_{k=0}^{\infty} \frac{x^{2k}}{(2k)!} = cosh(x)$$

$$E_{2,2}(x^2) = \sum_{k=0}^{\infty} \frac{x^{2k}}{\Gamma(2k + 2)} = \sum_{k=0}^{\infty} \frac{x^{2k}}{(2k+1)!} = \frac{sinh(x)}{x}$$

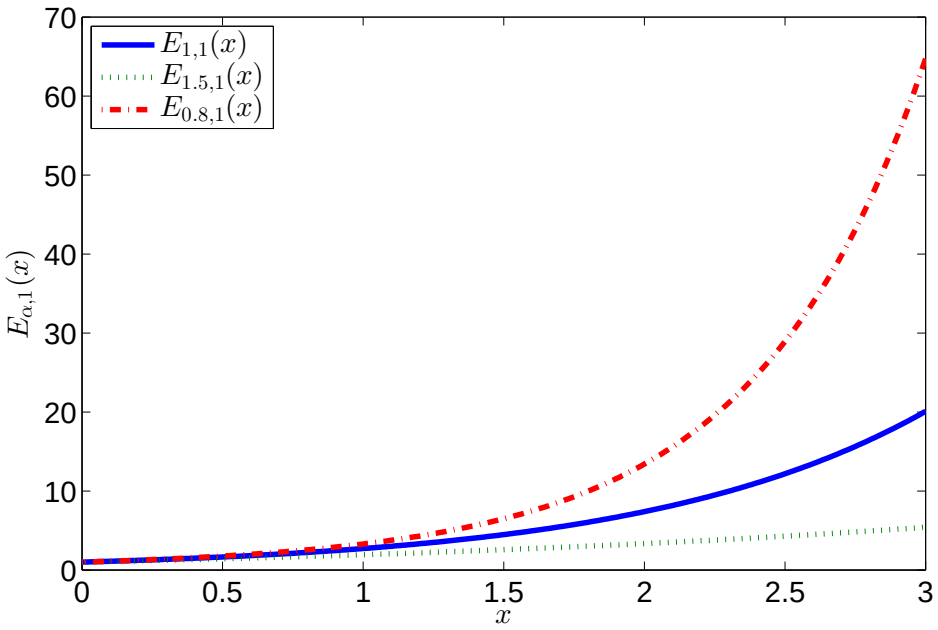

Fig. 1.4. Mittag-Leffler function $E_{\alpha,1}(x)$ for $\alpha = 0.8, 1, 1.5$

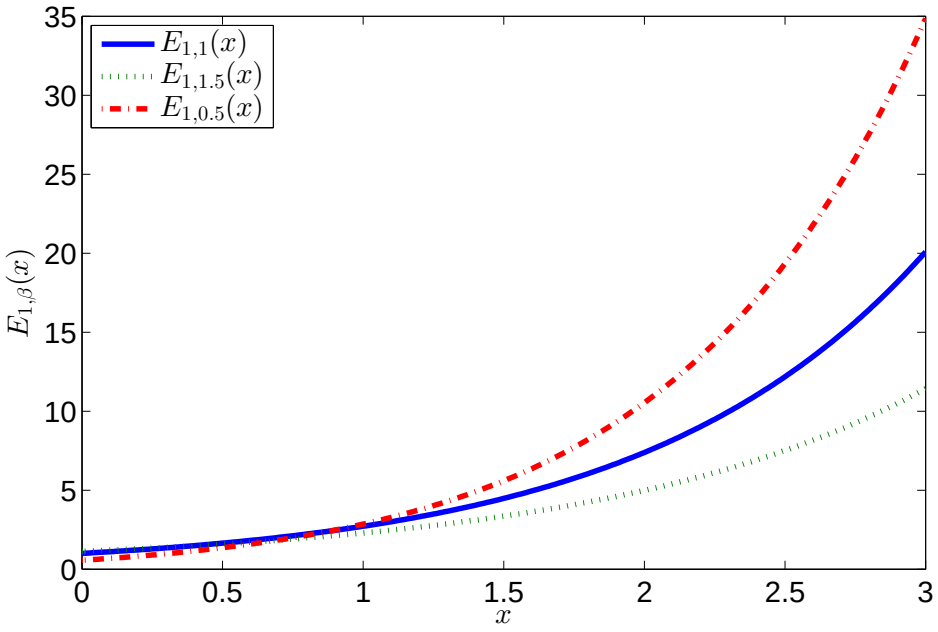

Fig. 1.5. Mittag-Leffler function $E_{1,\beta}(x)$ for $\beta = 0.5, 1, 1.5$

1.3.2 Laplace Transform of Two Parameters Mittag-Leffler Function

In Example 1.7 the generalisation of the e^x function using the Mittag-Leffler function was presented. Here, the way to obtain the Laplace transform of the Mittag-Leffler function using the analogy to exponential function is shown [72].

To derive the formula for calculation the Laplace transform of two parameters Mittag-Leffler function first let us prove that

$$\int_0^\infty e^{-t} e^{\pm zt} dt = \frac{1}{1 \mp z}, \ |z| < 1. \tag{1.9}$$

Using the series representation for e^{-bz}:

$$e^{-bz} = \sum_{k=0}^{\infty} \frac{(-1)^k (bz)^k}{k!}, \tag{1.10}$$

we obtain:

$$\int_0^\infty e^{-t} e^{\pm zt} dt = \sum_{k=0}^{\infty} \frac{(\pm z)^k}{k!} \int_0^\infty e^{-t} t^k dt = \sum_{k=0}^{\infty} \frac{(\pm z)^k}{k!} k! = \sum_{k=0}^{\infty} (\pm z)^k = \frac{1}{1 \mp z}. \tag{1.11}$$

Next, differentiating both sides of equation (1.9) with respect to z the following result was achieved

$$\int_0^\infty e^{-t} t^k e^{\pm zt} dt = \frac{k!}{(1 \mp z)^{k+1}}, \ |z| < 1, \tag{1.12}$$

what after substitutions gives the well-known pair of Laplace transform and the function $t^k e^{\pm at}$:

$$\mathscr{L}\left\{t^k e^{\pm at}\right\} = \int_0^\infty e^{\pm at} t^k e^{-st} dt = \frac{k!}{(s \mp a)^{k+1}}, \ Re(s) > |a|. \tag{1.13}$$

The Mittag-Leffler function (1.7) after substitution in the integral is given as:

$$\int_0^\infty e^{-t} t^{\beta-1} E_{\alpha,\beta}(zt^\alpha) dt = \frac{1}{1-z}, \ |z| < 1, \tag{1.14}$$

and from the above equations the Laplace transform of the function $t^{\alpha k+\beta-1} E^{(k)}_{\alpha,\beta}(\pm z t^\alpha)$, where $E^{(k)}_{\alpha,\beta}(y) \equiv \frac{d^k}{dy^k} E^{(k)}_{\alpha,\beta}(y)$ was obtained:

$$\mathscr{L}\left\{t^{\alpha k+\beta-1} E^{(k)}_{\alpha,\beta}(\pm a t^\alpha)\right\} = \int_0^\infty t^{\alpha k+\beta-1} E^{(k)}_{\alpha,\beta}(\pm a t^\alpha) e^{-st} dt = \frac{k! s^{\alpha-\beta}}{(s^\alpha \mp a)^{k+1}}, . \tag{1.15}$$

where $Re(s) > |a|^{\frac{1}{\alpha}}$. From relation (1.15) can be written another important Laplace pairs of the one and two parameters Mittag-Leffler function.

$$\mathscr{L}\left\{t^{-\frac{1}{2}} E_{\frac{1}{2},\frac{1}{2}}\left(\pm a\sqrt{t}\right)\right\} = \frac{1}{\sqrt{s} \mp a}$$

$$\mathscr{L}\left\{t^{\beta-1} E_{\alpha,\beta}\left(\pm a t^\alpha\right)\right\} = \frac{s^{\alpha-\beta}}{s^\alpha \mp a}$$

$$\mathscr{L}\left\{E_\alpha\left(\pm a t^\alpha\right)\right\} = \frac{s^\alpha}{s\left(s^\alpha \mp a\right)}$$

The Mittag-Leffler function is a natural extension of the Laplace transform pairs for the exponential function in terms of integer powers of s to the fractional powers of the transform parameters s. This analogies are presented in Table 1.1.

Table 1.1. Laplace Transform Pairs Involving Corresponding Representations for the Exponential and Mittag-Leffler Function [56]

$f(s)$	$F(t)$	$f(s)$	$F(t)$
$\frac{1}{s+a}$	e^{-at}	$\frac{1}{\sqrt{s}+a}$	$\frac{1}{\sqrt{t}} E_{\frac{1}{2},\frac{1}{2}}(-a\sqrt{t})$
$\frac{1}{s(s+a)}$	$\frac{1-e^{-at}}{a}$	$\frac{1}{\sqrt{s}(\sqrt{s}+a)}$	$E_{\frac{1}{2}}(-a\sqrt{t})$
$\frac{1}{s^2(s+a)}$	$\frac{1}{a^2}\left(e^{-at}+at-1\right)$	$\frac{1}{s(\sqrt{s}+a)}$	$\frac{1}{a}\left(1 - E_{\frac{1}{2}}(-a\sqrt{t})\right)$
$\frac{1}{(s+a)^2}$	te^{-at}	$\frac{1}{(\sqrt{s}+a)^2}$	$\left(1+2a^2t\right) E_{\frac{1}{2}}(-a\sqrt{t}) - 2a\sqrt{\frac{t}{\pi}}$
$\frac{s}{s^2+a^2}$	$\cos(at)$	$\frac{\sqrt{s}}{s+a^2}$	$\frac{1}{\sqrt{t}} E_{1,\frac{1}{2}}\left(-a^2t\right)$
$\frac{1}{s(s^2+a^2)}$	$\frac{1}{a^2}\left(1-\cos(at)\right)$	$\frac{1}{\sqrt{s}+a^2}$	$\sqrt{t} E_{1,\frac{3}{2}}\left(-a^2t\right)$

1.4 Confluent Hypergeometric Function

The Confluent Hypergeometric Function is a solution of a Confluent Hypergeometric Equation, which is a degenerate form of a hypergeometric differential equation where two of the three regular singularities merge into an irregular singularity. (The term "confluent" refers to the merging of singular points of families of differential equations; "confluere" is Latin for "to flow together".)

To define the Confluent Hypergeometric Function first let us focus on the Confluent Hypergeometric Equation.

Definition 1.8. *Confluent Hypergeometric Equation (Kummer's Equation) with respect to $u(z)$ is defined as:*

$$z\frac{d^2u(z)}{dz^2} + (c - z)\frac{du(z)}{dz} - au(z) = 0,$$

where $z \in \mathbb{C}$ and a, c are the constant parameters.

The general solution of this equation is the linear combination of two independent constituents. This solution has the following form:

$$u(z) = C\,{}_1F_1(a, c, z) + Dz^{1-c}\,{}_1F_1(a - c + 1, 2 - c, z), \tag{1.16}$$

where C and D are constant and depend on the boundary conditions.

The function ${}_1F_1(a, c, z)$ is called Confluent Hypergeometric Function and is presented below.

Definition 1.9. *Confluent Hypergeometric Function is defined as:*

$${}_1F_1(a; c; z) = \sum_{n=0}^{\infty} \frac{(a)_n}{(c)_n}\frac{x^n}{n!} \quad -\infty < x < \infty,$$

where $(a)_n$ and $(c)_n$ are the Pochhammer symbols defined by

$$(g)_n = \frac{\Gamma(g + n)}{\Gamma(g)},\ n = 0,\ 1,\ 2, \ldots$$

Below some relation of confluent hypergeometric function are presented:

Example 1.10.

$${}_1F_1(1; 1; x) = e^x$$

$${}_1F_1(1; \alpha + 1; ax) = \Gamma(\alpha + 1)E_{1,\alpha+1}(ax)$$

$${}_1F_1(1; 1.5; x^2) = \frac{e^{x^2}\sqrt{\pi}}{2x}\,\mathrm{erf}(x)$$

$${}_1F_1(0.5; 1.5; -x^2) = \frac{\sqrt{\pi}}{2x}\,\mathrm{erf}(x)$$

1.5 Continuous Fractional Systems

In this section the fundamental definitions of the fractional calculus are shown. The name: fractional calculus describes the theory of integrals and derivatives of arbitrary order, which generalize and unify the notions of integer order differentiation and n-fold integration. The infinite sequence of n-fold integrals and derivatives can be expressed as:

$$\ldots, \qquad \int_a^t d\tau_2 \int_a^{\tau_2} f(\tau_1) d\tau_1, \qquad \int_a^t f(\tau_1) d\tau_1, \qquad f(t), \qquad \frac{df(t)}{dt}, \qquad \frac{d^2 f(t)}{dt^2}, \qquad \ldots$$

The α, a real order of derivative, can be considered as an interpolation of presented sequence of operators. The operator proposed by Davis [18] called *fractional derivative* is shown as follows:

$$ {}_aD_t^{\alpha} f(t), \tag{1.17}$$

where a and t are the limits related to the operation of fractional differentiation. Following Ross [79] we will call them the *terminals* of fractional differentiation. The notation (1.17) unify the definition of an integrals and a derivative operator. For the positive value of the order ($\alpha > 0$) we achieve the fractional derivative operator, for negative value of the order ($\alpha < 0$) we achieve fractional integrals operator and for ($\alpha = 0$) we have identity operator and achieve function $f(t)$ itself. Hence this operator is called a differ-integral.

At the beginning the Riemman-Liouville (R-L) definition, which is the extension of the Cauchy formula for the n-fold integration, is presented. Than, the Caputo definition, which is modification of R-L definition, is shown. Finally, the Grünwald-Letnikow (G-L) definition, which is the extension of the n-fold derivation formula for the integer order, is described. Also, the main properties of this operators are discussed.

At the end of this section the transfer function of the fractional order system is presented. Also the Bode diagrams of the fractional order integrator are shown.

1.5.1 Riemann-Liouville Derivatives

Let us consider the Cauchy formula for the n-fold integration [38]:

$$ {}_aI_t^n f(x) = \int_a^t d\tau_1 \int_a^{\tau_1} d\tau_2 \ldots \int_a^{\tau_{n-1}} f(\tau_n) d\tau_n = \frac{1}{(n-1)!} \int_a^t f(t-\tau) d\tau, \tag{1.18}$$

where a, x are terminals of the integration $f(\tau)$ function.

Using the relation (1.2) equation (1.18) can be extended for the $n \in \mathbb{R}$. In this case we obtained the Riemann-Liouville formula for the fractional integral:

$$ {}_a^R I_t^\alpha f(t) = \frac{1}{\Gamma(\alpha)} \int_a^t f(t-\tau)^{\alpha-1} f(\tau) d\tau, \tag{1.19} $$

where $\alpha \in \mathbb{R}^+$ is the order of integral in terminals (a, t) of the $f(t)$ function.

Extending equation (1.19) for $\alpha \leq 0$ the following definition was obtained:

Definition 1.11. *Riemann-Liouville (R-L) fractional order differ-integral is defined as:*

$$ {}_a^R D_t^\alpha f(t) = \frac{1}{\Gamma(m-\alpha)} \frac{d^m}{dt^m} \int_a^t \frac{f(\tau)}{(t-\tau)^{\alpha-m+1}} d\tau, $$

where $\alpha \in \mathbb{R}$ is a fractional order of the differ-integral of a function $f(t)$.
For $\alpha > 0 \quad m-1 < \alpha \leq m,\ m \in \mathbb{N}$ and for $\alpha \leq 0 \quad m = 0$.

As we see, when $\alpha > 0$ the result of this function is equivalent to the fractional order derivative, for $\alpha < 0$ to fractional order integral and for $\alpha = 0$ to the function itself. This is why above definition is called a differ-integral.

The main property of the operator ${}_a^R D_t^\alpha f(t)$ is the linearity for the integer-order differentiation and also for the fractional differentiation. More properties are described in: [61, 63, 72].

The Laplace transform of the fractional order differ-integral in Riemann-Liouville form is given as follows [72]:

$$ \mathcal{L}[{}_0^R D_t^\alpha f(t)] = \begin{cases} s^\alpha F(s) & \text{for } \alpha < 0 \\ s^\alpha F(s) - \sum_{k=0}^{n-1} s^k \ {}_0^R D_t^{\alpha-k-1} f(0) & \text{for } \alpha > 0, \end{cases} $$

where

$$ n-1 < \alpha \leq n,\ n \in \mathbb{N}. $$

It has to be noticed that the Laplace transform of the Riemann-Liouville definition possesses the fractional order derivatives of the initial conditions.

1.5.2 Caputo Derivatives

The non-integer order of the initial conditions implies the problem with utilization of the R-L definition in real applications. Despite the fact that initial values problems can be successfully solved mathematically (see e.g. [80]) their solutions are practically useless, because the physical interpretation of such types of initial condition is not known. A certain solution of this problems was proposed by M. Caputo in paper [11] and in book

[12], and recently (in Banach spaces) by El-Sayed [28, 29]. This new definition has the following form:

Definition 1.12. *Caputo (C) definition of the fractional order differ-integral*

$$ {}_a^C D_t^\alpha f(t) = \frac{1}{\Gamma(m-\alpha)} \int_a^t \frac{f^{(m)}(\tau)}{(t-\tau)^{\alpha-m+1}} d\tau, $$

where $\alpha \in \mathbb{R}$ is a fractional order of the differ-integral of the function $f(t)$.
For $\alpha > 0 \quad m-1 < \alpha \leq m,\ m \in \mathbb{N}$ and for $\alpha \leq 0 \quad m = 0$.

Caputo operator is also linear but this definition is more restrictive then the Riemann-Liouville because it requires the absolute integrability of the mth-order derivative of the function $f(t)$. In general, this two definitions are not equivalent, except in the case of being zero at $t = 0^+$ for the function $f(t)$ and its first $(m-1)$th-order derivatives. In fact, between R-L and C definition there are following relations [62]:

$$ {}_a^R D_t^\alpha f(t) = {}_a^C D_t^\alpha f(t) + \sum_{k=0}^{m-1} \frac{tk-\alpha}{\Gamma(k-\alpha+1)} f^{(k)}(0^+), \tag{1.20} $$

$$ {}_a^R D_t^\alpha f(t) \left(f(t) - \sum_{k=0}^{m-1} f^{(k)}(0^+) \frac{t^k}{k!} \right) = {}_a^C D_t^\alpha f(t). \tag{1.21} $$

The Laplace transform of the fractional order differ-integral in Caputo form is given as follows [72]:

$$ \mathcal{L}[{}_0^C D_t^\alpha f(t)] = \begin{cases} s^\alpha F(s) & \text{for } \alpha < 0 \\ s^\alpha F(s) - \sum_{k=0}^{n-1} s^{\alpha-k-1} f^{(k)}(0) & \text{for } \alpha > 0, \end{cases} $$

where

$$ n-1 < \alpha \leq n,\ n \in \mathbb{N}. $$

The Laplace transform formula of the Caputo definition involves the value of the function $f(t)$ and its derivatives at the lower terminal $t = 0$, for which the certain physical interpretations exist. Hence Caputo formula is very useful for solving applied problem leading to linear fractional differential equation.

1.5.3 Left-sided Grünwald-Letnikov Derivatives

The different way of derivation the formula for calculating the fractional order derivatives was presented by Grünwald and Letnikov [35]. Their definition is the generalisation of the backward difference for fractional order.

Let us consider a continuous function $y = f(t)$. The first-order derivative is described as following formula:

$$f^{'}(t) = \frac{df}{dt} = \lim_{h \to 0} \frac{f(t-h) - f(t)}{h}. \tag{1.22}$$

The second-order derivative can be written as:

$$f^{''}(t) = \frac{d^2 f}{dt^2} = \lim_{h \to 0} \frac{f^{'}(t-h) - f^{'}(t)}{h} = \lim_{h \to 0} \frac{f(t-2h) - 2f(t-h) + f(t)}{h^2}. \tag{1.23}$$

By the induction, the relation for the n-fold derivative can be achieved:

$$f^{n}(t) = \frac{d^n f}{dt^n} = \lim_{h \to 0} \frac{1}{h^n} \sum_{r=0}^{n} (-1)^r \binom{n}{r} f(t - rh). \tag{1.24}$$

Finally, using the generalization of (1.24) the derivative for non-integer order can be defined.
Grünwald-Letnikov definition:

Definition 1.13. *Grünwald-Letnikov definition of the fractional order differ-integral*

$$f^{\alpha}(t) = \frac{d^\alpha f}{dt^\alpha} = \lim_{h \to 0} \frac{1}{h^\alpha} \sum_{r=0}^{\alpha} (-1)^r \binom{\alpha}{r} f(t - rh),$$

where $\alpha \in \mathbb{R}$.

The approximation of this definition is very useful in case of computer applications.

1.5.4 Fractional Order Transfer Function

The equation for a continuous-time dynamic system of fractional-order can be written as follows:

$$H(\mathcal{D}^{\alpha_0 \alpha_1 \alpha_2 \ldots \alpha_m})(y_1, y_2, \ldots, y_l) = G(\mathcal{D}^{\beta_0 \beta_1 \beta_2 \ldots \beta_n})(u_1, u_2, \ldots, u_k), \tag{1.25}$$

where y_i, u_i are the functions of the time and $H(\cdot)$, $G(\cdot)$ are the combination laws of the fractional-order derivative operator. Fot the linear time-invariant single-variable case, the following equation would be obtained:

$$\begin{aligned} &a_n \mathcal{D}^{\alpha_n} y(t) + a_{n-1} \mathcal{D}^{\alpha_{n-1}} y(t) + \ldots + a_0 \mathcal{D}^{\alpha_0} y(t) = \\ &= b_m \mathcal{D}^{\beta_m} u(t) + b_{m-1} \mathcal{D}^{\beta_{m-1}} u(t) + \ldots + b_0 \mathcal{D}^{\beta_0} u(t) \end{aligned} \tag{1.26}$$

where $a_n \ldots a_0$ and $b_m \ldots b_0 \in \mathbb{R}$.

If all the orders of system are integer multiples of a base order, α, ($\alpha_k, \beta_k = k\alpha$, $\alpha \in \mathbb{R}^+$), the system is named *commensurate-order* and in addition if $\alpha = \frac{1}{q}$, $q \in \mathbb{Z}^+$, the system is called *rational-order*.

Applying the Laplace transform to (1.27) with zero initial conditions, the input-output representation of fractional order system can be obtained.

Definition 1.14. *The continuous fractional order transfer function is defined as:*

$$G(s) = \frac{Y(s)}{U(s)} = \frac{b_m s^{\beta_m} + b_{m-1} s^{\beta_{m-1}} + \ldots + b_0 s^{\beta_0}}{a_n s^{\alpha_n} + a_{n-1} s^{\alpha_{n-1}} + \ldots + a_0 s^{\alpha_0}},$$

where $U(s)$,$Y(s)$ are the Laplace transform of input, output signal respectively, assuming zero initial conditions $u(0), y(0) = 0$ and $m, n \in \mathbb{N}_+$.

In case of a commensurate-order system, the continuous-time transfer function is given by:

$$G(s) = \frac{\sum_{k=0}^{m} b_k (s^\alpha)^k}{\sum_{k=0}^{n} a_k (s^\alpha)^k} \tag{1.27}$$

1.5.5 Fractional Order Integrator

The fractional order integrator is described using following equation:

$$G(s) = \frac{1}{(Ts)^\alpha} \tag{1.28}$$

The spectral transfer function of (1.28) is given as:

$$G(j\omega) = \frac{1}{(Tj\omega)^\alpha} = \frac{1}{T\omega^\alpha(\cos\frac{\pi}{2}\alpha + j\sin\frac{\pi}{2}\alpha)} \tag{1.29}$$

and the magnitude of the transfer function is [40]

$$A(\omega) = \sqrt{\frac{\left(cos^2\frac{\pi}{2}\alpha + sin^2\frac{\pi}{2}\alpha\right)}{(T\omega)^{2\alpha}}} = \frac{1}{(T\omega)^\alpha}, \tag{1.30}$$

which yields

$$M(\omega) = 20\log A(\omega) = -\alpha 20\log(T) - \alpha 20\log(\omega). \tag{1.31}$$

The phase properties are obtained from the following relation:

$$\varphi(\omega) = \arg\left[\frac{1}{(T\omega)^\alpha} j^{-\alpha}\right] = -\alpha\frac{\pi}{2}.$$

The Bode diagrams of the fractional order integrator for different values of α is presented in Fig. 1.6.

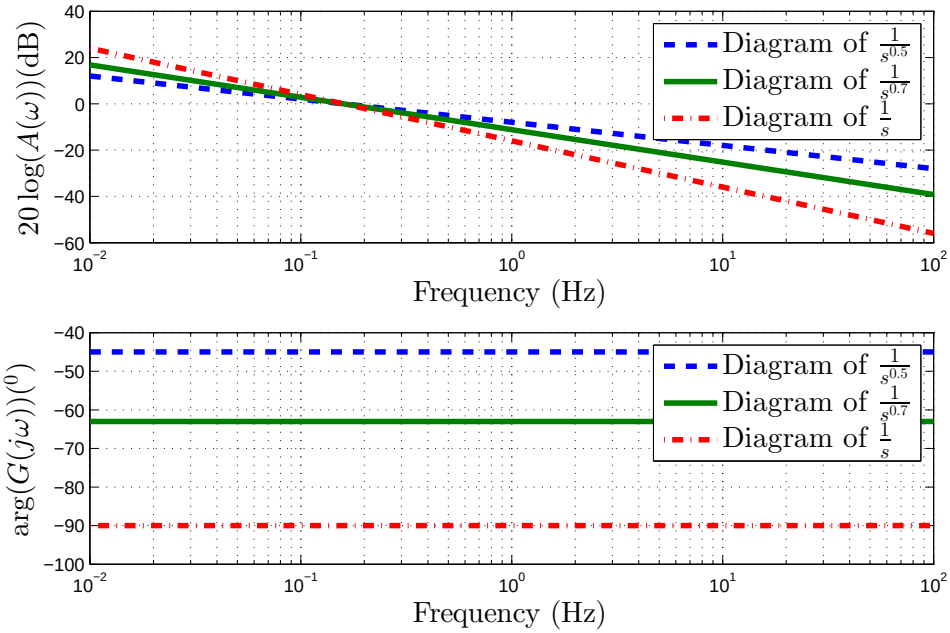

Fig. 1.6. Bode diagrams of $G(s) = \frac{1}{s^\alpha}$ systems for $\alpha = 0.5, 0.7, 1$.

1.6 Discrete Fractional Order Systems

In the following section a short introduction to the fractional order discrete time system is presented. On the contrary to the continuous systems in the discrete systems there exists only one type of definition of the fractional order difference. This definition is the generalisation of the traditional definition of integer difference for the fractional order and it is the extension of the Grünwald-Letnikov (1.13) definition for the constant step h.

1.6.1 Fractional Order Difference

To present the definition of the fractional order difference let us introduce the first order backward difference:

$$\Delta x_k = x_k - x_{k-1}. \tag{1.32}$$

This difference is more useful in physics than the forward difference because usually one operates on the known samples.
The second (backward) difference is presented as:

$$\Delta^2 x_k = x_k - 2x_{k-1} + x_{k-2}. \tag{1.33}$$

The integer order difference at any order n can be calculated by the following relation:

$$\Delta^n x_k = \sum_{r=0}^{n} (-1)^r \binom{n}{r} x_{k-r}. \tag{1.34}$$

Using the relation above the fractional order difference can be defined:

Definition 1.15. *Fractional order (backward) difference is defined as [24]:*

$$\Delta^{\alpha} x_k = \sum_{j=0}^{k} (-1)^j \binom{\alpha}{j} x_{k-j}, \tag{1.35}$$

where $\alpha \in \mathbb{R}$ is a fractional order and $k \in \mathbb{N}$ is a number of sample for which the difference is obtained.

The operator of fractional order difference Δ^{α} is linear like its equivalent continuous operator.

1.6.2 Discrete Fractional Order State-Space System

The linear discrete time fractional order state-space system (DFOSS) was introduced by Dzieliński and Sierociuk [24, 25]. Their definition contains three main equations for calculating:

- fractional difference of state variable,
- next value of state variable,
- system output.

The DFOSS is used from the following definition:

Definition 1.16. *Linear discrete fractional order system (DFOSS) in the state-space representation is defined as [24]:*

$$\Delta^{\alpha} x_{k+1} = A_d x_k + B u_k \tag{1.36}$$

$$x_{k+1} = \Delta^{\alpha} x_{k+1} - \sum_{j=1}^{k+1} (-1)^j \binom{\alpha}{j} x_{k-j+1} \tag{1.37}$$

$$y_k = C x_k + D u_k \tag{1.38}$$

where $x_k \in \mathbb{R}^N$, $A_d \in \mathbb{R}^{N \times N}$, $B \in \mathbb{R}^{N \times m}$, $C \in \mathbb{R}^{p \times N}$, $D \in \mathbb{R}^{p \times m}$ and m is a number of system inputs, p is a number system outputs, $k \in \mathbb{Z}_+$ is a number of sample for which the difference is obtained and $\alpha \in \mathbb{R}$ is a system order.

The solution of such defined system is:

$$x_k = \Phi(k) x_0 + \sum_{j=0}^{k-1} \Phi(k-j-1) B u_j, \tag{1.39}$$

where $\Phi(k)$ is a transition matrix described for the following equation:

$$\Phi(k+1) = \left(A_d + I\binom{n}{1}\right)\Phi(k) - \sum_{j=2}^{k+1}(-1)^j\binom{n}{j}\Phi(k+j-1), \tag{1.40}$$

for the initial condition $\Phi = I$. Presented system is linear what was shown in Ph.D. thesis of D.Sierociuk [85].

From DFOSS the following non-linear discrete fractional order system is proposed.

Definition 1.17. *Non-linear discrete fractional order system in a state-space representation is defined as:*

$$\Delta^\alpha x_{k+1} = f(x_k, u_k) \tag{1.41}$$

$$x_{k+1} = \Delta^\alpha x_{k+1} - \sum_{j=1}^{k+1}(-1)^j\binom{\alpha}{j}x_{k-j+1} \tag{1.42}$$

$$y_k = h(x_k) \tag{1.43}$$

where $\alpha \in \mathbb{R}$ is a system order, $f()$ and $h()$ are non-linear functions.

This system can be used for modelling a non-linear fractional order system. Example of modelling ultracapacitor non-linearity is shown in this work.

Chapter 2

Analytical Model of Ultracapacitors

In this chapter a derivation of an analytical ultracapacitor model is presented. To explain use of the fractional calculus in the ultracapacitor modelling process, the internal ultracapacitor structure is described. In addition to the new model derivation, classical ultracapacitor models based on the RC ladder are shown. Also neural network ultracapacitor models which deal with the complicated internal structure are briefly described.

2.1 Introduction to Ultracapacitors

Ultracapacitors (aka supercapacitors or double-layer capacitors) are electrical devices which are used to store energy and offer high power density that is not possible to achieve with traditional capacitors. The capacity order of ultracapacitor is thousands of times greater than a high capacity traditional electrolytic capacitor (even up to 5000 farads). The amount of energy stored per unit weight is generally lower than that of an electrochemical battery (2-9 Wh/kg for an standard ultracapacitor, although 85 Wh/kg has been achieved in the lab compared to 30-40 Wh/kg for a lead acid battery), and about 1/1000th the volumetric energy density of gasoline. These features make it possible to use the ultracapacitors in many industrial applications e.g. electric storage devices for solar and wind power, electric-car, elevator and power supply supplement or balance. They can be also used in PC Cards, flash, photography devices in digital cameras, portable media players, and in automated meter reading, wherever extremely fast charging is desirable. The parameters of the supercapacitors are the results of highly intricate internal structure. [34]

An ultracapacitor can be shown (Fig.2.1) as two non reactive porous plates, or collectors, suspended within an electrolyte, with a voltage potential applied across the collectors. These plates are typically constructed with activated carbon which is characterized by high degree of microporosity (1 gram of activated carbon has surface area in excess of 500m^2). In an ultracapacitor the applied potential to the positive electrode attracts the negative ions in the electrolyte, while the potential to the negative electrode attracts

the positive ions. A dielectric separator between the two electrodes prevents the charge from moving between the two electrodes. Electrical energy storage devices, such as capacitors, store electrical charge on an electrode. In other devices like electrochemical cells or batteries, the energy is created by chemical reaction of electrodes. In both of these, the ability to store or create electrical charge is a function of the surface area of the electrode. In an ultracapacitor the energy is also the function of the electrodes surface but this energy is collected in ions movement, differently from electrolyte capacitor where energy is collected in the ions polarization.

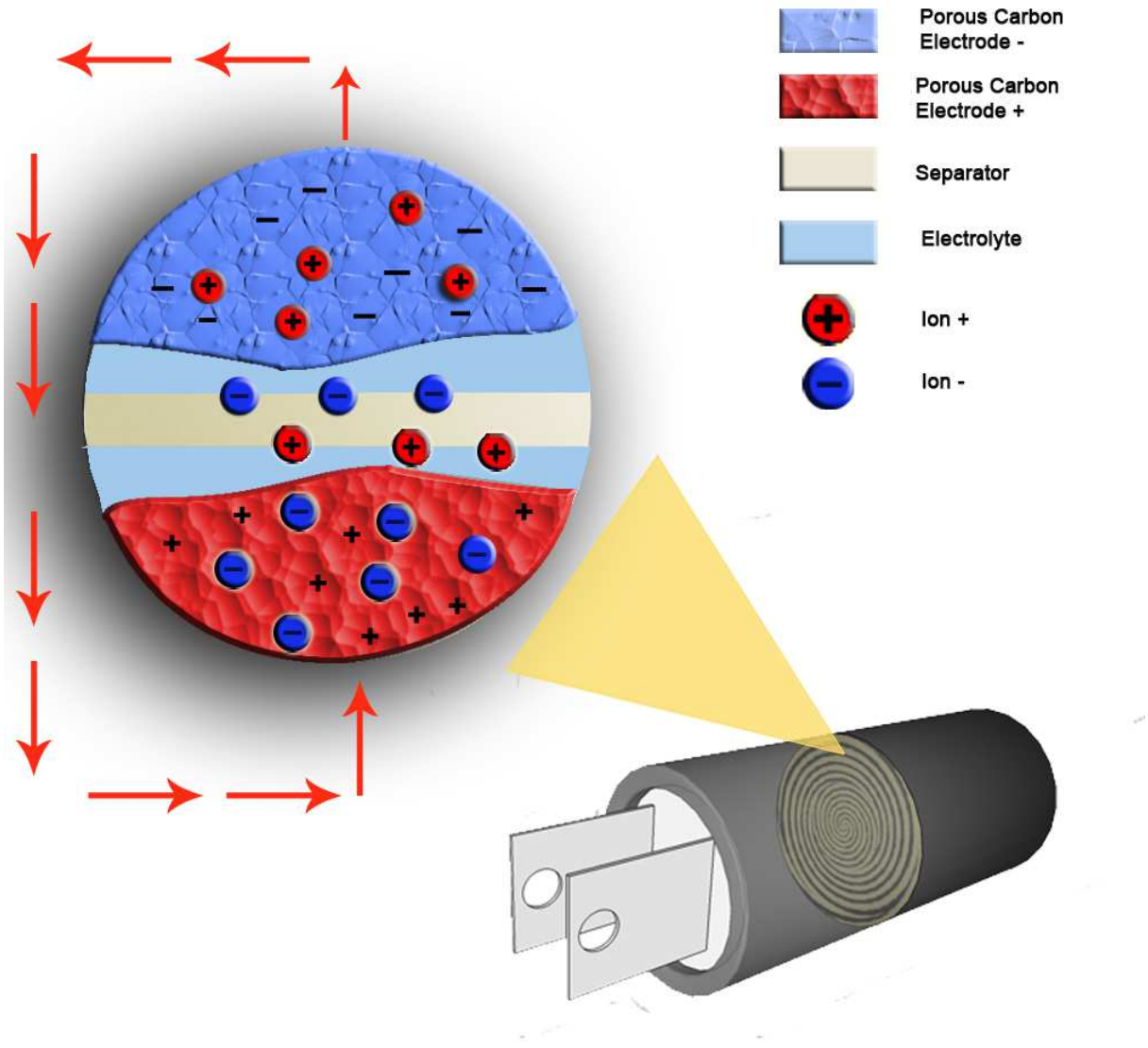

Fig. 2.1. Ultracapacitor scheme

As a storage device, the ultracapacitor, relies on the microscopic charge separation at an electrochemical interface to store energy. This separation is made because of the double-layer phenomenon. At low voltage at the boundary of two substances are contained

electrically charged particles which create a thin separating region across which an electrical field exists, hence the ultracapacitor is also called double-layer capacitor. Employment of this phenomenon enforces the parameters of supercapacitor (single ultracapacitor can be used only in tight range of Voltage 0-5V). This can be avoided by building a cascade of ultracapacitors. Since, the capacity of supercapacitor devices is proportional to the active electrode area and inversely proportional to the width of separation layer, it is not possible to control the width of spread region, so to change the amount of energy that can be stored and the capacity one gets changing the electrode surface area. This need for high surface area causes the use of materials such as activated carbon or sintered metal powders. However, in both situations, there is an intrinsic limit to the porosity of these materials, that determines an upper limit to the electrodes surface area.

A complicated structure of supercapacitor and utilization of ions movement to store the energy have a large influence on its dynamics. Therefore, it is different than in traditional capacitor. Modelling and description of this devices requires the use of more sophisticated methods, from which we can distinguish tree main groups using the following:

1. fractional order model,
2. RC cascade,
3. artificial neural network (ANN).

Some examples of models from these groups are presented in the next sections.

2.2 Analytical Derivation of Fractional Order Ultracapacitor Model

The high porosity of electrodes internal kinetic effects differ from those observed in conventional planar electrodes and have great influence on the impedance of ultracapacitor. To derive an analytical model of double-layer capacitor it is necessary to focus on the porous structure and the electrode-electrolyte interface. The current in supercapacitor is composed of an ionic current through the electrolyte, an electronic current through the electrode material and a displacement current at the electrode-electrolyte interface [8]. Since, the two order of magnitude higher conductivity of electrode than the insulator layer the electrode resistance can be neglected. However, in a full model of ultracapacitor this resistance should be taken into consideration because of high current work conditions. For the double-layer capacitor impedance, the main influence have the ions diffusion at the electrode-electrolyte interface layer. The diffusion process can be modelled using the finite model of transmission line presented in Fig: 2.2 [6].

To derive a simplified model of an ultracapacitor it was assumed that the distributions of resistance r and capacitance c are constant and the cylindrical pores are uniformly filled with electrolyte, and d is a length of transmission line.

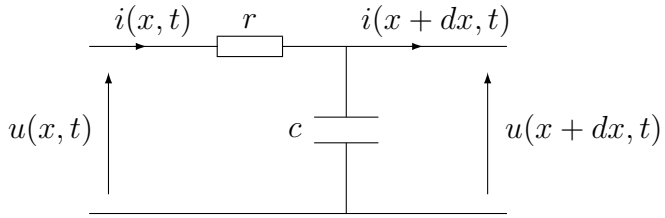

Fig. 2.2. Scheme of transmission line mathematical model

The current $i(x,t)$ and the voltage $u(x,t)$ are related by using the diffusion partial differential equation presented as follows:

$$\begin{cases} \frac{\partial u(x,t)}{\partial x} = -r \cdot i(x,t) \\ \frac{\partial i(x,t)}{\partial x} = -c \cdot \frac{\partial u(x,t)}{\partial t} \end{cases} \tag{2.1}$$

Parameters r and c being constant, equation (2.1) can be rewritten as:

$$\begin{cases} \frac{\partial^2 u(x,t)}{\partial x^2} = r \cdot c \cdot \frac{\partial u(x,t)}{\partial t} \\ \frac{\partial^2 i(x,t)}{\partial x^2} = r \cdot c \cdot \frac{\partial i(x,t)}{\partial t} \end{cases} \tag{2.2}$$

The above relation can be solved like one dimensional transient heat conduction equation using the Laplace domain. The Laplace transform derivative with respect to time of the first equation from (2.2) is presented as follows:

$$\frac{\partial^2 U(x,s)}{\partial x^2} = r \cdot c \cdot s \cdot U(x,s) - r \cdot c \cdot U(x,0) \tag{2.3}$$

For the zero initial condition above equation can be rewritten as:

$$\frac{\partial^2 U(x,s)}{\partial x^2} - r \cdot c \cdot s \cdot U(x,s) = 0 \tag{2.4}$$

The roots of this equation are as follows:

$$\omega_{1,2} = \pm\sqrt{r \cdot c \cdot s}$$

and the solution of the equation (2.4) is:

$$U(x,s) = C_1(s) \sinh\left(x\sqrt{r \cdot c \cdot s}\right) + C_2(s) \cosh\left(x\sqrt{r \cdot c \cdot s}\right) \tag{2.5}$$

where $C_1(s)$ and $C_2(s)$ are the constants of the equation.
To appoint constants of above equation it is necessary to use the boundary condition. For

the $x = 0$ we have:

$$U(0,s) = C_1(s)\sinh(0) + C_2(s)\cosh(0) \tag{2.6}$$

what gave the relation for the second constant $C_2(s)$ presented as:

$$C_2(s) = U(0,s) \tag{2.7}$$

The constant $C_1(s)$ can be calculated from the first equation from the set of equation (2.1):

$$-r \cdot i(x,t) = \frac{\partial u(x,t)}{\partial x}$$

Using the Laplace transform with respect to time and the equation (2.5) we obtained:

$$-r \cdot I(x,s) = C_1(s)\sqrt{r \cdot c \cdot s} \cdot \cosh\left(x\sqrt{r \cdot c \cdot s}\right) + U(0,s)\sqrt{r \cdot c \cdot s} \cdot \sinh\left(x\sqrt{r \cdot c \cdot s}\right) \tag{2.8}$$

In the case of ultracapacitors, the limit condition in $x = d$ is $i(d,t) = 0$, which implies $I(d,s) = 0$, so the equation (2.8) becomes:

$$0 = C_1(s)\sqrt{r \cdot c \cdot s} \cdot \cosh\left(d\sqrt{r \cdot c \cdot s}\right) + U(0,s)\sqrt{r \cdot c \cdot s} \cdot \sinh\left(d\sqrt{r \cdot c \cdot s}\right) \tag{2.9}$$

what can be rewritten as:

$$C_1(s) = -\tanh\left(d\sqrt{r \cdot c \cdot s}\right) U(0,s). \tag{2.10}$$

Let us go back to the equation (2.8). For $x = 0$ we obtaine:

$$-r \cdot I(0,s) = -\tanh\left(d\sqrt{r \cdot c \cdot s}\right) U(0,s)\sqrt{r \cdot c \cdot s} \cdot 1 + 0 \tag{2.11}$$

what can be rewritten as:

$$I(0,s) = \frac{\sqrt{r \cdot c \cdot s}}{r} \tanh\left(d\sqrt{r \cdot c \cdot s}\right) U(0,s) \tag{2.12}$$

Finally we obtained the transfer function of the transmission line:

$$Z_{imp}(s) = \frac{U(0,s)}{I(0,s)} = \frac{r}{\sqrt{r \cdot c \cdot s}} \coth\left(d\sqrt{r \cdot c \cdot s}\right) \tag{2.13}$$

This allows us to introduce a total capacity of the line C where $C = c \cdot d$ and a total resistance $R_l = r \cdot d$. The pulse impedance of transmission line can be rewritten as:

$$\bar{Z}_{imp}(s) = \frac{R_l}{\sqrt{R_l \cdot C \cdot s}} \cdot \coth\left(\sqrt{R_l \cdot C \cdot s}\right) \tag{2.14}$$

Using a Taylor series it is possible to approximate $\coth(x)$ through the following equation

[77]:

$$\coth(x) = \frac{\cosh(x)}{\sinh(x)} \cong \frac{1 + \frac{x^2}{2}}{x} \tag{2.15}$$

The expression in numerator $1 + \frac{x^2}{2}$ is the approximation of $\sqrt{1 + x^2}$. For low frequency equation (2.15) becomes:

$$\coth(x) \underset{x \to 0}{\cong} \frac{\sqrt{1 + x^2}}{x} \tag{2.16}$$

This development is also available for high frequencies as:

$$\coth(x) \underset{\infty}{\cong} \frac{e^{\frac{x}{2}}}{e^{\frac{x}{2}}} = 1 \underset{\infty}{\cong} \frac{\sqrt{1 + x^2}}{x} \tag{2.17}$$

Putting the above relation to equation (2.14) we achieved a simplified fractional model of ultracapacitor porous impedance:

$$Z_{imp}(s) = \frac{\sqrt{1 + R \cdot C \cdot s}}{Cs} = \frac{\sqrt{1 + Ts}}{Cs} \tag{2.18}$$

Model (2.18) was derived using the idealistic assumptions, however the real electrodes should be modelled using a more complicated method. The diffusion of liquids [7, 37], suspension in the fractional structures like granular substances or a transport of electrons, holes, ions, spine, etc., in disordered solids should be described by anomalous(fractional) diffusion equations [47].

In normal diffusion the particle average movement is proportional to $t^{\frac{1}{2}}$, however in the case of subdiffusion it is smaller, proportional to the $t^{\frac{\alpha}{2}}$, where $\alpha \in (0, 1)$. As a result, we can formulate the following Lemma:

Lemma 2.1. *New model of ultracapacitor impedance based on subdiffusion equation is:*

$$Z_{imp}(s) = \frac{\sqrt{1 + Ts^{\alpha}}}{C_{\alpha} s^{\alpha}} \tag{2.19}$$

where C_{α} is the ultracapacitor fractional capacity and T is the parameter responsible for the changes capacity with frequency.

Proof. The subdiffusion process can be modelled using the finite model of fractional transmission line presented in Fig: 2.3.

To derive ultracapacitor model based on the anomalous diffusion equation it is assumed that the distributions of resistance r_{α} and capacitance c_{α} are constant and the cylindrical pores are uniformly filled with electrolyte, and d is the length of transmission line.

In case of anomalous diffusion this model should be described by the following equation:

$$\begin{cases} \frac{\partial^2 u(x,t)}{\partial x^2} = r_{\alpha} c_{\alpha} \frac{\partial^{\alpha} u(x,t)}{\partial t^{\alpha}} \\ \frac{\partial^2 i(x,t)}{\partial x^2} = r_{\alpha} c_{\alpha} \frac{\partial^{\alpha} i(x,t)}{\partial t^{\alpha}}, \end{cases} \tag{2.20}$$

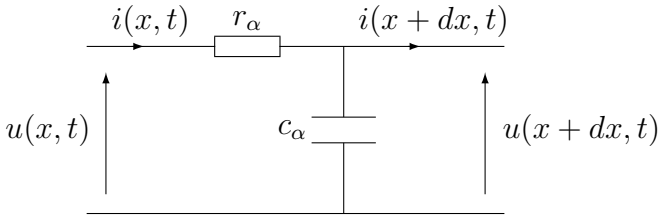

Fig. 2.3. Transmission line mathematical model

where for the subdiffusion $\alpha \in (0,1)$.

Then, based on the derivation presented for the impedance model (2.18) we can proof above Lemma.

The Laplace transform derivative with respect to time of the first equation from (2.20) for the zero initial condition is presented as follows:

$$\frac{\partial^2 U(x,s)}{\partial x^2} - r_\alpha c_\alpha s^\alpha U(x,s) = 0 \tag{2.21}$$

The roots of this equation are following:

$$\omega_{1,2} = \pm\sqrt{r_\alpha c_\alpha s^\alpha}$$

and the solution of the equation (2.21) is:

$$U(x,s) = C_1(s)\sinh\left(x\sqrt{r_\alpha c_\alpha s^\alpha}\right) + C_2(s)\cosh\left(x\sqrt{r_\alpha c_\alpha s^\alpha}\right) \tag{2.22}$$

where $C_1(s)$ and $C_2(s)$ are the constants of the equation.
To establish the constants of above equation it is necessary to use the boundary condition. For the $x = 0$ we have:

$$U(0,s) = C_1(s)\sinh(0) + C_2(s)\cosh(0) \tag{2.23}$$

which gave the relation for the second constant $C_2(s)$ presented as:

$$C_2(s) = U(0,s) \tag{2.24}$$

The constant $C_1(s)$ can be calculated from the first equation of the set of equations (2.21):

$$-r_\alpha i(x,t) = \frac{\partial u^\alpha(x,t)}{\partial x^\alpha}$$

Using the Laplace transform with respect to time and the equation (2.22) we obtained:

$$-r_\alpha I(x,s) = C_1(s)\sqrt{r_\alpha c_\alpha s^\alpha}\cosh\left(x\sqrt{r_\alpha c_\alpha s^\alpha}\right) + U(0,s)\sqrt{r_\alpha c_\alpha s^\alpha}\sinh\left(x\sqrt{r_\alpha c_\alpha s^\alpha}\right)$$

In the case of ultracapacitors, the limit condition in $x = d$ is $i(d,t) = 0$, which implies $I(d,s) = 0$, so the equation (2.25) becomes:

$$0 = C_1(s)\sqrt{r_\alpha c_\alpha s^\alpha}\cosh\left(d\sqrt{r_\alpha c_\alpha s^\alpha}\right) + U(0,s)\sqrt{r_\alpha c_\alpha s^\alpha}\sinh\left(d\sqrt{r_\alpha c_\alpha s^\alpha}\right) \tag{2.25}$$

what can be rewritten as:

$$C_1(s) = -\tanh\left(d\sqrt{r_\alpha c_\alpha s^\alpha}\right) U(0,s) \tag{2.26}$$

Let us get back to the equation (2.25). For $x = 0$ we obtained:

$$-r_\alpha I(0,s) = -\tanh\left(d\sqrt{r_\alpha c_\alpha s^\alpha}\right) U(0,s)\sqrt{r_\alpha c_\alpha s^\alpha} \tag{2.27}$$

what can be rewritten as:

$$I(0,s) = \frac{\sqrt{r_\alpha c_\alpha s^\alpha}}{r_\alpha}\tanh\left(d\sqrt{r_\alpha c_\alpha s^\alpha}\right) U(0,s) \tag{2.28}$$

Finally we obtained the transfer function of the transmission line:

$$Z_{imp}(s) = \frac{U(0,s)}{I(0,s)} = \frac{r_\alpha}{\sqrt{r_\alpha c_\alpha s^\alpha}}\coth\left(d\sqrt{r_\alpha c_\alpha s^\alpha}\right) \tag{2.29}$$

This allows us to introduce a total capacity of the line C_α where $C_\alpha = c_\alpha d$ and a total resistance $R_\alpha = r_\alpha d$. The pulse impedance of transmission line can be rewritten as:

$$\bar{Z}_{imp}(s) = \frac{R_\alpha}{\sqrt{R_\alpha C_\alpha s^\alpha}}\coth\left(\sqrt{R_\alpha C_\alpha s^\alpha}\right) \tag{2.30}$$

Finally, using the approximation of $\coth(x)$ presented in equation (2.15) and putting to the above relation we achieve a fractional model of ultracapacitor porous impedance presented in Lemma 2.19:

$$Z_c(s) = \frac{\sqrt{1 + R_\alpha C_\alpha s^\alpha}}{C_\alpha s^\alpha} = \frac{\sqrt{1 + T s^\alpha}}{C_\alpha s^\alpha} \tag{2.31}$$

■

The full model of supercapacitor including the resistance of the electrodes is presented in Fig. 2.4. The transfer function of the modelled system in Fig. 2.4 is defined as:

$$G_{uc}(s) = \frac{U_{uc}(s)}{I(s)}\ ,$$

where $U_{uc}(s)$ is a Laplace transform of the capacitor voltage and $I(s)$ is a Laplace transform of the capacitor current. The whole transfer function of an ultracapacitor is presented

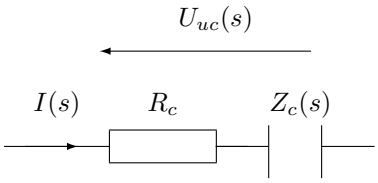

Fig. 2.4. Ultracapacitor equivalent model

in Fig. 2.4 is:

$$G_{uc}(s) = \frac{U_{uc}(s)}{I(s)} = R_c + Z_c(s), \tag{2.32}$$

where R_c is the resistance of the ultracapacitor and $Z_c(s)$ can be any of the ultracapacitor capacity model. Using the impedance model from (2.19) the whole double-layer capacitor model is presented as follows:

$$G_{uc}(s) = R_c + \frac{\sqrt{1+Ts^{\alpha}}}{Cs^{\alpha}}, \tag{2.33}$$

where $R_c \in \mathbb{R}_+$, $T \in \mathbb{R}_+$ and $\alpha \in (0,1)$.

In [76] J.J. Quintana presented one of the well-known fractional order capacity model presented below:

$$Z_{c_q}(s) = \frac{(1+Ts)^{\alpha}}{Cs^{\beta}}. \tag{2.34}$$

Actually the analytical derivation of this model has not been presented. It was developed from a realistic capacity model $Z_c = \frac{1}{Cs^{\alpha}}$ presented in [91]. The Quintana's model is the conclusion of results from impedance spectroscopy experiments on the ultracapacitor and can very precisely describe the dynamics of supercapacitor, hence it was meticulously examined and described in the following chapters. The whole Quintana's model of ultracapacitor is:

$$G_{uc_q}(s) = R_c + \frac{(1+Ts)^{\alpha}}{Cs^{\beta}}, \tag{2.35}$$

where $R_c \in \mathbb{R}_+$, $T \in \mathbb{R}_+$ and $\alpha \in (0,1)$.

Neither model (2.33) nor model (2.35) have capacity which can be compared with the capacity of traditional capacitor. In denominator is the Cs^v, where $v \in \mathbb{R}_+$, what can be called fractional capacity. To create more physically model capable of compeering with the traditional model of capacitor, the Quintana capacitance model with the $\beta = 1$ is used:

$$G_{DC}(s) = R_c + \frac{(1+Ts)^{\alpha}}{Cs}, \tag{2.36}$$

Historically this model was proposed by Davidson and Cole in 1951 like a dielectric model to fit the complex dielectric constant data observed for glycerine [16, 17].

In next chapters the properties of presented model are discussed. Also the experiments

of ultracapacitor identification and advisability of presented models are described.

2.3 Other Methods for Ultracapacitor Modelling

Before the invention of the fractional order model many authors tried to describe the behaviour of supercapacitors using the RC cascade. These models were based on the double layer equivalent model [48], that was constituted by a complicated net of RC branches with non-linear capacitors in parallel connected by resistances Fig. 2.5. The value of the resistances depend on the parameters, such as:

- resistance of the electrode materials,
- resistance of the electrolytic solvent,
- pores width,
- membrane porosity,
- quality of the connection electrode-collector.

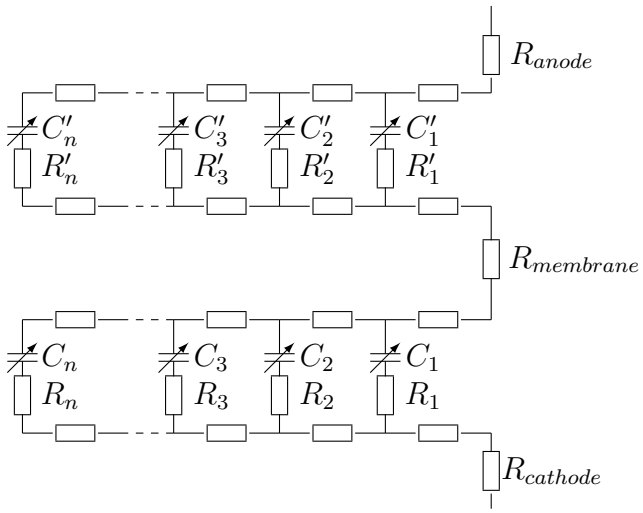

Fig. 2.5. Supercapacitors theoretical model

Since, the presented model is intractable to manage and practically useless, several simplified models have been invented [6, 9, 31, 34]. These models are simplified and easier to use. Some of them are presented in Fig. 2.6. Shortcuts ESR and EPR mean the equivalent series resistance and the equivalent parallel resistance respectively. The first (Fig. 2.6a) is the classical model of ultracapacitor without non-linear elements. The second (Fig. 2.6b)is the variable capacity model. Two next models (Fig. 2.6c, 2.6d) are the three, four branches models respectively. The last one (Fig. 2.6e) is the transmission

line model. Despite the simplifications in presented models they are very hard to fit to the physical devices. The parameter values of the equivalent circuits in Fig. 2.6a, 2.6b, 2.6c and 2.6d were tuned using the the current step response analysis of physical devices. The transmission line model 2.6e requires more sophisticated laboratory instruments and tests then others.

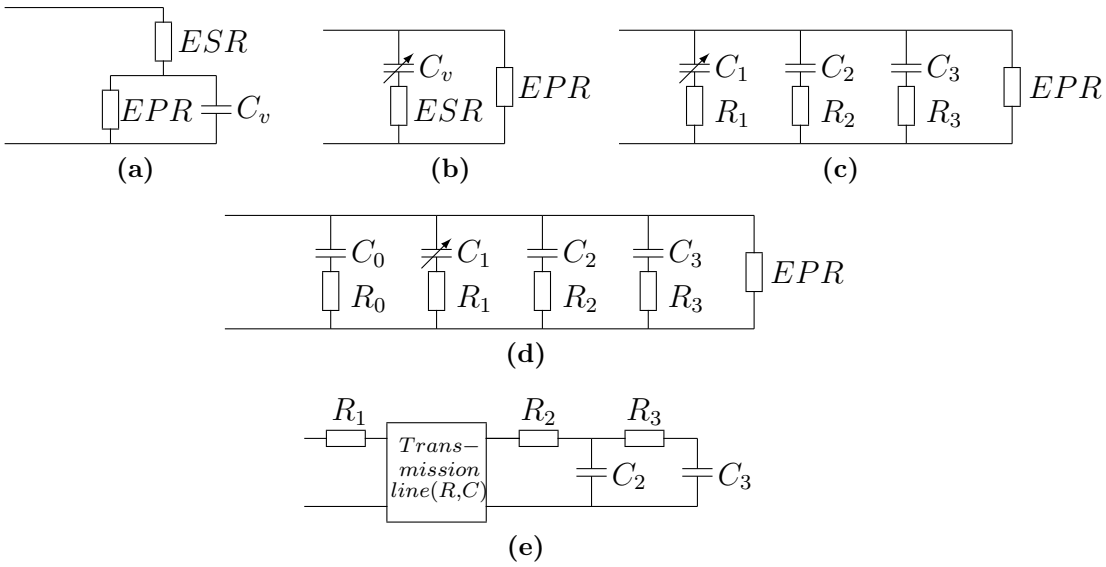

Fig. 2.6. Examples of supercapacitors RC models

The problem of model fitting can be seen clearly in the case of these systems dynamics. Presented models can describe it only in some range of frequency, what forced the use of non-linear elements for correction. More accurate dynamic can be also obtained using more branches in the model, but the infinite model cannot be implemented and a huge number of branches in a physical model are more prone to damages.

To solve a problem of using huge, non-linear models one started to adapt an artificial neural network (ANN) for ultracapacitor modelling. This solution can also omit using precise fractional model of ultracapacitor, which usually is very hard to use. ANN solution can correct errors arising while model approximation and also to solve a non-linearity problem occurring in the whole system with ultracapacitor. The ANN works like a black box which can cover a lot of problem in system designing, therefore neural network is often used in the engineering application of the system with ultracapacitor [14, 57]. The ANN ultracapacitor model uses a direct approach (Fig.2.7), where parameters can be calculated from measurements carried out on the process. The adaptive mechanism is made by the network training algorithm. This algorithm uses decreasing gradient and parameter update of the network is performed thanks to the Lavenberg-Marquardt method to minimise the error between the output of the system y_p and the predicted output y_m.

One of the simplest net structure was presented in the article written by J.N. Marie-Francoise, H. Gualous and A. Berthon [58]. For ultracapacitor modelling a neural network

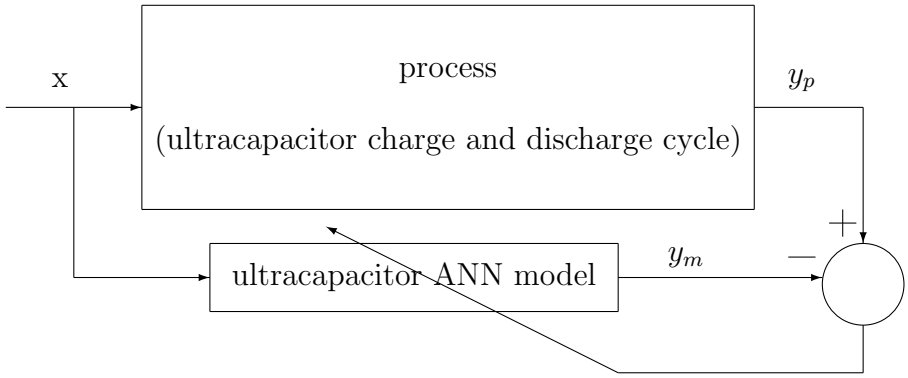

Fig. 2.7. Ultracapacitor-model direct approach

of multiple-input and single-output (MISO) was applied. The supercapacitor artificial neural network model was trained, tested and validated using diagram presented in Fig. 2.8. The neural network parameters were:

- Inputs: temperature T, current I_{uc}, value of capacity C;
- Output: ultracapacitor voltage U_{uc};
- 3 neurons in Hidden-layer;
- 1 neuron in Output-layer;
- Activation function: tanh function (hidden layer); linear function (output layer);
- Delays output number: $n_1 = 1$, $n_2 = 3$, $n_3 = 3$.

To update the parameters the Levenberg-Marquardt method was performed. This model accurately described the behaviour of ultracapacitor not only taking account of electrical but also thermal influences.

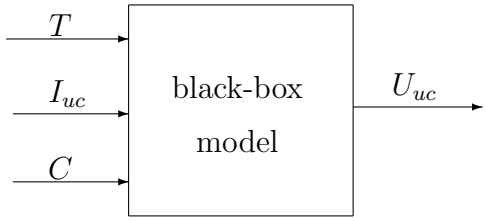

Fig. 2.8. Ultracapacitor ANN black-box model

2.4 Summary

In this chapter the different ultracapacitor models are presented. These models are the result of complicated system dynamics not able to modelling in classical simply way. The diffusion (subdiffusion) process, which for the ultracapacitors is the most important one, because of their internal structure, allowed to derive of a new ultracapacitor model and also to explain why the fractional calculus takes such important role in the ultracapacitor dynamics modelling. Hence, the main part of this work is focused on the fractional order model of ultracapacitor. In the next chapter the properties of presented models are discussed. In another chapters the experiments are presented. Achieved results confirmed usefulness of the fractional calculus in modelling dynamic system based on the diffusion. To control the ultracapacitor charging and discharging process a new type of model based on the fractional order neural network is proposed.

Chapter 3

Properties of Theoretical Models

In the prior chapter the fractional order models for modelling of ultracapacitors were presented. This chapter is devoted to the main properties of these models. In the Section 3.1 discussion about the new derived model is given. Section 3.2 presents most physical ultracapacitor model, which is the special case of the Quintana model for $\beta = 1$. For this model the derivation of ultracapacitor and quadripole with ultracapacitor step response in the time domain is shown.

3.1 Description of New Model

Let focus on the following fractional order capacitance model:

$$Z_c(s) = \frac{\sqrt{1 + Ts^\alpha}}{C_\alpha s^\alpha},$$

where $T \in \mathbb{R}_+$ and $\alpha \in (0, 1)$.

To underline that C_α in this model is not a capacity of capacitor in traditional way we use extra index C_α. The units of this parameter are the following units $\frac{Farads}{(sec)^{1-\alpha}}$. It is worth to notice that in fact C_α is not a value of ultracapacitor capacity but it is an ultracapacitor impedance dependent of frequency and α parameter.

Let us take this model into consideration. The behaviour at the ends of frequency ranges can be described using following relation:

$$G_c(s) = \begin{cases} \frac{\sqrt{T}}{C_\alpha s^{\alpha/2}} & \text{for } s \gg \frac{1}{T} \\ \frac{1}{C_\alpha s^\alpha} & \text{for } s \ll \frac{1}{T}. \end{cases}$$

For low frequency this model tends to the fractional integrator model presented by Westerlund [91]. This model can be rewritten in following form:

$$\frac{1}{C_\alpha s^\alpha} \underset{s=j\omega}{=} \frac{1}{C_\alpha \omega^\alpha \left(\sin \frac{\pi}{2}\alpha + j \cos \frac{\pi}{2}\alpha\right)} \tag{3.1}$$

what means that for the $\omega \to 0$ the ultracapacitor capacity is equal to the capacity of traditional capacitor. In Fig. 3.1 exemplary Bode diagrams of this model for $T = 1$, $C = 1$ and different $\alpha = 0.6,\ 0.8,\ 1$ are presented. It can be noticed that higher value of α (model order) implies faster system dynamics.

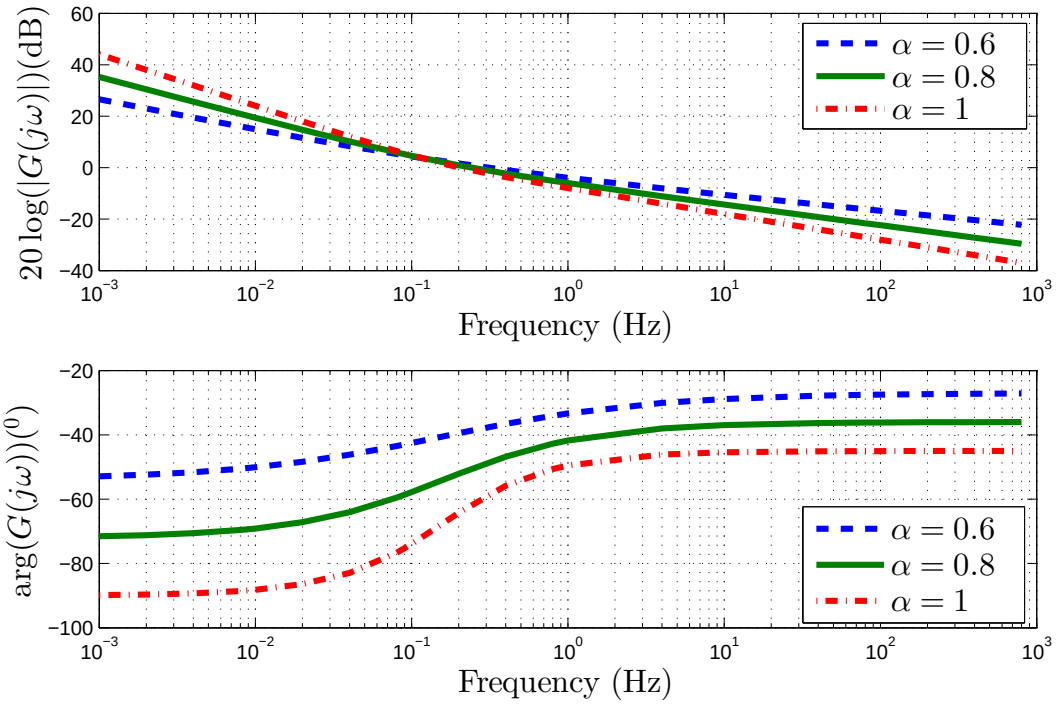

Fig. 3.1. Bode's diagrams of G_c capacitance model for $\alpha = 0.6,\ 0.8,\ 1$

Even though, this model is the most appropriate to describe the dynamics of ultracapacitor in the frequency domain, it is very hard to calculate the inverse Laplace transform to find the step response of this model in the time domain, therefore in this book, for ultracapacitor modelling, the Davidson-Cole model is used.

3.2 Davidson-Cole Model Properties

Let us take Davidson-Cole model (2.36), which can be also achieved from Quintana model for $\beta = 1$.

$$G_{DC} = \frac{(1+Ts)^{\alpha}}{Cs},$$

where C is a capacity of ultracapacitor, $\alpha \in (0, 1)$ is a model order and T is a parameter which meaning is presented in this subsection.

In this model parameter C is a traditional capacity with the unit $Farads$, therefore this model is more physically-oriented. The behaviour of this model on the ends of range

is following:

$$G_{DC}(s) = \begin{cases} \frac{T^{\alpha}}{Cs^{1-\alpha}} & \text{for } s \gg \frac{1}{T} \\ \frac{1}{Cs} & \text{for } s \ll \frac{1}{T}. \end{cases}$$

It can be noticed, that this model for low frequency ($\omega \to 0$) behaves like model of traditional capacitor with decrease of amplitude characteristic $20dB$ per decade. For high values of frequency this model reminds a fractional order integrator (1.28) with order equal to $1 - \alpha$. Figure 3.2 presents Bode diagrams of Davidson-Cole model for $T = 1$, $C = 1$ and three different values of α (0.4, 0.5, 0.6).

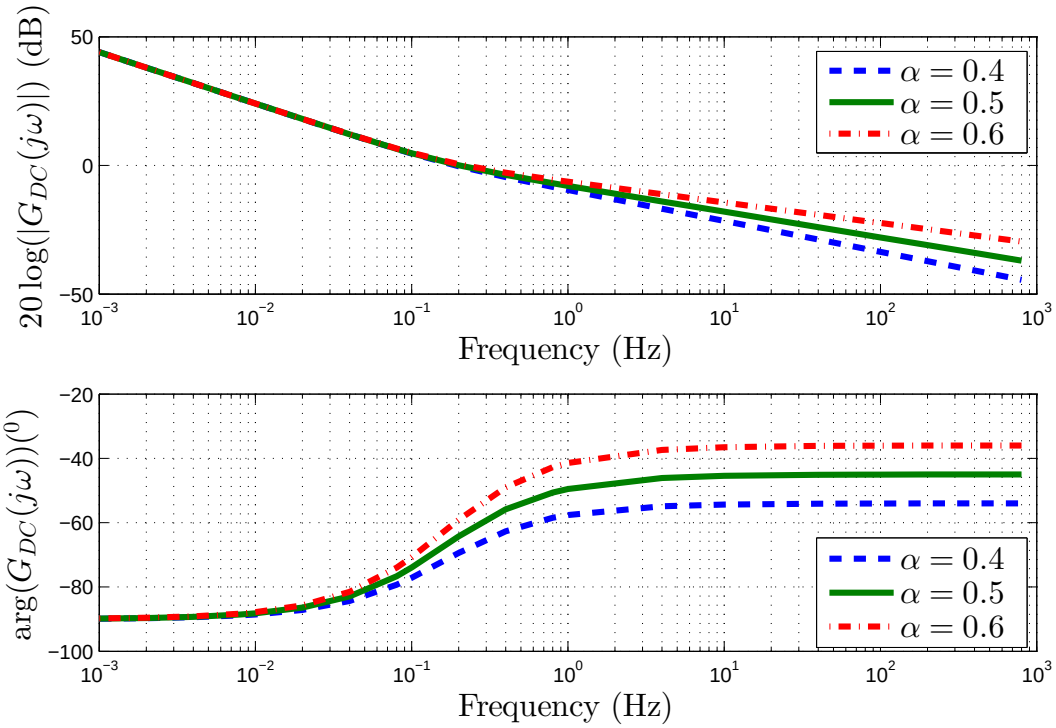

Fig. 3.2. Bode's diagrams of Davidson-Cole capacitance model for $\alpha = 0.4, 0.5, 0.6$

Now, let us try to describe the meaning of the T parameter. To explain its importance we have to consider the spectral transfer function of Davidson-Cole model given as follows:

$$G_{DC}(j\omega) = \frac{(Tj\omega + 1)^{\alpha}}{Cj\omega}. \tag{3.2}$$

The magnitude of this spectral transfer function is

$$A_{DC}(\omega) = \frac{((T\omega)^2 + 1)^{\frac{\alpha}{2}}}{C\omega}. \tag{3.3}$$

This magnitude is compared to the magnitude of a traditional capacitor of capacity C' is:

$$\frac{((T\omega)^2 + 1)^{\frac{\alpha}{2}}}{C\omega} = \frac{1}{C'\omega}, \tag{3.4}$$

which yields

$$C' = \frac{C}{((T\omega)^2 + 1)^{\frac{\alpha}{2}}}, \tag{3.5}$$

where C' is the capacity equivalent of the ultracapacitor for given frequency ω. This equivalent capacity illustrates what capacity the traditional capacitor should have in order to have the same magnitude for desired value of frequency. For $\alpha = 0.5$ we have:

$$C' = \begin{cases} C & \text{for } \omega \ll \frac{1}{T} \\ \frac{C}{\sqrt{T\omega}} & \text{for } \omega \gg \frac{1}{T} \end{cases} \tag{3.6}$$

The frequency f_c for which the capacity equivalent decreases 2 times is given as follows:

$$f_c = \frac{\sqrt{2^{\frac{2}{\alpha}} - 1}}{2\pi T}. \tag{3.7}$$

A fact of decrease of ultracapacitor capacity with frequency is known by the producers but only using of fractional order model of presented form for ultracapacitor modelling explains this behaviour.

Now let take a full ultracapacitor model based on the Davidson-Cole capacitance model:

$$G_c(s) = R_c + \frac{(1 + Ts)^\alpha}{Cs}.$$

The step response of this model in the time domain is discussed below:

Lemma 3.1. *The time domain step response of the ultracapacitor itself is as follows:*

$$u_c(t) = \mathcal{L}^{-1}\left[G_c(s)\frac{I}{s}\right] = \left(R_c + \frac{T^\alpha}{C}e^{-\frac{t}{T}}\frac{t^{1-\alpha}}{\Gamma(2-\alpha)}{}_1F_1\left(2; 2-\alpha; \frac{t}{T}\right)\right) I, \tag{3.8}$$

where the ${}_1F_1\left(2; 2-\alpha; \frac{t}{T}\right)$ *is a confluent hypergeometric function.*

Proof. [20, 21] To calculate the step response of $G_c(s)$ ultracapacitor capacity model form is necessary to find the inverse Laplace transformation presented below:

$$u_c(t) = \mathcal{L}^{-1}\left[\left(R_c + G_{DC}(s)\right)\frac{I}{s}\right]. \tag{3.9}$$

The hardest task in this calculus is finding the inverse Laplace transformation of unit step of the capacity part:

$$G_{DC}(s)\frac{1}{s} = \frac{(Ts+1)^\alpha}{Cs}\frac{1}{s}, \tag{3.10}$$

which can be rewritten as:

$$\mathcal{L}^{-1}\left[G_{DC}(s)\frac{1}{s}\right] = \mathcal{L}^{-1}\left[\frac{T^\alpha(s+\frac{1}{T})^\alpha}{Cs^2}\right]. \tag{3.11}$$

Using the theorem of the complex shift of the Laplace transformation, we obtain:

$$\mathcal{L}^{-1}\left[G_{DC}(s)\frac{1}{s}\right] = \frac{T^{\alpha}}{C}e^{-\frac{t}{T}}\mathcal{L}^{-1}\left[\frac{s^{\alpha}}{\left(s-\frac{1}{T}\right)^{2}}\right]. \tag{3.12}$$

To solve the inverse Laplace transformation from (3.12), the following formula is used:

$$\mathcal{L}^{-1}\left[\frac{s^{\gamma-\beta}}{(s-a)^{\gamma}}\right] = \frac{t^{\beta-1}}{\Gamma(\beta)}{}_1F_1(\gamma;\beta;at), \tag{3.13}$$

where $\gamma, \beta \in \mathcal{R}_+$, and the ${}_1F_1(\gamma;\beta;at)$ is a confluent hypergeometric function (1.4). Using (3.13) to (3.12) the step response of the ultracapacitor capacitance in time domain can be calculated:

$$\mathcal{L}^{-1}\left[G_{DC}(s)\frac{I}{s}\right] = \frac{T^{\alpha}}{C}e^{-\frac{t}{T}}\frac{t^{1-\alpha}}{\Gamma(2-\alpha)}{}_1F_1\left(2;2-\alpha;\frac{t}{T}\right)I. \tag{3.14}$$

Finally, adding the resistance part the Lemma thesis is achieved:

$$u_c(t) = \mathcal{L}^{-1}\left[G_c(s)\frac{I}{s}\right] = \left(R_c + \frac{T^{\alpha}}{C}e^{-\frac{t}{T}}\frac{t^{1-\alpha}}{\Gamma(2-\alpha)}{}_1F_1\left(2;2-\alpha;\frac{t}{T}\right)\right)I. \tag{3.15}$$

■

Analytically, the response of the ultracapacitor with the linear function of current ($i(t) = It$, where $I = \text{const}$) as an input signal can be also calculated:

$$\mathcal{L}^{-1}\left[\frac{G_c(s)I}{s^2}\right] = \left(R_cI + \frac{T^{\alpha}}{C}e^{-\frac{t}{T}}\frac{t^{2-\alpha}}{\Gamma(3-\alpha)}{}_1F_1\left(3;3-\alpha;\frac{t}{T}\right)\right)I. \tag{3.16}$$

Let us take it to consideration the RC quadripole presented in Fig. 3.3.

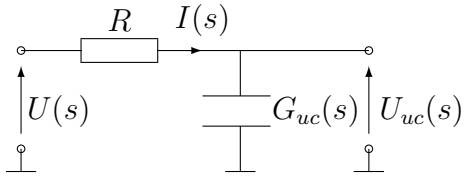

Fig. 3.3. RC quadripole model

The transfer function of this system is defined as follows:

$$G_{\mathrm{RC}}(s) = \frac{U_{uc}(s)}{U(s)} = \frac{G_{uc}(s)}{G_{uc}(s)+R}.$$

In our case using $G_c(s)$ like the ultracapacitor model $G_{uc}(s)$, this model has the following form:

$$G_{\mathrm{RC}}(s) = \frac{G_c(s)}{G_c(s)+R} = \frac{(Ts+1)^{\alpha}+R_cCs}{(Ts+1)^{\alpha}+(R+R_c)Cs},$$

where C, R_c is ultracapacitor capacity and resistance respectively, T is a parameter of capacity decreasing with frequency and R is a system resistance (matching resistance in experimental setup 4.1.1).

Examples of the frequency characteristics of this model for $C = 1$, $T = 1$, $R_c = 1$, $R = 100$ and three α orders equal 0.4, 0.5, 0.6 are presented in Fig. 3.4.

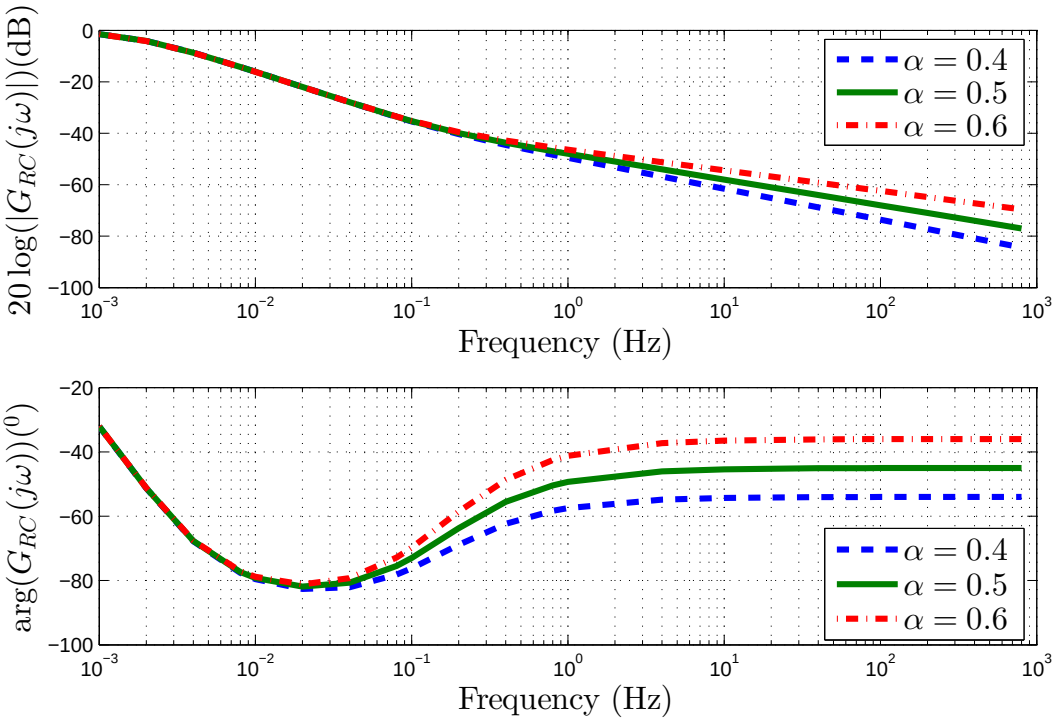

Fig. 3.4. Fractional order RC quadripole Bode diagrams for $\alpha = 0.4$, 0.5, 0.6

Calculation of the step response of RC quadripole with the ultracapacitor model $G_c(s)$ for arbitrary α is not easy. Therefore, the step response of this model for $\alpha = 0.5$ is presented. This order can describe the dynamics of low-capacity ultracapacitor what was confirmed in experiments and is presented in Section 4.2.

Lemma 3.2. *The unit step response of the system with the ultracapacitor for $\alpha = 0.5$ is given by the following equation:*

$$u_{uc}(t) = \mathcal{L}^{-1}\left[G_{RC}(s)\frac{1}{s}\right] = e^{-\frac{t}{T}}\sum_{i=1}^{4}\left(\frac{F_i}{t^{0.5}}\cdot E_{1,0.5}\left(H_i^2 t\right) + F_i H_i e^{H_i^2 t}\right), \tag{3.17}$$

where

$$\begin{aligned}
F_1 &= \frac{\sqrt{T}}{2}, \quad F_2 = -\frac{\sqrt{T}}{2}, \quad F_3 = \frac{(B-A)T}{\sqrt{T(T^2+4A^2)}}, \quad F_4 = \frac{(A-B)T}{\sqrt{T(T^2+4A^2)}},\\
H_1 &= \sqrt{\frac{1}{T}}, \quad H_2 = -\sqrt{\frac{1}{T}}, \quad H_3 = \frac{-T^{1.5}+\sqrt{T^3+4A^2T}}{2AT},\\
H_4 &= \frac{-T^{1.5}-\sqrt{T^3+4A^2T}}{2AT}, \quad A = (R+R_c)C, \quad B = R_cC
\end{aligned}$$

and $E_{1,0.5}\left(H_i^2 t\right)$ is a two-parameter Mittag-Leffler function. Parameters C, R_c, T are the parameters of the ultracapacitor $G_{uc}(s)$ model and R is the resistance of RC quadripole's resistor.

Proof. [20, 21] To calculate the step response of the system with the ultracapacitor in the time domain for $\alpha = 0.5$ it is necessary to find the inverse Laplace transformation of the following transfer function:

$$\mathcal{L}^{-1}\left[G_{RC}(s)\frac{1}{s}\right] = \mathcal{L}^{-1}\left[\frac{\sqrt{Ts+1}+R_cCs}{\sqrt{Ts+1}+(R+R_c)Cs}\frac{1}{s}\right]. \tag{3.18}$$

The above equation can be rewritten as:

$$\mathcal{L}^{-1}\left[G_{RC}(s)\frac{1}{s}\right] = \mathcal{L}^{-1}\left[\frac{\sqrt{Ts+1}+Bs}{\sqrt{Ts+1}+As}\frac{1}{s}\right], \tag{3.19}$$

where $B = R_cC$ and $A = (R+R_c)C$.

As a result of the applied theorem of the complex shift of the Laplace transformation, we obtain:

$$\mathcal{L}^{-1}\left[G_{RC}(s)\frac{1}{s}\right] = e^{-\frac{t}{T}}\mathcal{L}^{-1}\left[\frac{\sqrt{T}\sqrt{s}+B\left(s-\frac{1}{T}\right)}{\left(\sqrt{T}\sqrt{s}+A\left(s-\frac{1}{T}\right)\right)\left(s-\frac{1}{T}\right)}\right]. \tag{3.20}$$

Let us define the auxiliary variable:

$$G(s) = \frac{\sqrt{T}\sqrt{s}+B\left(s-\frac{1}{T}\right)}{\left(\sqrt{T}\sqrt{s}+A\left(s-\frac{1}{T}\right)\right)\left(s-\frac{1}{T}\right)}. \tag{3.21}$$

Using the auxiliary complex variable $w = s^{0.5}$ we have:

$$G(w) = \frac{(BTw^2 + T^{1.5}w - B)T}{(Tw^2 - 1)(ATw^2 + T^{1.5}w - A)}, \tag{3.22}$$

After decomposition of $G(w)$ into the partial fractions and inverse Laplace transform, back in the complex variable s we find:

$$\begin{aligned} G(s) \;=\; & \frac{1}{2\sqrt{\frac{1}{T}}\left(s^{0.5} - \sqrt{\frac{1}{T}}\right)} - \frac{1}{2\sqrt{\frac{1}{T}}\left(s^{0.5} + \sqrt{\frac{1}{T}}\right)} \\ & - \frac{(-B+A)\,T}{\sqrt{T\left(T^2+4A^2\right)}\left(s^{0.5} - \frac{-T^{1.5}+\sqrt{T^3+4A^2T}}{2AT}\right)} \\ & + \frac{(-B+A)\,T}{\sqrt{T\left(T^2+4A^2\right)}\left(s^{0.5} - \frac{-T^{1.5}-\sqrt{T^3+4A^2T}}{2AT}\right)}. \end{aligned}$$

By linearity of the Laplace transformation, the goal of finding the inverse Laplace transformation can be decomposed to four identical problems.

$$\mathcal{L}^{-1}\left[G_{\mathrm{RC}}(s)\frac{1}{s}\right] = e^{-\frac{t}{T}}\mathcal{L}^{-1}\left[G_1(s) + G_2(s) + G_3(s) + G_4(s)\right], \tag{3.23}$$

where $G_1(s), G_2(s), G_3(s),$ and $G_4(s)$ are the individual partial fraction. All of them can be transformed using new parameters to the presented form:

$$G_i(s) = \frac{F_i}{s^{0.5} - H_i}.$$

Using the following equation for decomposition of rational function to partial fraction:

$$\frac{1}{s^\nu - a} = \frac{1}{a}\sum_{k=1}^{n} \frac{a^k}{s^{(\nu k-1)}\left(s - a^{\frac{1}{\nu}}\right)}, \tag{3.24}$$

where $\nu = \frac{1}{n} \in \mathbb{R}_+$, we obtain:

$$G_i(s) = \frac{F_i}{s^{0.5} - H_i} = F_i \cdot \left(\frac{s^{0.5}}{s - H_i^2} + \frac{H_i}{s - H_i^2}\right).$$

The inverse Laplace transformation can be calculated using the following relation:

$$\mathcal{L}^{-1}\left[\frac{1}{s^\kappa\left(s \pm a^2\right)}\right] = t^\kappa E_{1,\kappa+1}\left(\mp at\right), \tag{3.25}$$

where function $E_{1,\kappa+1}\left(\mp at\right)$ is a two-parameter Mittag-Leffler function, defined in Section 1.3.

Finally, from (3.23), (3.24), and (3.25) we obtain the unit step response of the system with a ultracapacitor:

$$u_{uc}(t) = \mathcal{L}^{-1}\left[G_{RC}(s)\frac{1}{s}\right] = e^{-\frac{t}{T}}\sum_{i=1}^{4}\left(\frac{F_i}{t^{0.5}}\cdot E_{1,0.5}\left(H_i^2 t\right) + F_i H_i e^{H_i^2 t}\right), \tag{3.26}$$

where

$$\begin{aligned} F_1 &= \frac{\sqrt{T}}{2}, \quad F_2 = -\frac{\sqrt{T}}{2}, \quad F_3 = \frac{(B-A)T}{\sqrt{T(T^2+4A^2)}}, \quad F_4 = \frac{(A-B)T}{\sqrt{T(T^2+4A^2)}}, \\ H_1 &= \sqrt{\frac{1}{T}}, \quad H_2 = -\sqrt{\frac{1}{T}}, \quad H_3 = \frac{-T^{1.5}+\sqrt{T^3+4A^2T}}{2AT}, \\ H_4 &= \frac{-T^{1.5}-\sqrt{T^3+4A^2T}}{2AT}, \quad A = (R+R_c)C, \quad B = R_cC. \end{aligned}$$

■

3.3 Summary

In this chapter the properties of the different fractional order model are discussed. Additionally, the exemplars bode diagram are presented. The most important results presented in this chapter is explanation of the ultracapacitor capacity decreasing with frequency. This fact has been known by the producers and engineers but this phenomenon can be only explain using fractional calculus for the ultracapacitor dynamic description, what confirm that fractional calculus is the proper tool for modelling and control ultracapacitor and all electrical devices with the similar internal construction.

In the next chapter the results of ultracapacitors modelling are presented. This chapter shows fractional calculus like a proper tool for ultracapacitor modelling.

Chapter 4

Experiments of Ultracapacitor Modelling and Identification

In this chapter results of the experiments are shown. In Section 4.1 description of measurement setups are presented. In the Section 4.2 the experiments are described and their results are shown. In the research two types of ultracapacitor were used. First three ultracapacitors of nominal capacity $0.047F$, $0.1F$, $0.33F$ (Fig. 4.1), produced by Panasonic® [15], are called in this paper low capacity ultracapacitors. Their maximum operation voltage, provided by the manufacturer, is 5.5V. Another type of ultracapacitors contained two devices produced by Maxwell® of the nominal capacity 1500F/2.7V (BCAP1500) and 3000F/2.7V (BCAP3000) (Fig. 4.2). These ultracapacitors are named high capacity ultracapacitors.

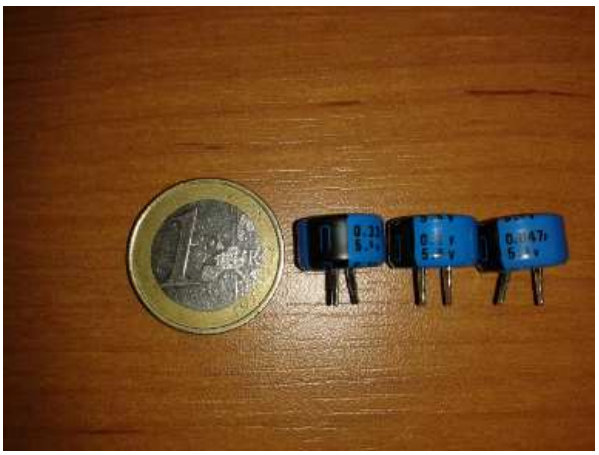

Fig. 4.1. Ultracapcitor: $0.33F$, $0.1F$, $0.047F$

Fig. 4.2. Ultracapcitor: $3000F$, $1500F$

Examination of such different capacity ultracapacitors required to build two systems for performing the experiments. At the end of this chapter the whole results of described experiments are concluded.

4.1 Measurement Setups

Using two types of ultracapacitors with so huge differences of capacity required to build two systems for their charging and discharging. System for examining low capacity ultracapacitor is simpler because of using only the relatively small value of current. For them the most important goal was to create a setup which can measure a current flowing through capacitor and a voltage on it with as smallest possible noise to signal ratio. Second system had to be able to provide the high value of current for fast charging and discharging high capacity ultracapacitors. This system is much more complicated and it is definitely bigger then the first one. Now let us focus on the system for examining low capacity ultracapacitor.

4.1.1 Setup for Low Capacity Ultracapacitor Measurement

The experimental setup for low capacity ultracapacitor measurements contains two main parts. First it is the system built in accordance with the scheme presented in Fig. 4.3. This circuit has the high-voltage/high-current operational amplifier OPA544 and the matching resistor $R_m = 180\Omega$. The amplifier works in the voltage follower configuration. This system is connected with the symmetrical power supply PowerLab 305D–II and the DS1102 Control Card in PC. The most useful advantage of DSpace Cards is the ability to cooperate with the Matlab and Simulink programs. The entire test stand is presented in Fig. 4.4. Presented structure of circuit allowed for examining the frequency response of ultracapacitor and also the step response but only for the voltage forcing. The methods and results of experiments are described in the next section.

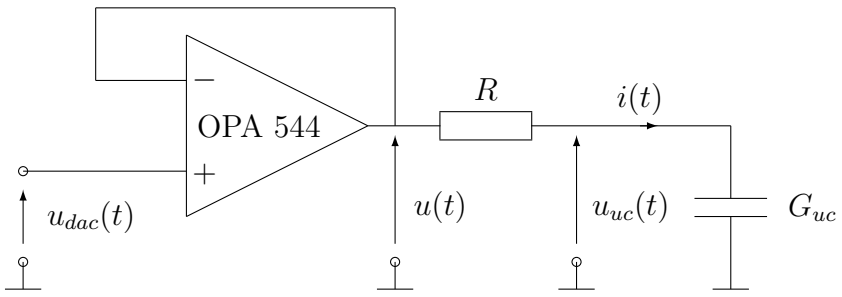

Fig. 4.3. Electronic circuit

4.1.2 Setup for High Capacity Ultracapacitor Measurement

The electronic circuit for high capacity ultracapacitor measurements is more complicated than the one used for low capacity ultracapacitors. To generate the high level of current

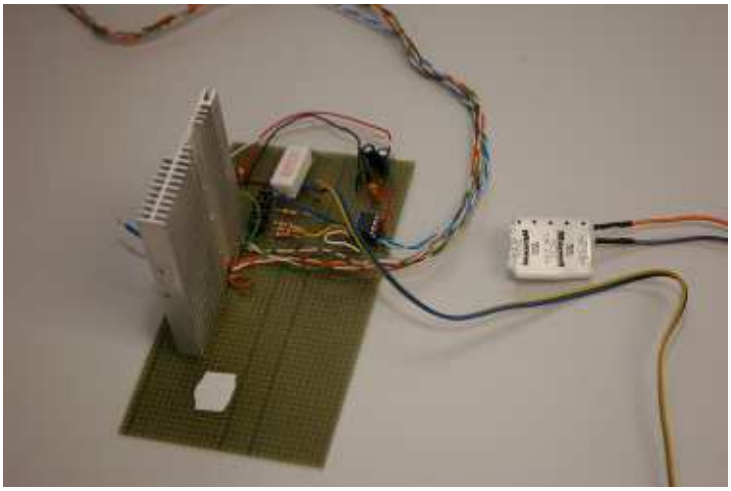

Fig. 4.4. Low Capacity Measurement System

the MOSFET power converter based on an H-Bridge was built. Four MOSFETs are grouped in two sets where each of them are connected to the Semikron Medium Power Double IGBT Drivers SKHI 23/12 (R). These controllers are connected to the DSpace DS1104 Control Card. The H-Bridge required the use of low pass filter in the form of a parallel electrolytic capacitor. A converter power supply applied the Instek PSH-10100A 1000 Watt Programmable Switching DC Power Supply and the energy storage, which contains four Maxwell ultracapacitors 3000F/2.7V (BCAP3000) connected in series. DC power supply protected by high current diode to prevent it in the ultracapacitor discharging process. Energy storage holds their own voltage meter and the group of resistors for after work setup discharging . Described configuration allows to generate even more than 100A on charging or discharging process. Figure 4.5 presents scheme of this circuit.

The measured system is also expanded. Charging and discharging current is measured by Hall effect current sensor. This sensor like the voltage measured ultracapacitor is connected to the built active filter and than to DSpace card. In addition to electronic safeguards system setup has a safety button for switching the MOSFET off. Another additional device which works in this system is UPS allowing the maintain stability of the network power. This type of circuit configuration allows the study of ultracapacitor step response for input current and for ultracapacitors measurement in frequency domain. Whole research position is presented in Fig. 4.6

4.2 Results of Experiments

First experiments were focused on the ultracapacitors modelling using the fractional order model. Values of the parameters were obtained as a result of Bode diagram matching. The model parameters were adjusted using the Matlab function *fmincon* by minimizing

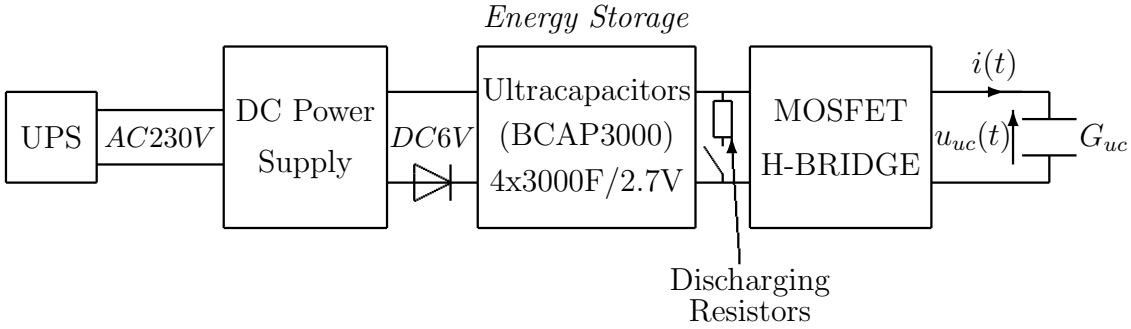

Fig. 4.5. Scheme of High Capacity Measurement System

Fig. 4.6. High Capacity Measurement System

a sum of Root Mean Square Error (RMSE) from amplitude and phase identification. It is very important to remember that ultracapacitors are electrolytic capacitors and they can accept only positive voltages, consequently in case of measuring low capacity ultracapacitor, using the voltage follower, the input signal with a constant component was:

$$u(t) = 2V + \sin(\omega t).$$

Capacitor voltage (in steady state) in this case was equal to

$$u_{uc}(t) = A_c(\omega)\sin(\omega t + \varphi_u)$$

and the capacitor current was:

$$i(t) = A_i(\omega)\sin(\omega t + \varphi_i).$$

In case of using the type of setup with a current converter, to model high capacity ultracapacitor, input signal was a current sine wave:

$$i(t) = A_i(\omega)\sin(\omega t + \varphi_i).$$

Capacitor voltage in this case contained initial value of voltage (u_0) depending on signal frequency, thus the output voltage signal was equal to:

$$u_{uc}(t) = u_0 + A_c(\omega)\sin(\omega t + \varphi_u).$$

The Bode diagram was obtained from the following relations:

$$M(\omega) = 20\log\left(\frac{A_c(\omega)}{A_i(\omega)}\right), \varphi(\omega) = \varphi_i(\omega) - \varphi_u(\omega).$$

In effect of measurements two diagrams were obtained. First one represents the magnitude of the system examined and the second one expresses the phase shift frequency response.

4.2.1 Ultracapacitor Modelling Using Davidson-Cole Model

Let us recall the Davidson-Cole model:

$$G_c = R_c + \frac{(1+Ts)^\alpha}{Cs},$$

where R_c is the ultracapacitor resistance, C is the ultracapacitor capacity in the traditional definition and T is a parameter of capacity decrease with frequency, which is explained in the Section 3.2.

Model parameters achieved as a result of identification by diagrams matching are presented in the Table 4.1.

Table 4.1. Identified Ultracapacitors Parameters

Capacitor	T	C(F)	$R_c(\Omega)$	α
0.047F	5.2261	0.06	32	0.6
0.1F	14.7979	0.094	52	0.6
0.33F	56.9669	0.27	29	0.57
1500F	1.006	1348	$0.25m$	0.62
3000F	0.6369	2410	$0.13m$	0.7

Table 4.2. RMSE of Davidson-Cole Model Identification

Capacitor	RMSE Magnitude	RMSE Phase
0.047F	0.0985	0.6152
0.1F	0.1521	0.6366
0.33F	1.3146	0.7857
1500F	0.9932	1.6518
3000F	0.8154	1.5344

RMSE of identification for this model is shown in the Table 4.2. Values presented in this table highlighted good matching of identified model. Mean error for magnitude and phase digram is lower than 1.5dB and 1.66^0 respectively. The examples of ultracapacitor identification in frequency domain in Fig.: 4.7, 4.9 are presented. Figures: 4.8, 4.10 present the absolute error between theoretical model and measured samples. These diagrams confirm that Davidson-Cole model can describ ultracapacitor dynamics in the fairly wide range of frequencies. For high capacity ultracapacitors the identification absolute error of magnitude is lower than $1,5dB$ for all samples and phase absolute error is lower than 4 degrees almost for all samples. The last sample has probably some measured error what can be noticed in the phase diagram. In case of identification Low capacity ultracapacitor diagrams matching has great accuracy in whole range of measured frequencies. Also, it is worth to notice that the $\alpha = 0.6$ is constant for all identified ultracapacitors, what means that its value is close to the model derived from normal diffusion equation, therefore acceptable results of modelling (especially for low capacity ultracapacitor) can be achieved using $\alpha = 0.5$. Results of ultracapacitors modelling using half-order ultracapacitor model are also presented in this section.

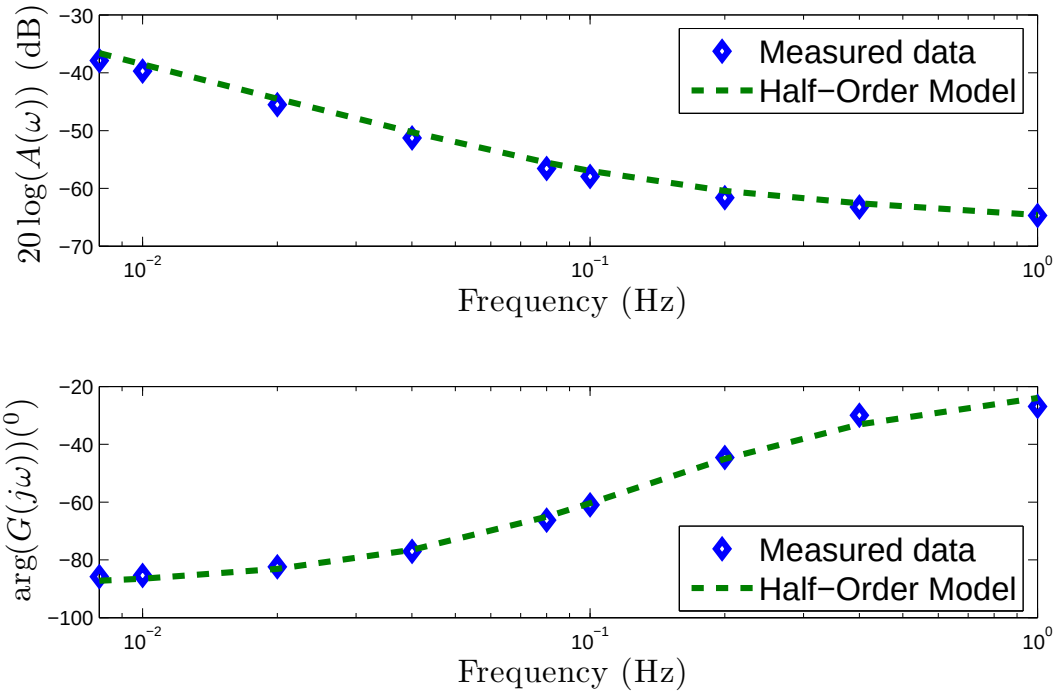

Fig. 4.7. Measured and D-C Model theoretical Bode diagrams of ultracapacitor 1500F

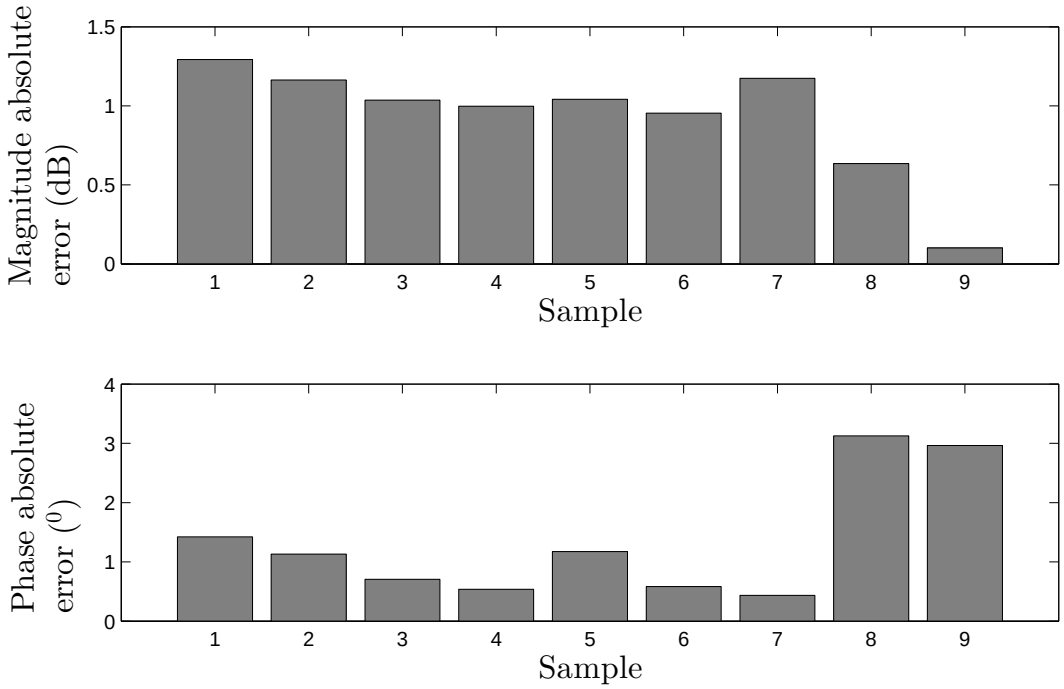

Fig. 4.8. D-C Model absolute identification error of ultracapacitor 1500F

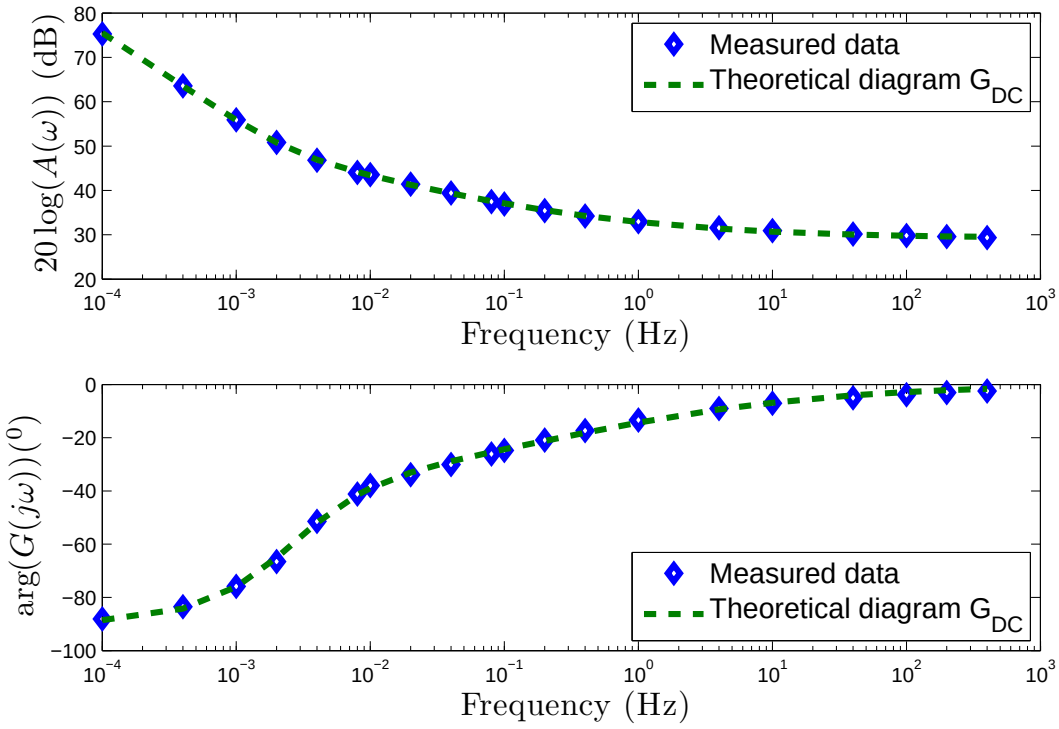

Fig. 4.9. Measured and D-C Model theoretical Bode diagrams of ultracapacitor 0.33F

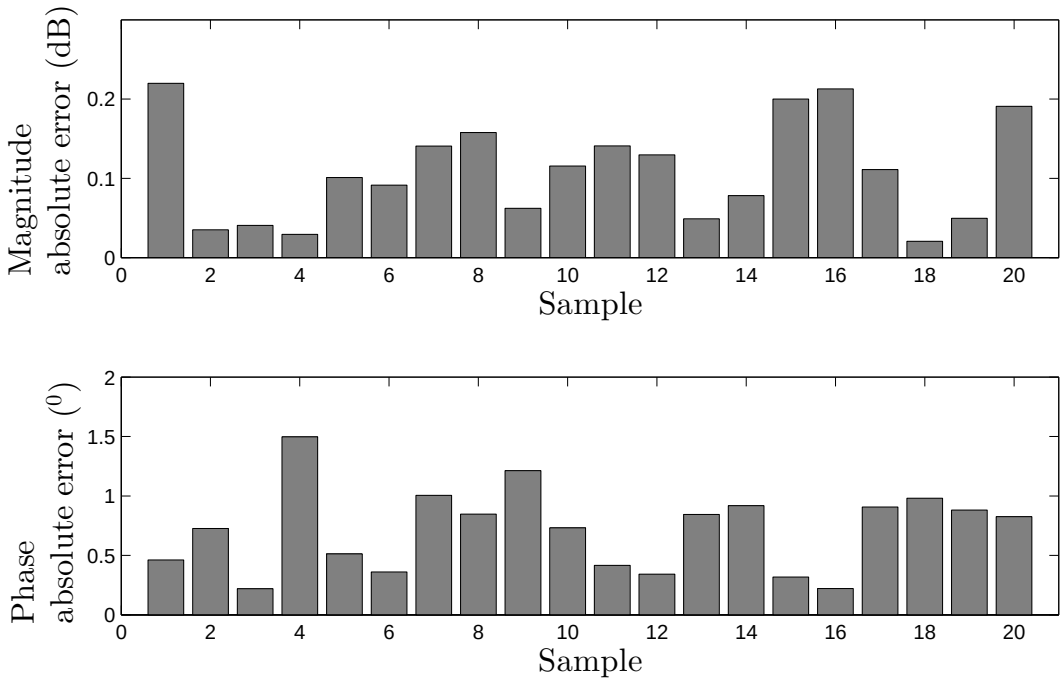

Fig. 4.10. D-C Model absolute identification error of ultracapacitor 0.33F

Now, let us focus on the T parameter. This parameter is responsible for ultracapacitor capacity decreasing with the frequency. The f_c, for which the equivalent capacity decreases two times is given as follows (3.5):

$$f_c = \frac{\sqrt{2^{\frac{2}{\alpha}} - 1}}{2\pi T}$$

and this values for tested ultracapacitors are summarized in Table 4.3:

Table 4.3. Values of frequency for which equivalent decreases capacity two times

capacitor	T	α	$f_c(mHz)$
0.047F	5.2261	0.6	91.8
0.1F	14.7979	0.6	32.4
0.33F	56.9669	0.57	9
1500F	1.006	0.62	457
3000F	0.6369	0.7	625

Following the Table 4.3 same dependencies can be noted. For high capacity ultracapacitors produced by Maxwell the value of f_c frequency increases with capacity, what means that bigger ultracapacitor have more stable capacity as a function of frequency. In the case of low capacity ultracapacitor higher capacity causes less stationarity of the capacitance parameter.

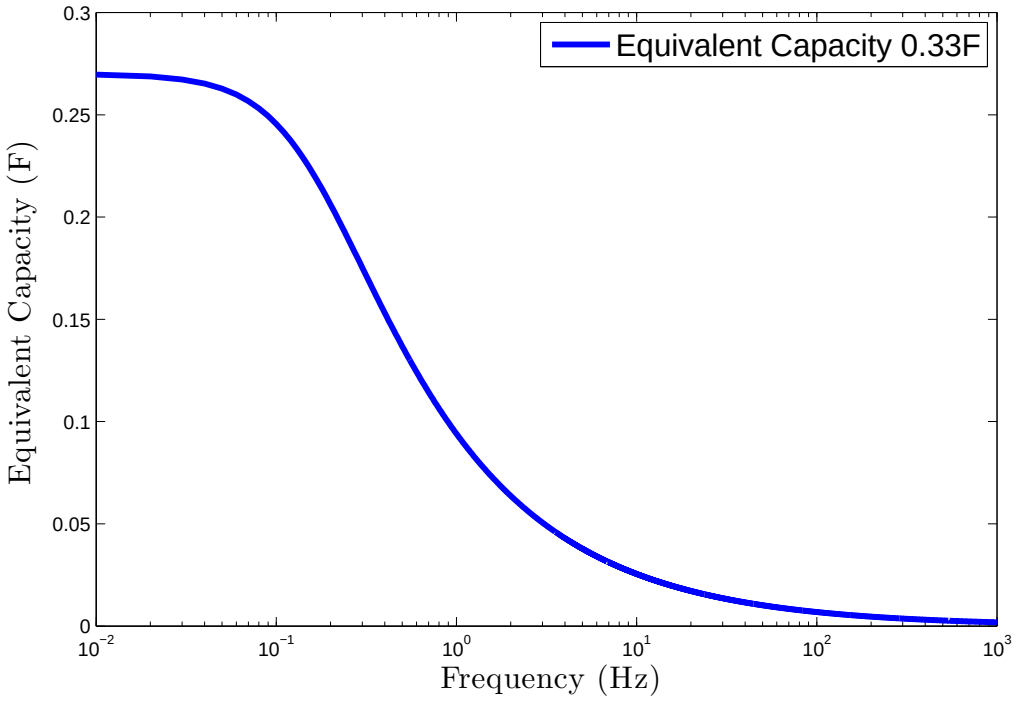

Fig. 4.11. Equivalent capacity C' of ultracapacitor 0.33F

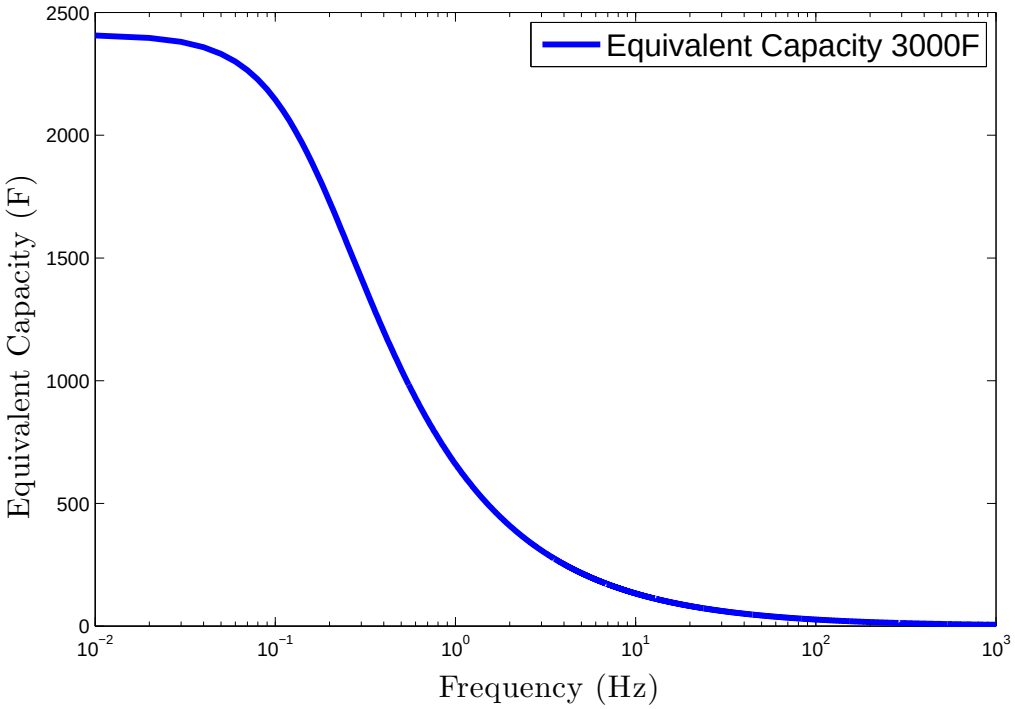

Fig. 4.12. Equivalent capacity C' of ultracapacitor 3000F

Figures 4.11, 4.12 present examples of the equivalent value capacity as a function of frequency for ultracapacitors of a nominal capacity $0.33F$, $3000F$.

Subsequently identified parameters with parameters measured directly from ultracapacitors were compared. Use of Davidson–Cole model allows for this validation, because, unlike other fractional order models presented in the Section 2.2, this model contains resistance $R_c(\Omega)$ and capacity $C(\mathrm{F})$ in traditional form. To measure real values of ultracapacitors resistance and capacity, the step response of the circuit was examined. The value of real resistance $R_{real}(\Omega)$ was measured like an ultracapacitor voltage step for state current immediately after starting charging process and the value of real capacity $C_{real}(\mathrm{F})$ was measured like charge stored on a ultracapacitor divided by its voltage. Parameters comparison is presented in the Table 4.4.

Table 4.4. Parameters comparison

capacitor	$C(\mathrm{F})$	$R_c(\Omega)$	$C_{real}(\mathrm{F})$	$R_{real}(\Omega)$
0.047F	0.06	32	0.06	32
0.1F	0.094	52	0.1	42
0.33F	0.27	29	0.27	28
1500F	1348	$0.25m$	1189	$0.26m$
3000F	2446	$0.13m$	2435.4	$0.15m$

Table 4.4 confirms that using fractional order model G_c one can very precisely identify real parameters of ultracapacitors. Identification results are equivalent to these obtained from real ultracapacitor by different methods e.g. step response. Differences between C parameter achieved in identification process and the real values in case of modelling of high capacity ultracapacitors are the effect of not precise enough measurements of fast changing signals. Lack of high frequency samples alaso had some influence on the identification process.

Having identified models for each measured ultracapacitors we can validate them in the time domain through the comparison of theoretical step responses of achieved models (3.8) with step responses of circuit. The result of this validation is presented in Fig.: 4.13 and 4.14. First of these figures show the step response of ultracapacitor with nominal capacity 1500F for current input signal equal to 100A and second presents the step response of ultracapacitor with nominal capacity 3000F for current equal to 50A.

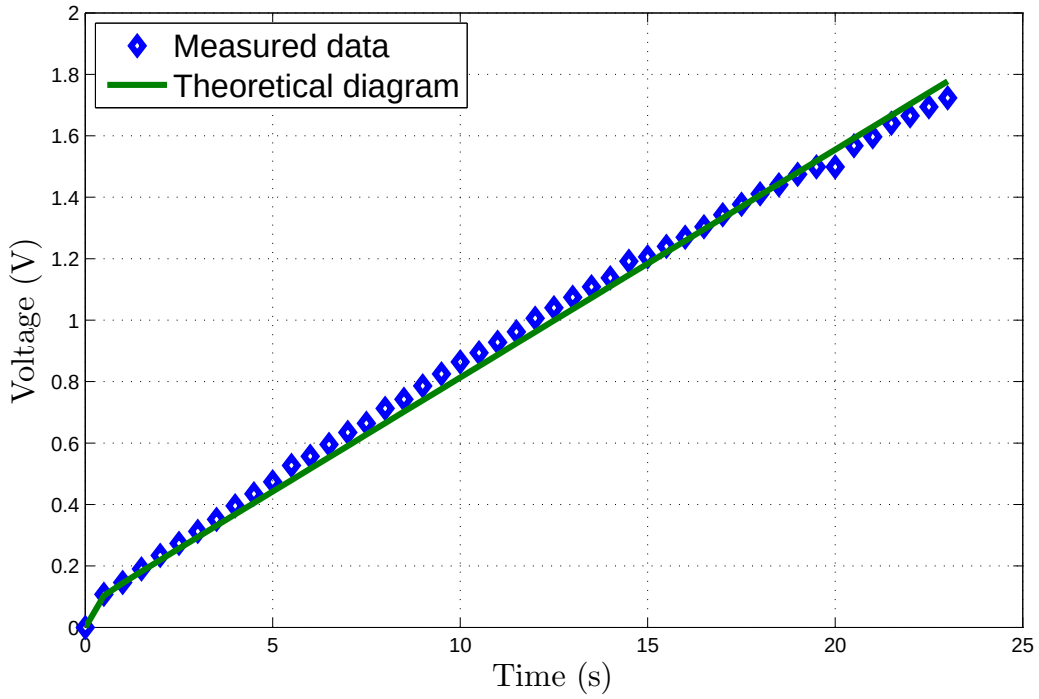

Fig. 4.13. Step response of model $G_c(s)$ for 1500F and current I(t)=100A

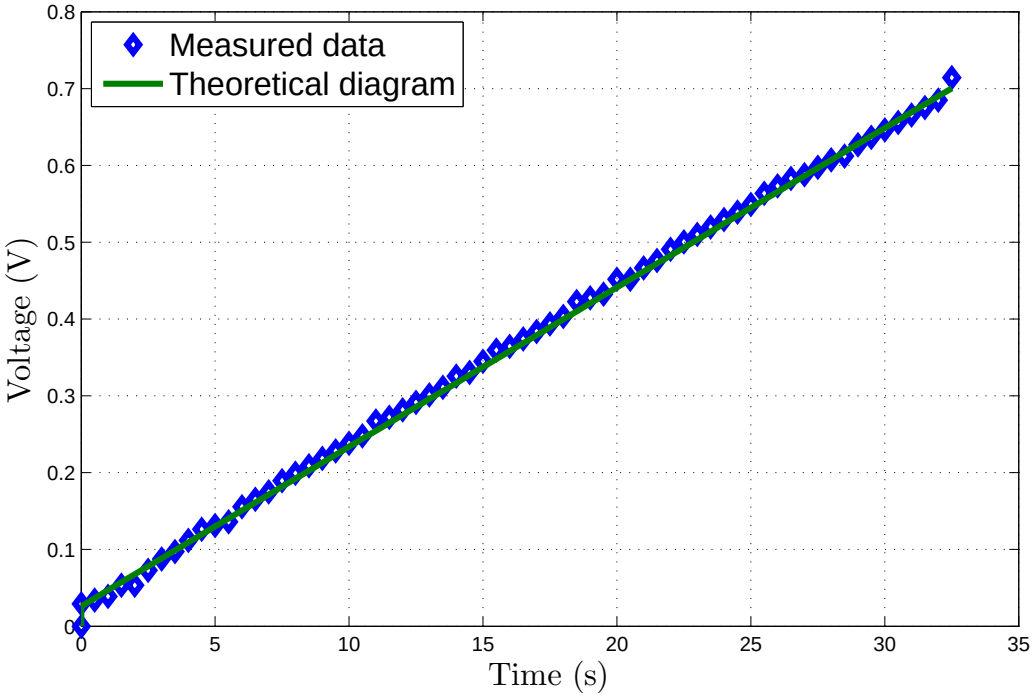

Fig. 4.14. Step response of model $G_c(s)$ for 3000F and current I(t)=50A

4.2.2 Ultracapacitor Modelling Using New Model

New Model is an ultracapacitor model derived using the anomalous diffusion partial differential equation:

$$G_{c_\alpha} = R_c + \frac{\sqrt{1 + T_\alpha s^\alpha}}{C_\alpha s^\alpha},$$

where R_c is the ultracapacitor resistance, C_α is the ultracapacitor fractional capacity with units $\frac{farads}{(sec)^{1-\alpha}}$ and T_α is the parameter of capacity decrease with frequency.

Comparison of the model parameters achieved as a result of identification by diagrams matching with real ultracapacitors parameters are presented in Table 4.5.

Table 4.5. Identified Ultracapacitors Parameters for New Model

capacitor	T	$C_\alpha(\frac{F}{s^{1-\alpha}})$	$R_c(\Omega)$	α	C_{real}(F)	$R_{real}(\Omega)$
0.047F	5.9257	0.0533	35	0.9887	0.06	32
0.1F	18.0459	0.0941	58	0.9969	0.1	42
0.33F	64.4422	0.2512	32	0.9870	0.27	28
1500F	1.0132	1490	$0.3m$	0.9945	1189	$0.26m$
3000F	0.5	2497	$0.18m$	0.9810	2435	$0.15m$

In fact we cannot compare the decrease of ultracapacitor capacity with frequency, because parameter C_α should be interpreted rather as ultracapacitor impedance than capacity like in the case of parameter C for traditional capacitor (see Section 3.1), but

we have to notice that the values of the α parameters in Table 4.5 demonstrate that for this model the best results of ultracapacitor modelling can be achieved for α slightly less than 1, what means that also for $\alpha = 1$ we should achieve similar results. Although the parameters C and C_α have different units, for α approximately equal 1 we can try to put this parameters together to see if their values are identified correctly. Presented table confirms that achieved results are proper, because their values are quite close to the real values of ultracapacitor parameters.

The RMSE of identification is presented in the Table 4.6.

Table 4.6. Error of New Model Identification

Capacitor	Magnitude RMSE	Phase RMSE
0.047F	0.3121	1.4608
0.1F	0.3513	1.4979
0.33F	0.4190	1.7736
1500F	0.3555	1.8486
3000F	0.3729	0.7570

Achieved values confirm good results of the model identification. In the case of using new model, we can see that Magnitude diagram has better accuracy than the Phase one. Examples of the results of ultracapacitor modelling for the new model are presented in the Fig.: 4.15 and 4.17. Figures 4.16, 4.18 present the absolute identification error of ultracapacitors 3000F and 0.047F. It can be noticed that maximum identification error of magnitude and phase is less than 0.8db and 3^o respectively. One of the identification confirmation we can see in the Fig.: 4.19. These plots present the measured and theoretical diagram for the quadripole system with ultracapacitor of an approximately capacity equal to 0.047F.

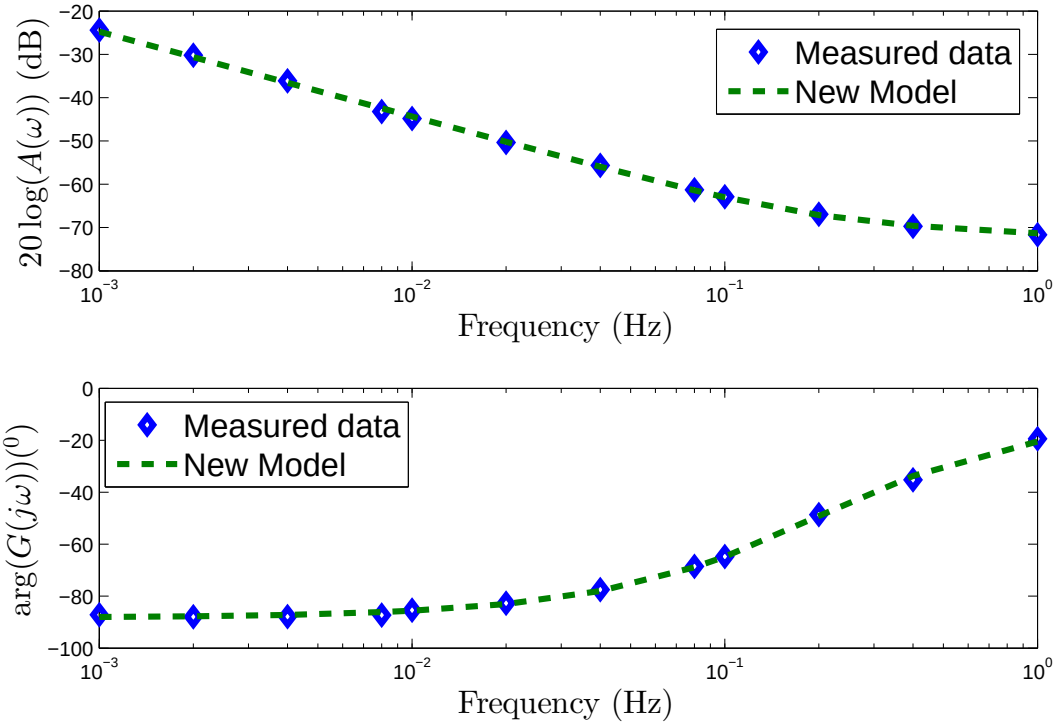

Fig. 4.15. Measured and New Model theoretical Bode's diagrams of ultracapacitor $3000F$

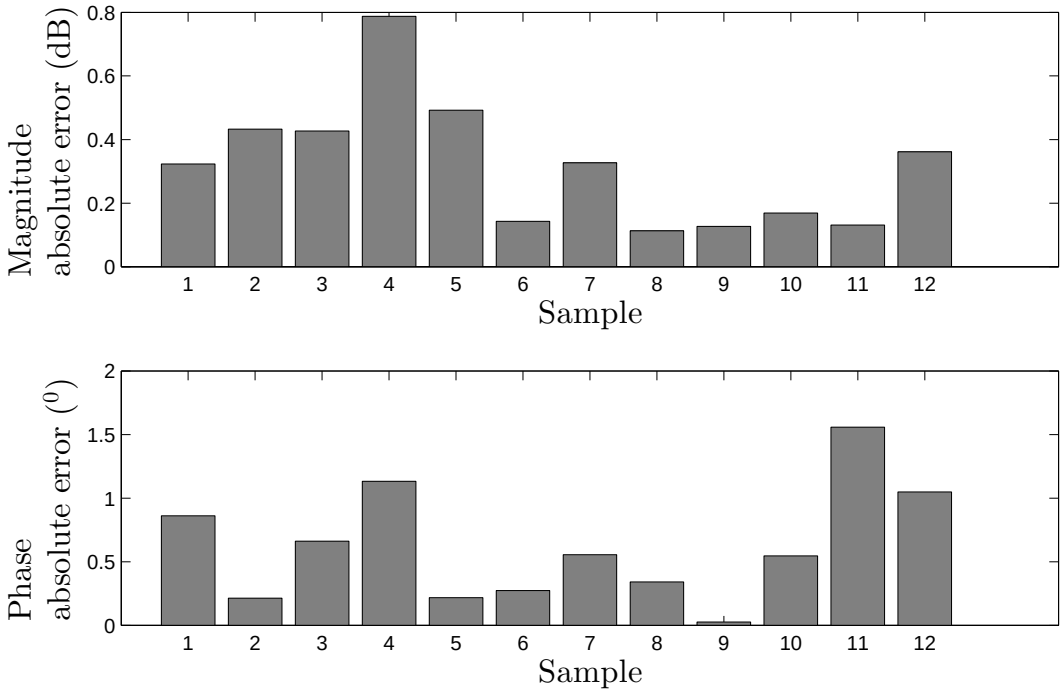

Fig. 4.16. New Model absolute identification error of ultracapacitor $3000F$

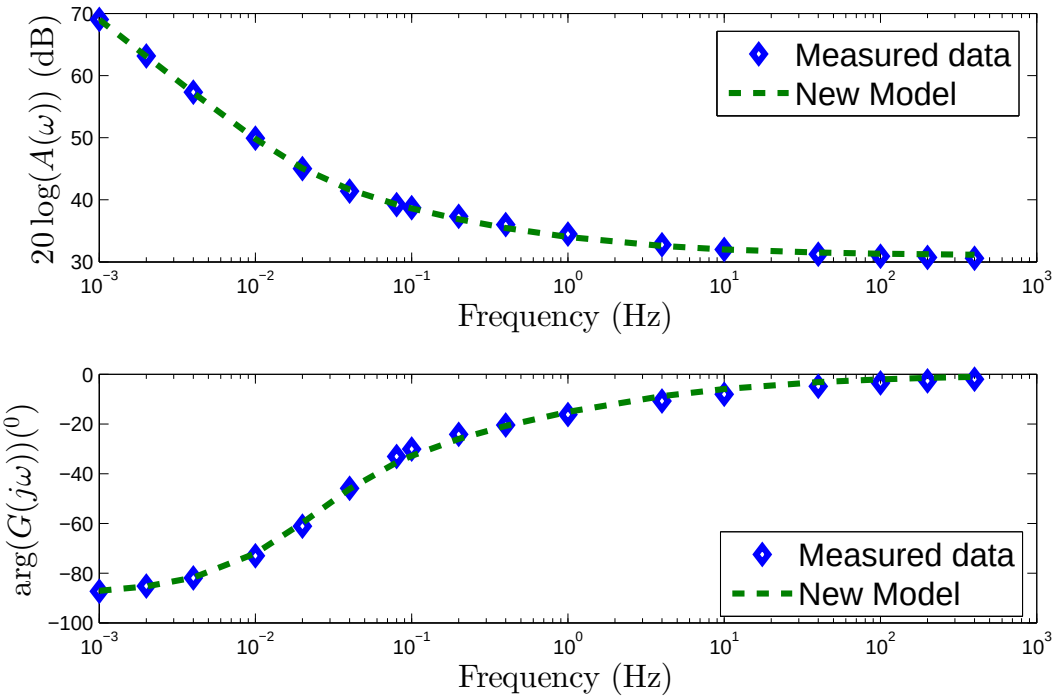

Fig. 4.17. Measured and New Model theoretical Bode's diagrams of ultracapacitor $0.047F$

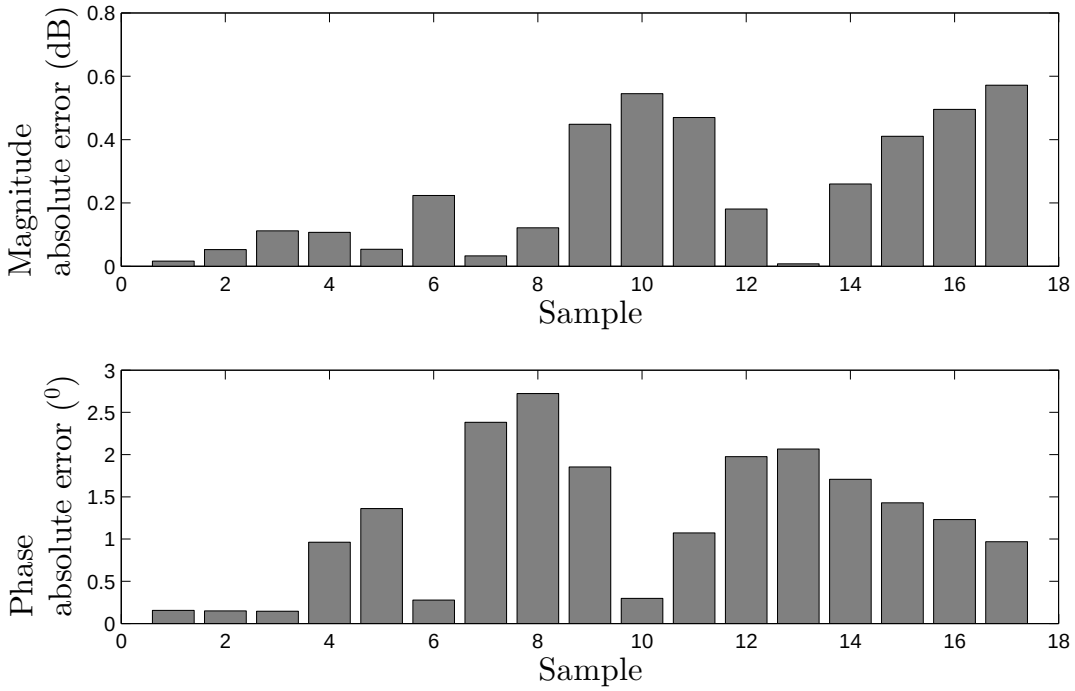

Fig. 4.18. New Model absolute identification error of ultracapacitor $0.047F$

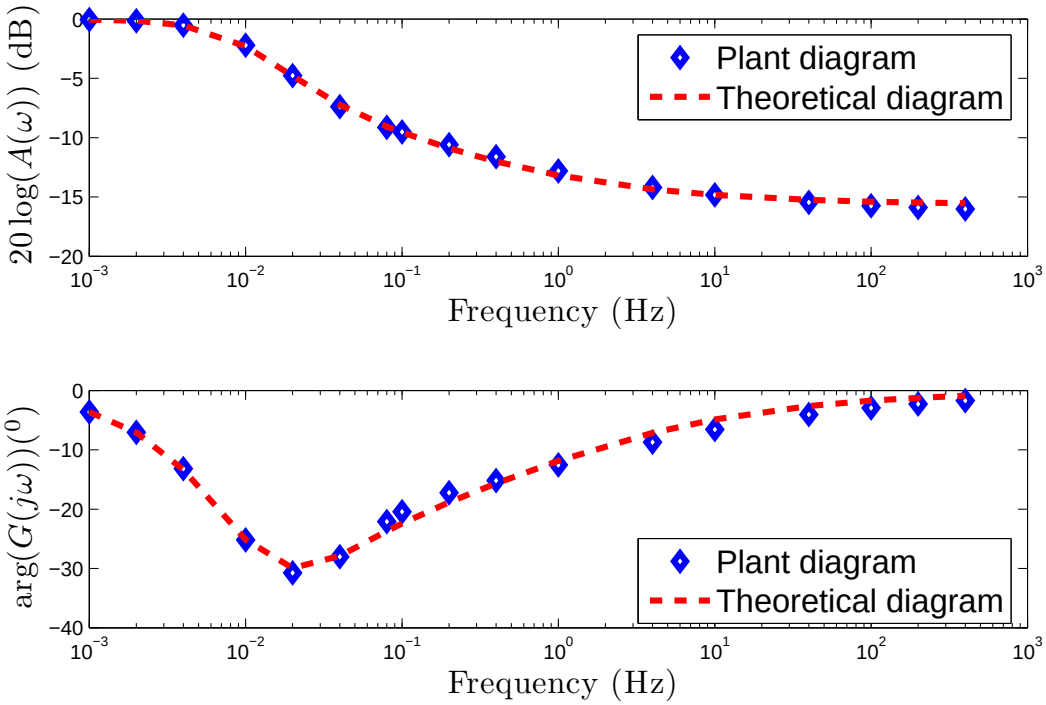

Fig. 4.19. Measured and New Model theoretical Bode's diagrams of system for ultracapacitor $0.047F$

Having a confirmation of good ability of new model for ultracapacitor modelling we can exam Half Order Model which has more useful construction because of their capacity parameters in a traditional form.

4.2.3 Ultracapacitor Modelling Using Half–Order Model

Half–Order Model is the ultracapacitor model derived using the diffusion partial differential equation:

$$G_{0.5} = R_c + \frac{\sqrt{1+Ts}}{Cs},$$

where R_c is the ultracapacitor resistance, C is the ultracapacitor capacity in the traditional definition and T is a parameter of capacity decrease with frequency. This model can be also achieved as a particular case of the Davidson–Cole model for $\alpha = 0.5$. However this model has the simplest structure, its construction allows for model validation in the time domain not only for high capacity ultracapacitor but also for low capacity using experimental setups presented at the beginning of this chapter.

Comparison of the model parameters achieved as a result of identification by diagrams matching with real ultracapacitors parameters are presented in Table 4.7.

The summary of the identification process in the Table 4.8 is presented. It can be noticed that the Root Mean Square Error of this experiment is also small what means that Half-Order model is precise enough for ultracapacitor modelling. The examples of

Table 4.7. Identified Ultracapacitors Parameters for Half–Order Model

capacitor	T	C(F)	$R_c(\Omega)$	C_{real}(F)	$R_{real}(\Omega)$
0.047F	6.5231	0.056	35	0.06	32
0.1F	18.5672	0.1	58	0.1	42
0.33F	73.2900	0.27	32	0.27	28
1500F	1.3059	1371	$0.25m$	1189	$0.26m$
3000F	0.9668	2446	$0.13m$	2435	$0.13m$

achieved Bode diagrams are presented in Fig. 4.20 and 4.22. The absolute error for all samples are shown in Fig. 4.21 and 4.23.

Table 4.8. Error of Half Order Model Identification

Capacitor	Magnitude RMSE	Phase RMSE
0.047F	0.3175	1.5169
0.1F	0.3546	1.4971
0.33F	0.5053	2.0026
1500F	0.9533	2.7004
3000F	0.6875	2.8670

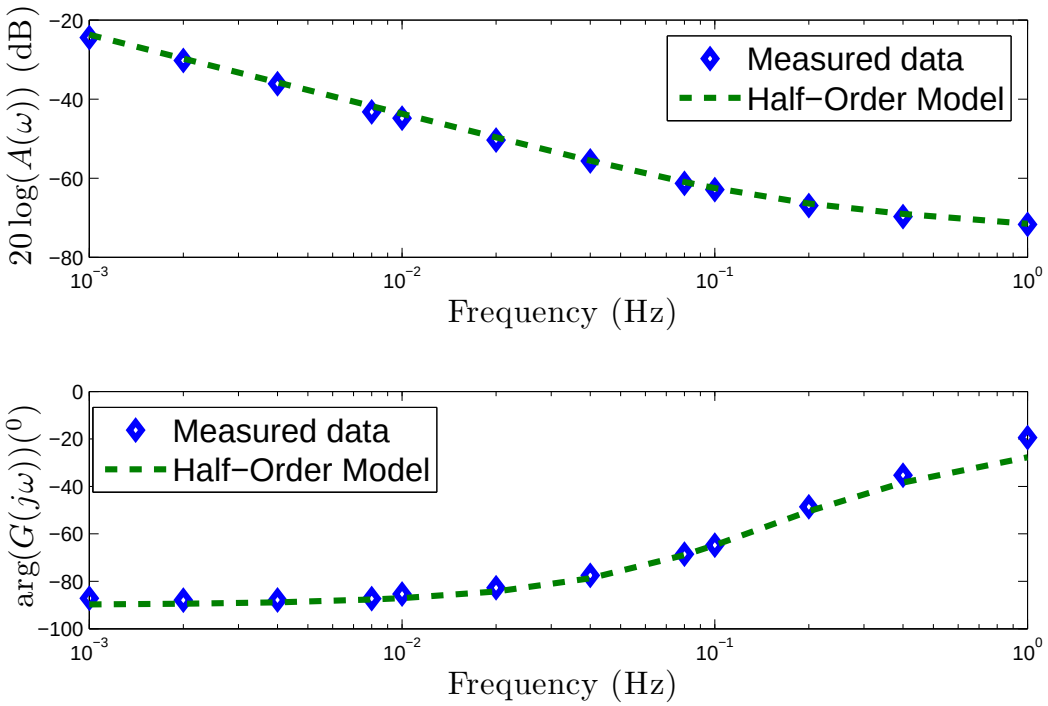

Fig. 4.20. Measured and theoretical Bode's diagrams of ultracapacitor $3000F$

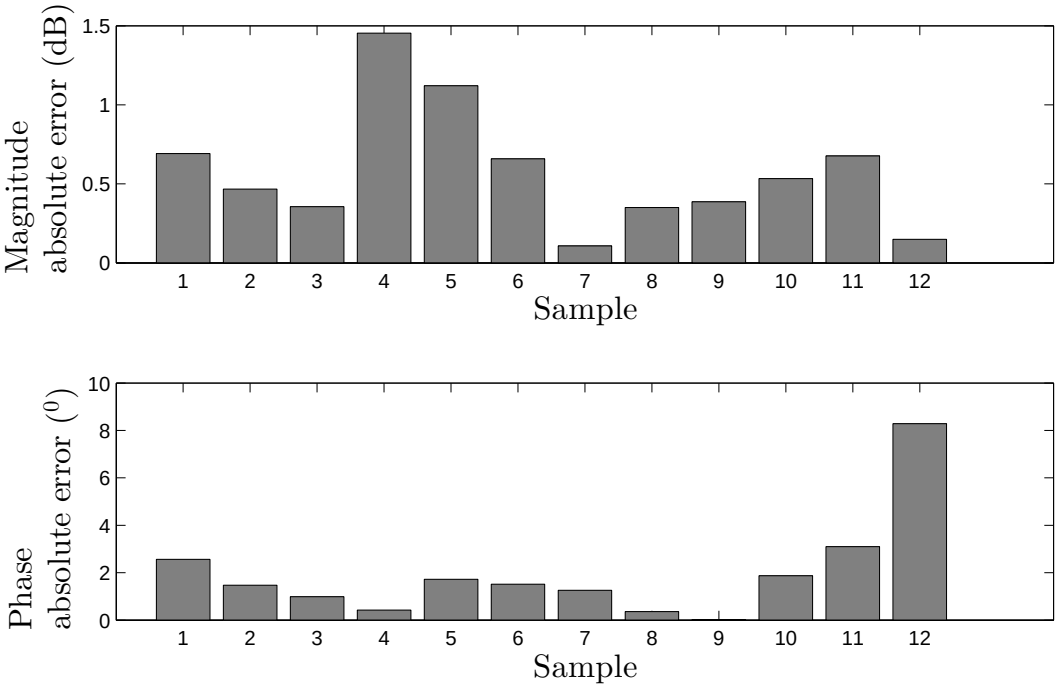

Fig. 4.21. Absolute identification error of ultracapacitor $3000F$

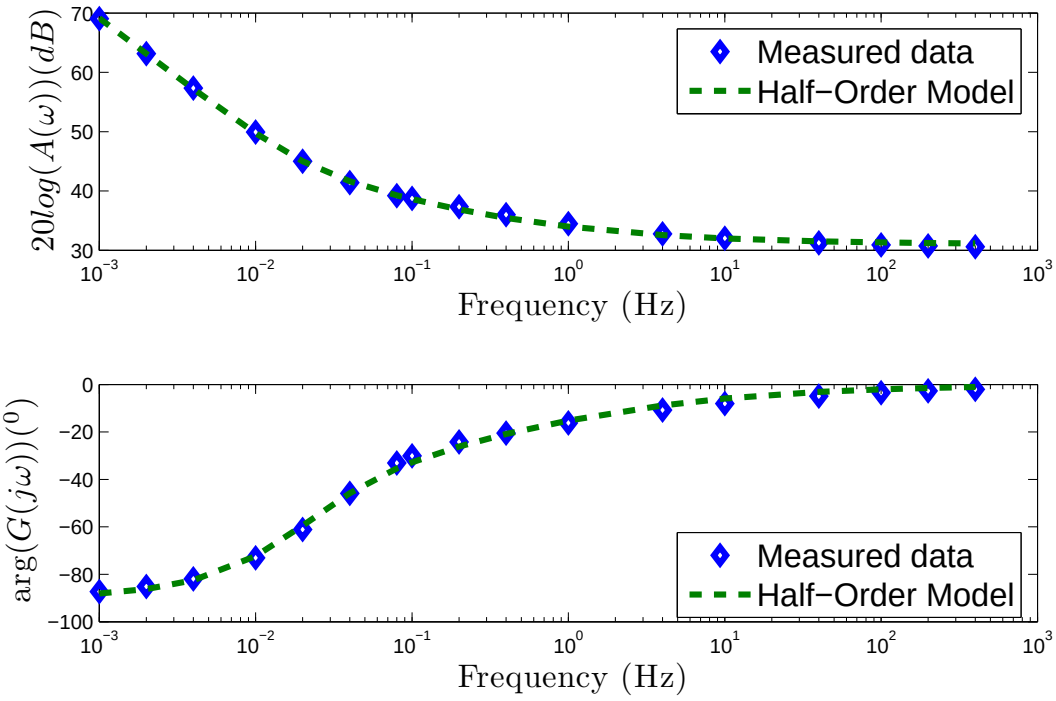

Fig. 4.22. Measured and theoretical Bode's diagrams of ultracapacitor $0.047F$

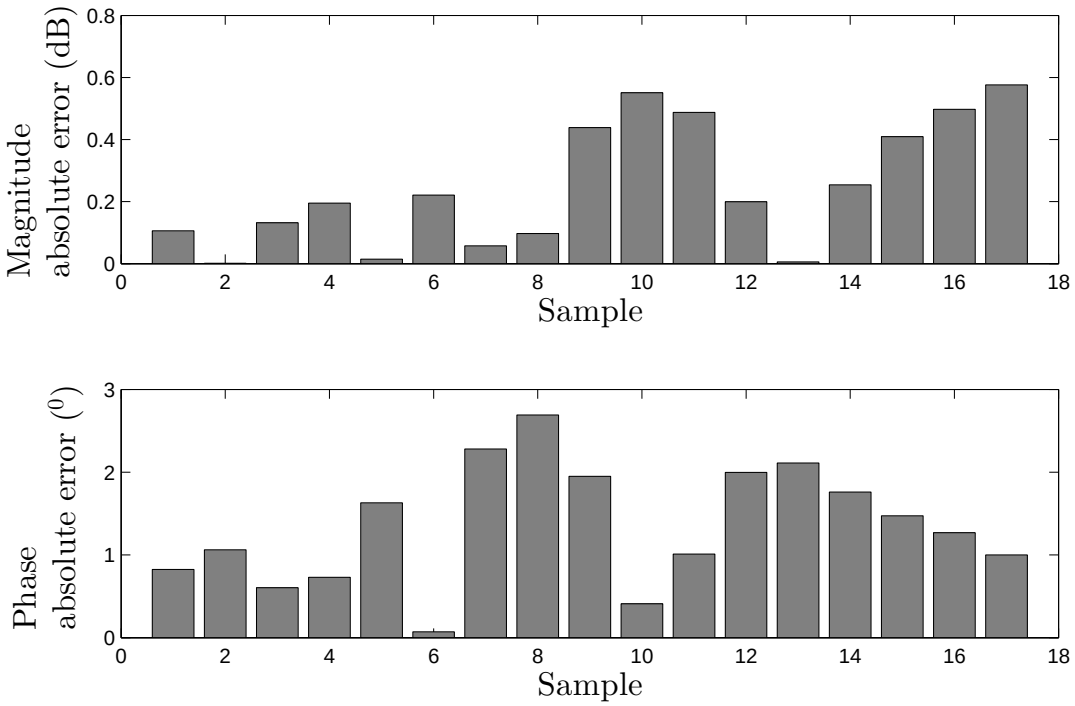

Fig. 4.23. Absolute identification error of ultracapacitor $0.047F$

Since in the Half order model parameter C describes the device capacity in the traditional form, then it can be compared with the traditional capacity. The f_c dependent on T, for which the equivalent capacity decreases two times for Half Order Model is given as follows:

$$f_c = \frac{\sqrt{2^4 - 1}}{2\pi T}$$

and this values for tested ultracapacitors are summarized in Table 4.9:

Table 4.9. Values of frequency for which equivalent capacity decreases two times

capacitor	T	$f_c(mHz)$
0.047F	6.5231	94.5
0.1F	18.5672	33.2
0.33F	73.29	8.41
1500F	1.3059	472
3000F	0.9668	637.6

Achieved values are very close to the values obtained for the Davidson-Cole model. Also this model shown that for low capacity ultracapacitor produced by Panasonic frequency of two time capacity decreasing is smaller for higher capacity and in case of high capacity supercapacitor produced by Maxwell the value of this parameter is increasing with a capacity of the device.

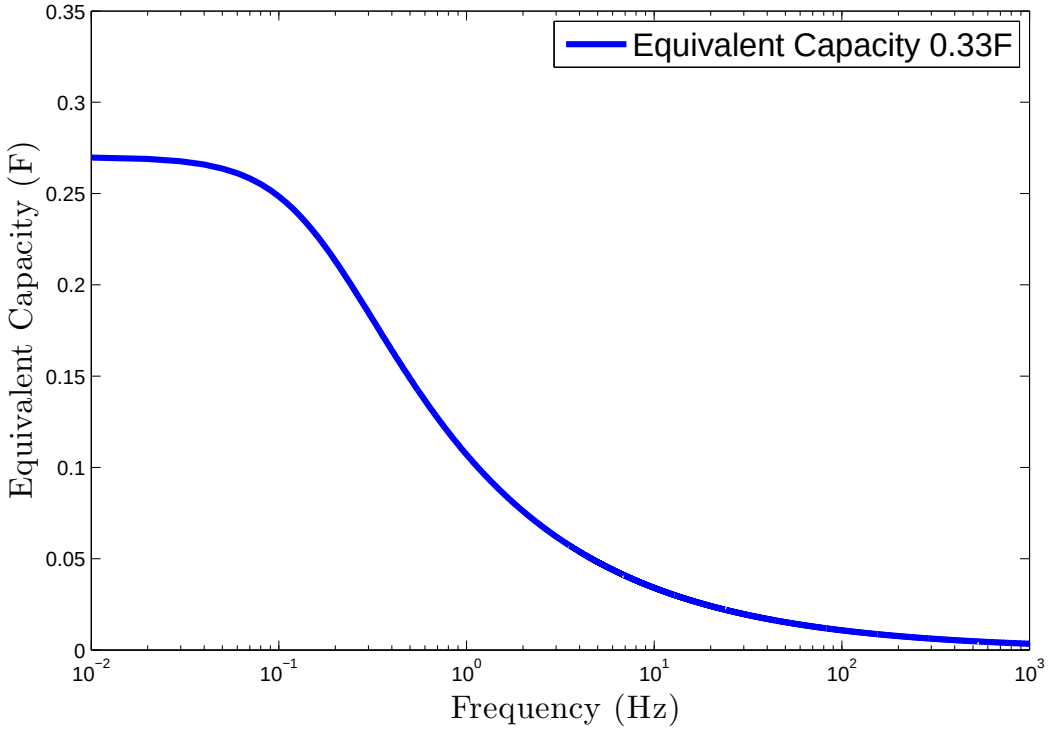

Fig. 4.24. Equivalent capacity C' of ultracapacitor 0.33F

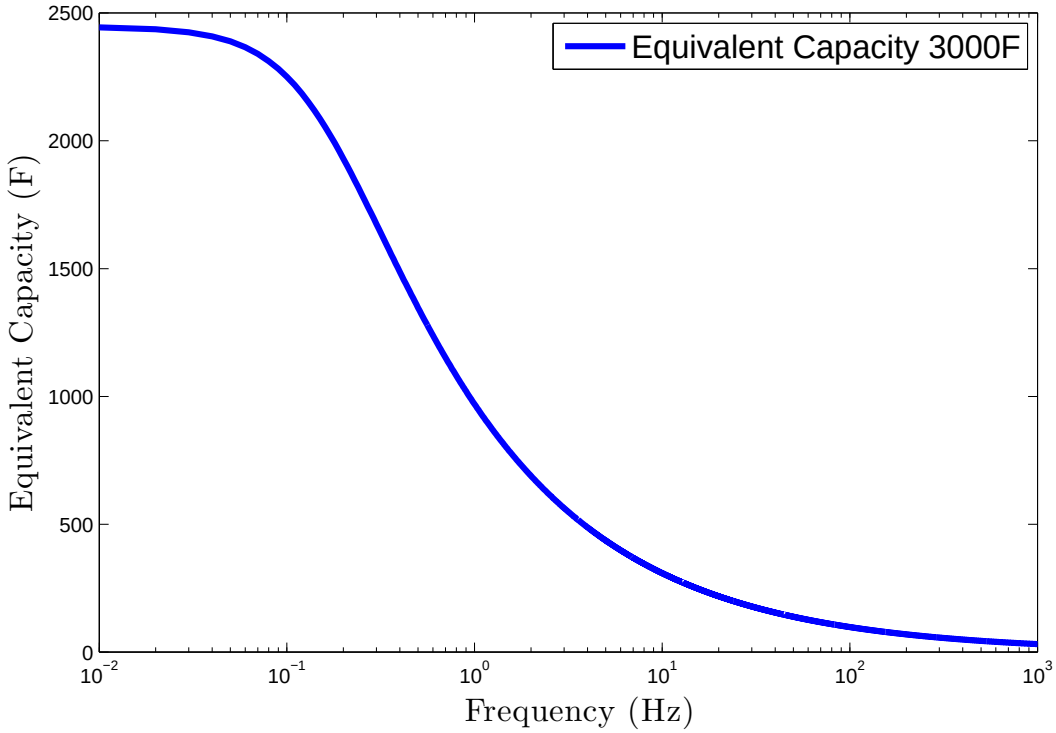

Fig. 4.25. Equivalent capacity C' of ultracapacitor 3000F

Figures 4.24, 4.25 present examples of the equivalent value of capacity as a function of frequency for ultracapacitors of a nominal capacity $0.33F$, $3000F$. After achieved modelling results in the frequency domain it was able to validate them in the time domain. Exemplary comparison between the theoretical model step responses in time domain with values measured in the experiment are presented in the Fig.: 4.26, 4.27. The first of them presents the step response of the ultracapacitor of the nominal capacity 1500F for the input current equal 100A. Second shows step response of ultracapacitor 3000F for the current 50A.

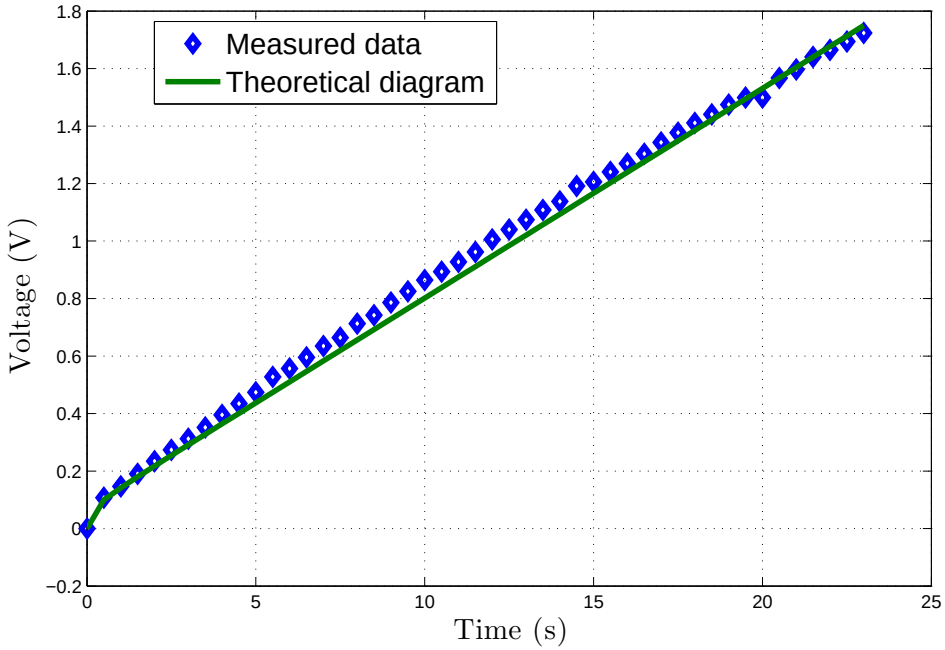

Fig. 4.26. Step response of model $G_{0.5}$ for ultracapacitor 3000F and current $I(t) = 100A$

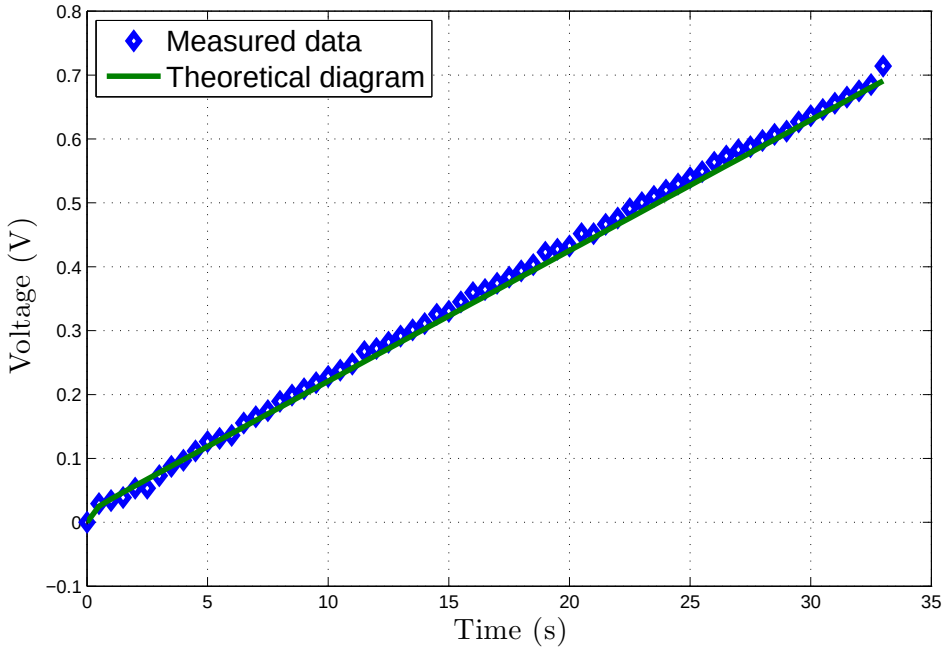

Fig. 4.27. Step response of model $G_{0.5}$ for ultracapacitor 1500F and current $I(t) = 50A$

Because of physical model parameters and order $\alpha = 0.5$ it is possible to validate achieved model for low capacity ultracapacitors using the relation presented in Lemma 3.2. In Fig. 4.28, 4.29 the step responses of ultracapacitor of a nominal capacity $0.33F$ and 0.047 and for the voltage input signal $v(t) = 5V$ are presented. Presented validation also confirms that achieved model it is proper for ultracapacitor modelling.

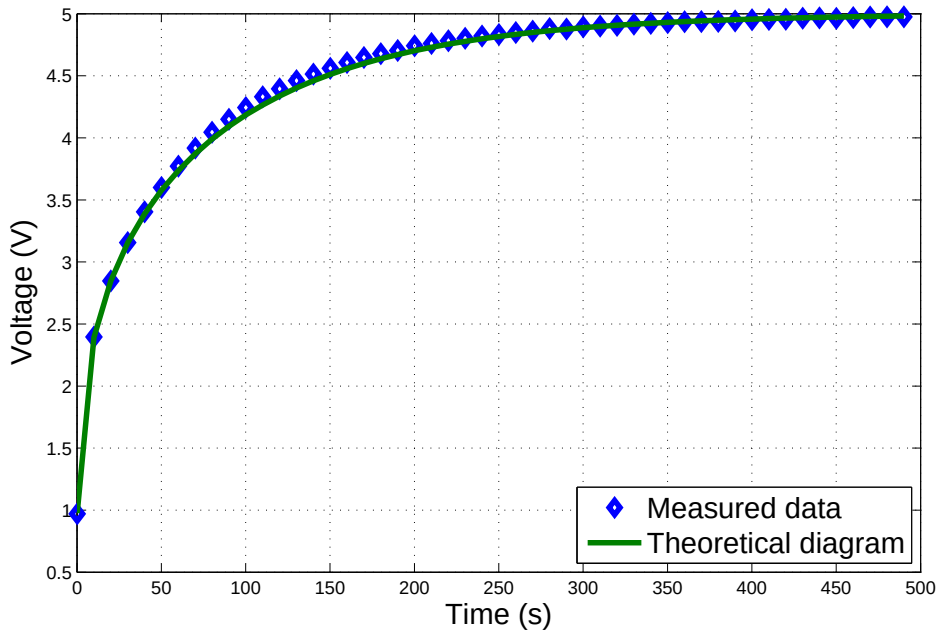

Fig. 4.28. Step response of model $G_{0.5}$ for system with ultracapacitor 0.33F.

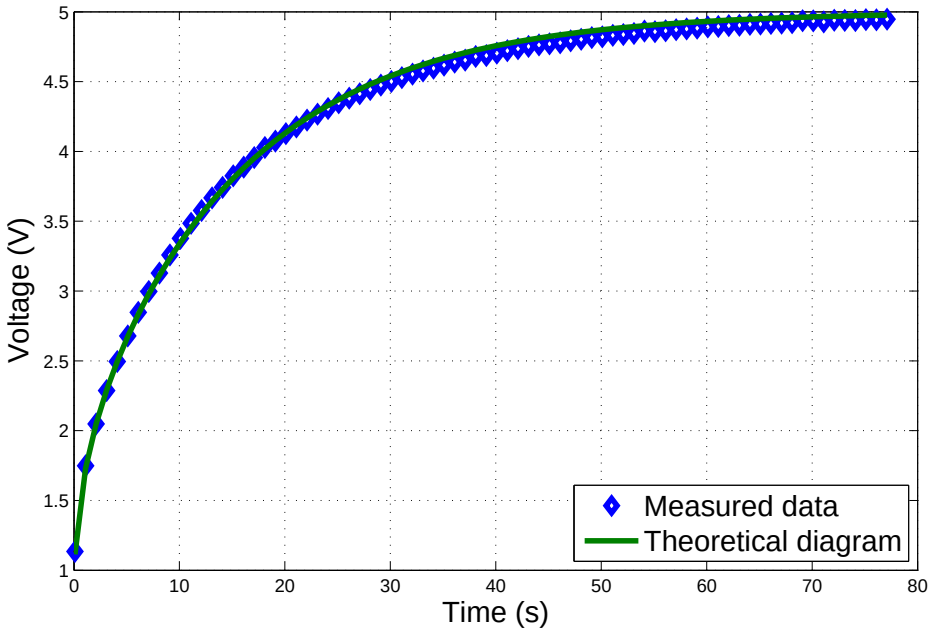

Fig. 4.29. Step response of model $G_{0.5}$ for system with ultracapacitor 0.047F.

Presented results confirm good accuracy of model achieved from normal diffusion equation with the dynamics of physical systems, however they are a little worse than results achieved for Davidsona-Cola's model. The greatest advantage of Half-Order model is the integer system order in the denominator what implies the use of physical system parameters able to compare with parameters of traditional capacitor.

4.3 Summary

In this chapter the experiments of ultracapacitors modelling using fractional order ultracapacitor model are presented. Achieved results confirm that fractional order model can very precisely represent the dynamics of ultracapacitor in the frequency domain and in the time domain. The model which can describe ultracapacitor dynamics in the best way and for a wide range of frequencies is the model derived from the subdiffusion equation (New Model), but for this model it is impossible to compare achieved parameters with the parameters of traditional capacitor because of a non physical parameters in the denominator. However, using this model we proved that value of the order for which it was achieved the best dynamics accuracy is slightly smaller than 0.5 what could have been expected. The subdiffusion, which is a basic phenomenon used in ultracapacitor for energy storing is a process very similar to the normal diffusion, so the order 0.5 is good enough for approximating the ultracapacitor dynamics. Half-Order model, which was derived from the traditional diffusion equation, is not as precise, but it has one very important advantage, all parameters of used model are in the traditional, well know form,

what allows to compare the parameters and properties of ultracapacitor with traditional capacitor. The results of ultracapacitor modelling were also achieved using Davidson-Cole model, which can be also derived from the Quintan's model using the denominator order equal 1. This model combines the physical parameters of ultracapacitors with dynamics which is an effect of anomalous diffusion ions movement. Full model presented by Quintan has not been considered in this chapter because, first it does not have capacity which can be represented in Farads and what is also important, in literature there is no formal derivation which suggest the justification for using the presented model form. The structure of Quintan's model is only the result of a characteristic matching for the enlarged Westerlund's model in the spectroscopy impedance experiments.

In this chapter it has been used only the linear models of capacity. It was necessary to check if the errors achieved in the modelling process were not effects of system nonlinearity. In effect there was prepared another experiment which had confirmed some ultracapacitor nonlinearity. The results of this trial are presented in the Fig. 4.30.

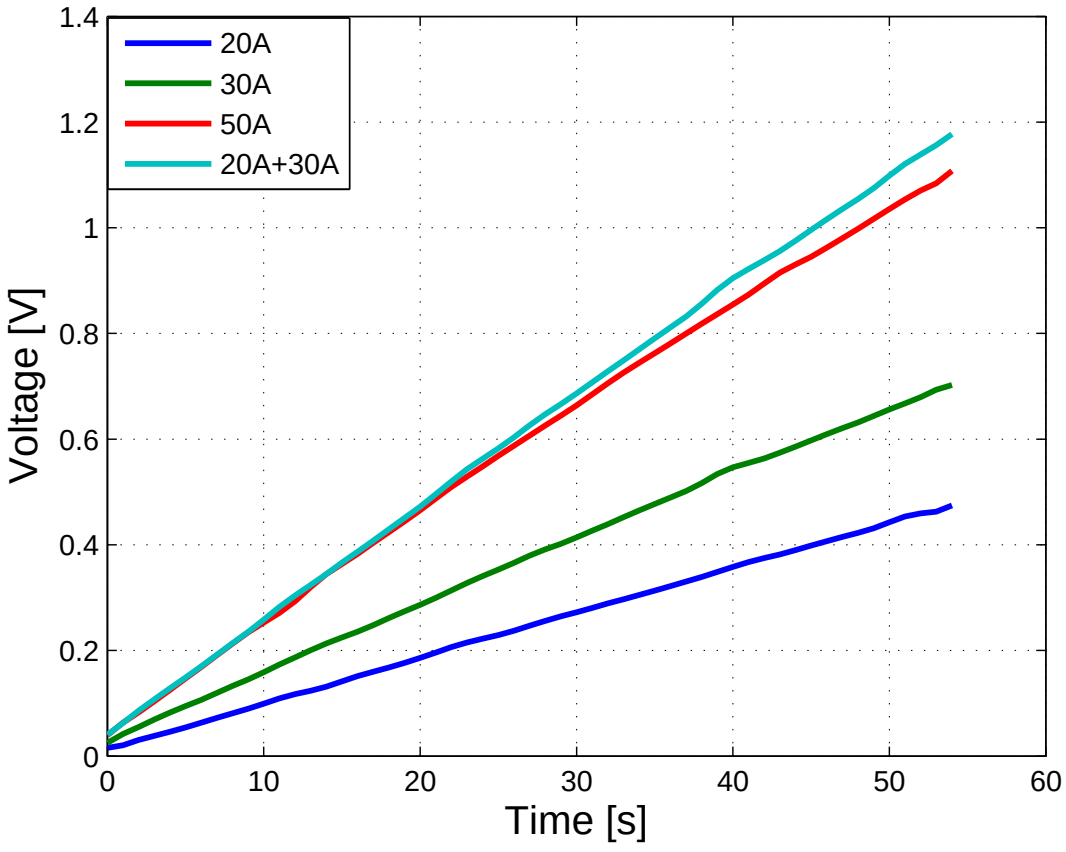

Fig. 4.30. Result of 3000F ultracapacitor nonlinearity

Collected results for the ultracapacitor of a nominal capacity equal 3000F shown that ultracapacitors have some nonlinearity what leads to the conclusion that the most precise ultracapacitor modelling and control can be achieved only using nonlinear fractional order

model. Since a solution of such a system is not trivial so for solving the nonlinearity problem and for precise modelling of ultracapacitor dynamics fractional order neural network has been studied. This is described in the next chapter

Chapter 5

Control of Ultracapacitor Charging and Discharging

This chapter is focused on the ultracapacitor charging and discharging. A problem of efficient charge transport in accordance with a preset characteristic is a problem of a control theory. At the end of the previous chapter it was shown that in fact the ultracapacitors are non-linear devices. In this respect, in order to a control algorithm develop, it was necessary to prepare a new ultracapacitor model including its nonlinearity. Because of non trivial problem of a solution of non-linear fractional order system, the most intuitive idea was to use the artificial neural network for supercapacitor modelling. To this purpose a fractional order artificial neural network (FANN) was developed. This neural network was used for ultracapacitor modelling and for preparing a fractional order controller. Designed controller bases on the idea of the neural network inverse controller. In this chapter the new idea of the fractional artificial neural network is presented. This network was adapted for ultracapacitor modelling. Using neural network ultracapacitor model the fractional order ultracapacitor controller was proposed. Also results of experiments and algorithm validation at the physical system control process using the new type of controller are shown.

5.1 Discrete Fractional Order Neural Network

At the beginning let us consider the non-linear system given in the following form:

$$\Delta^{n\alpha} y_{k+n} = g(\Delta^{(n-1)\alpha} y_{k+n-1}, ..., \Delta^{\alpha} y_{k+1}, y_k, u_k) \tag{5.1}$$

which we can rewrite as:

$$\begin{aligned}
\Delta^{\alpha} y_{1,k+1} &= x_{2,k} \\
\Delta^{\alpha} x_{2,k+1} &= x_{3,k} \\
&\vdots \\
\Delta^{\alpha} x_{n,k+1} &= g\left(y_k, x_{2,k}, ..., x_{n,k}, u_k\right).
\end{aligned}$$

Very good results of this system modelling can be achieved using the Discrete Fractional Order Neural Network (DFONN) proposed by Sierociuk, Sarwas and Dziliński [88]. This structure is a combination of a standard neural network and the linear discrete fractional state-space system (DFOSS 1.16). The schema of this structure useful for simulation of a fractional order neural network is presented in the Fig. 5.1. In this architecture

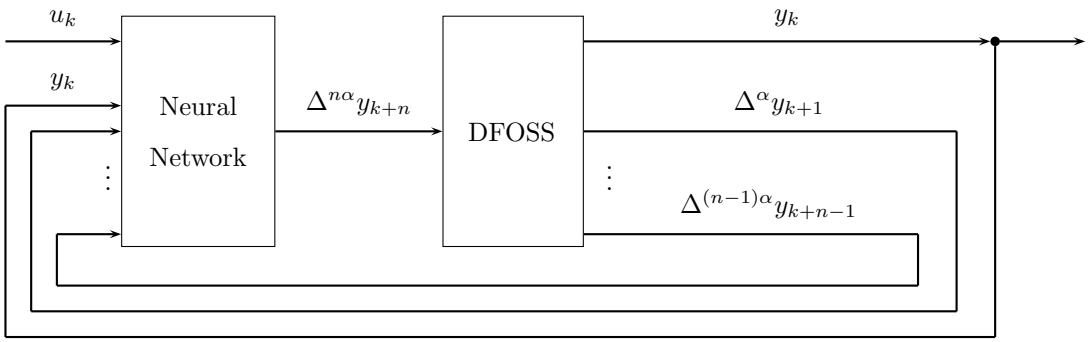

Fig. 5.1. Discrete time fractional neural network

the neural network is a traditional neural network structure in the form dependent on the modelling system. Input signals of the network are system input and output data for $k-th$ sample (u_k, y_k) and the vector differences between previous outputs from $\Delta^{(n-1)\alpha} y_{k+n-1}$ to $\Delta^{\alpha} y_{k+1}$. In the output of the neural network one obtains the prediction of next step difference $\Delta^{n\alpha} y_{k+n}$. Using this value DFOSS calculates value of the system output and the new differences vector. The size of DFOSS blocks depends of the modelled system structure and their matrices can be obtained in the following way:

$$\mathbb{A} = \begin{bmatrix} 0 & 1 & 0 & 0 & \cdots & 0 \\ 0 & 0 & 1 & 0 & \cdots & 0 \\ \vdots & \vdots & \vdots & \vdots & \ddots & \vdots \\ 0 & 0 & 0 & 0 & \cdots & 1 \\ 0 & 0 & 0 & 0 & \cdots & 0 \end{bmatrix}, \quad \mathbb{B} = \begin{bmatrix} 0 \\ \vdots \\ 0 \\ 1 \end{bmatrix}, \quad \mathbb{C} = [I], \quad \mathbb{D} = [0].$$

In fact, the presented structure can be only used for off-line simulation of a modelled fractional order dynamics. In order to apply it to on-line application in control one needs to use $\Delta^{n\alpha} y_{k+n}$ (output of the network) to calculate the system output using only previous

signals samples which are available. Results of modelling of non-linear systems in form presented in (5.1) were shown in [88]. Application of DFONN for modelling a non-linear fractional order dynamics gives very good results and allows to use a much simpler neural network, but for modelling ultracapacitor dynamic the description of non-linear system should by more complicated. Sierociuk and Petráš in [87] presented the fractional order non–linear system description in more general form for on–line modelling a heat transfer process. They used system in the following relation:

$$\Delta^{n\alpha} y_{k+n} = g\left(\Delta^{(n-1)\alpha} y_{k+n-1}, ..., \Delta^{\alpha} y_{k+1}, y_k, \Delta^{(n-1)\alpha} u_{k+n-1}, ..., \Delta^{\alpha} u_{k+1}, u_k\right) \tag{5.2}$$

This system apart from the differences of output signals has the differences of input signals. The calculation of the future samples needs only the samples from the past. Using time shift of (5.2) the following relation can be obtained:

$$\Delta^{n\alpha} y_{k} = g\left(\Delta^{(n-1)\alpha} y_{k-1}, ..., \Delta^{\alpha} y_{k-n+1}, y_{k-n}, \Delta^{(n-1)\alpha} u_{k-1}, ..., \Delta^{\alpha} u_{k-n+1}, u_{k-n}\right) \tag{5.3}$$

Above relation is applied for signal pre–filtering in the neural network training process. The schema of the DFONN which realizes this relation is presented in the Fig. 5.2. Following configuration system can be implemented in Simulink using Neural Network Toolbox and Fractional State–Space Toolkit [84, 86]. This signal processing schema can

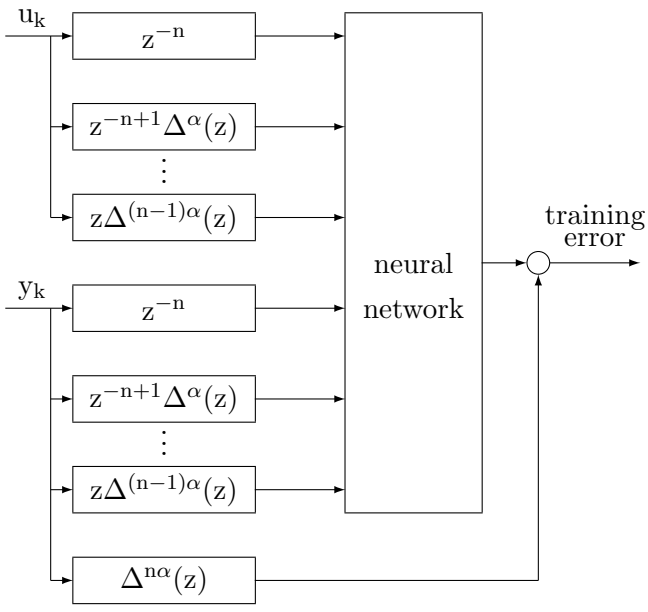

Fig. 5.2. Signal pre–filtering for neural network learning process

be transformed in order to adapt it for on–line simulation. The schema used for simulation of the non–linear discrete fractional order system based on the neural network

obtained in the training process is presented in Fig. 5.3. This Configuration of DFONN is very useful in modelling commensurate systems, otherwise it is necessary to use two or more system orders independent of each other. Despite the fact that presented neural network configuration is sufficient for modelling the heat transfer process in case of the ultracapacitor modelling the non–linear incommensurate system is needed. Description of this system configuration is presented in the next section.

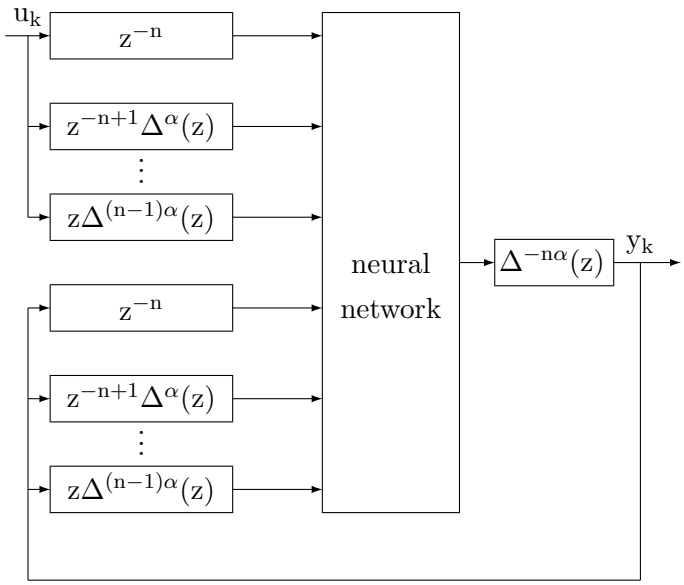

Fig. 5.3. Scheme for on–line simulation of discrete fractional order neural network

5.2 Ultracapacitor Modelling and Control Using DFONN

For ultracapacitors modelling the following non–linear system is proposed:

$$\Delta^{\alpha+\beta} y_k = g\left(u_{k-2}, \Delta^{\alpha} u_{k-1}, \Delta^{\beta} u_{k-1}, \Delta^{\alpha+\beta} u_k, y_{k-2}, \Delta^{\alpha} y_{k-1}, \Delta^{\beta} y_{k-1}\right) \tag{5.4}$$

This system is a particular case of an incommensurate non–linear fractional order system for two system orders (α and β) and the maximum delay amounting two samples. The general formula of this kind of system for any delay is much more complicated. It contains elements depended on higher order differences for α, β and $\alpha+\beta$ orders. Because of huge and complicated expression for general incommensurate non–linear system, in this book we limited ourselves only to present system in the form useful for ultracapacitor modelling. This system was realized for the model shown in Fig. 5.4. Presented schema of signal prefiltering was implemented for the fractional order neural network training process. For

on–line simulation of the system, achieved during modelling process, the link configuration presented in Fig. 5.5 was used.

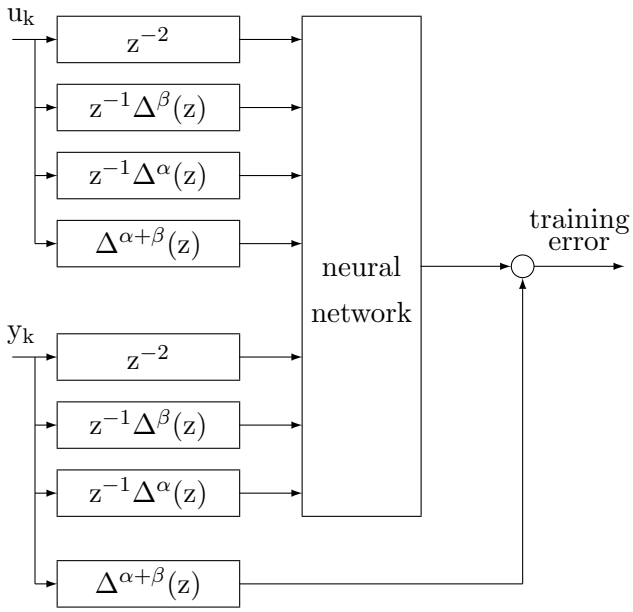

Fig. 5.4. Signal prefiltering for neural network training process

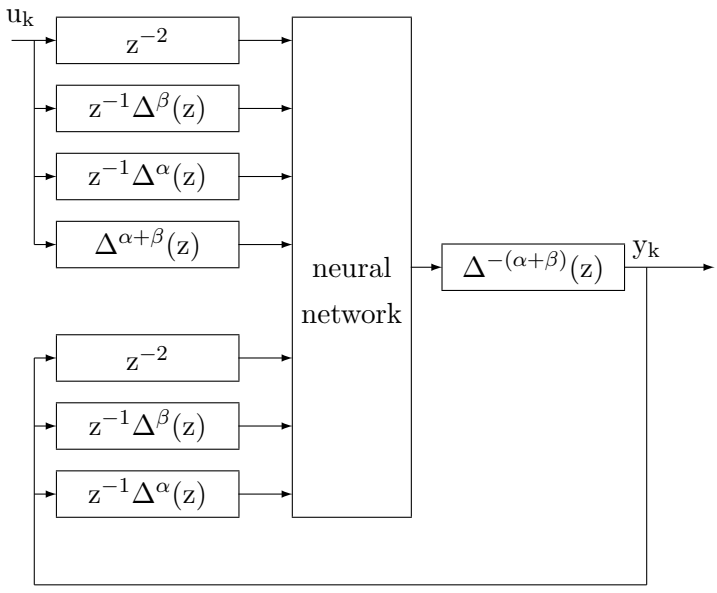

Fig. 5.5. Scheme of on–line simulation of DFONN ultracapacitor model

Experiments of ultracapacitor modelling were carried on of the Maxwell PC5 (4F, 2.5V) ultracapacitor. This ultracapacitor was connected for the experimental setup in the voltage to current converter configuration presented in Fig 5.6, where C is a modelled ultracapacitor, R is a matching resistor and OPA 549 is a High-Voltage, High-current Operational Amplifier. For the fractional order neural network training and testing step responses of the system with ultracapacitor were measured.

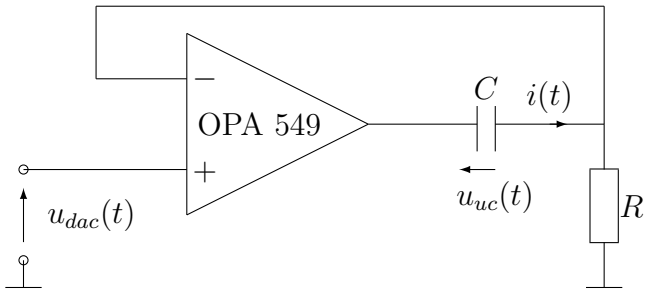

Fig. 5.6. Electronic circuit

For the fractional order neural network training and testing step responses of the quadripole system with ultracapacitor were measured. Using Matlab Simulink program and DSpace DS1103 card the $u_{dac}(t)$ signal were generated. This signal through the voltage to current follower presented in the Fig. 5.6 was amplified, what created the current input signal $i(t)$. Sampling time used in experiments was $t_s = 0.01s$. In the training process the input signals $i(t)$ presented in Fig. 5.7 were used.

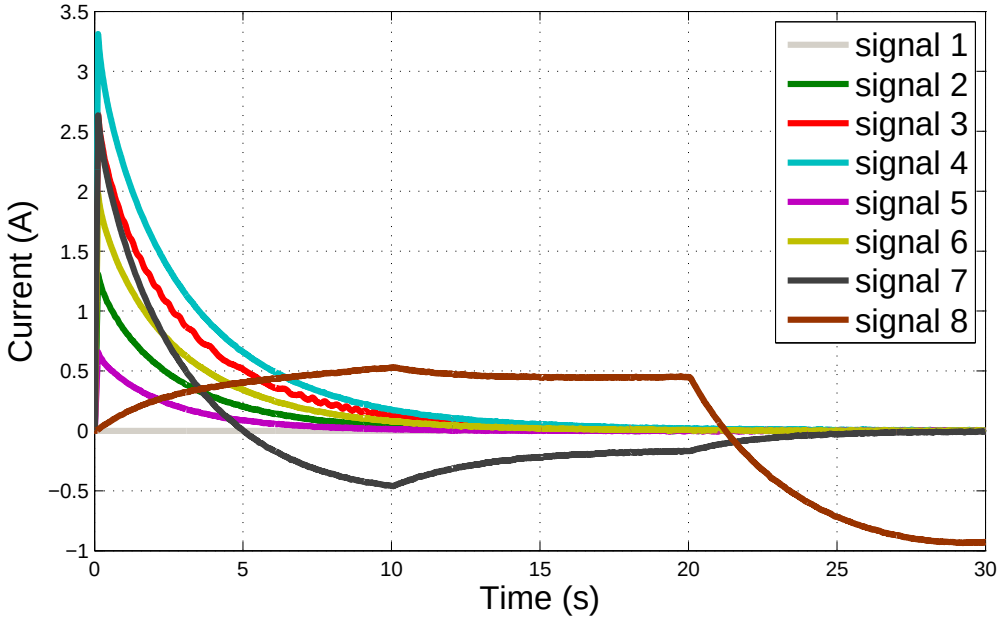

Fig. 5.7. Training input signals

Also, a very important move, was to take the zero signal for neural network training process. Without this signal the net had a huge problem with generalization in case of the steady state. To test the network ability for generalization the testing signal shown in the Fig. 5.8 was used.

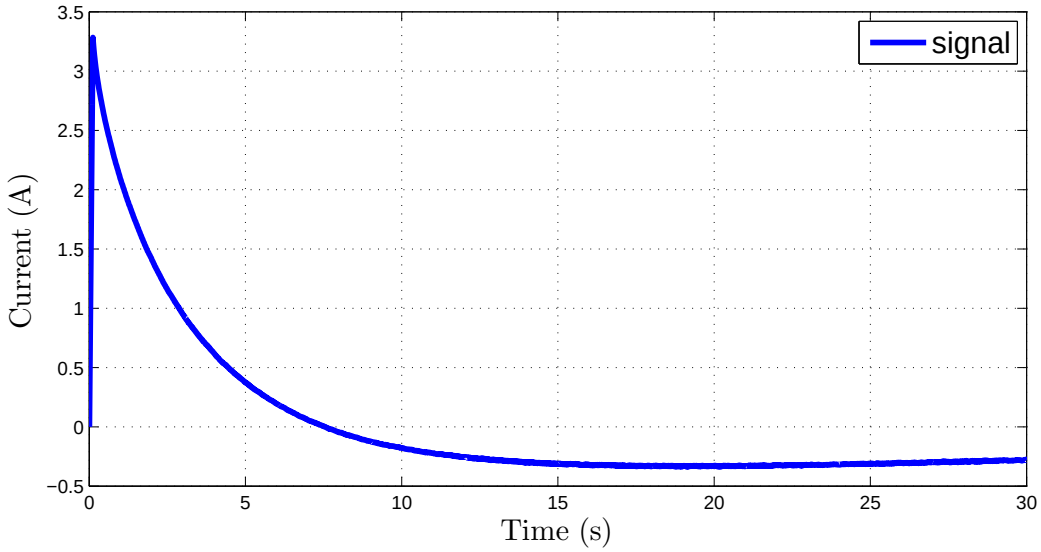

Fig. 5.8. Testing input signals

The voltage responses of the ultracapacitor $u_{uc}(t)$ for the presented input signals $i(t)$ measured directly from the ultracapacitor are presented in Fig. 5.9, where the response called *signal* is the output for the testing input signal and another responses are named like input signals presented in Fig. 5.7 respectively. These signals had been filtered for measurement noise elimination.

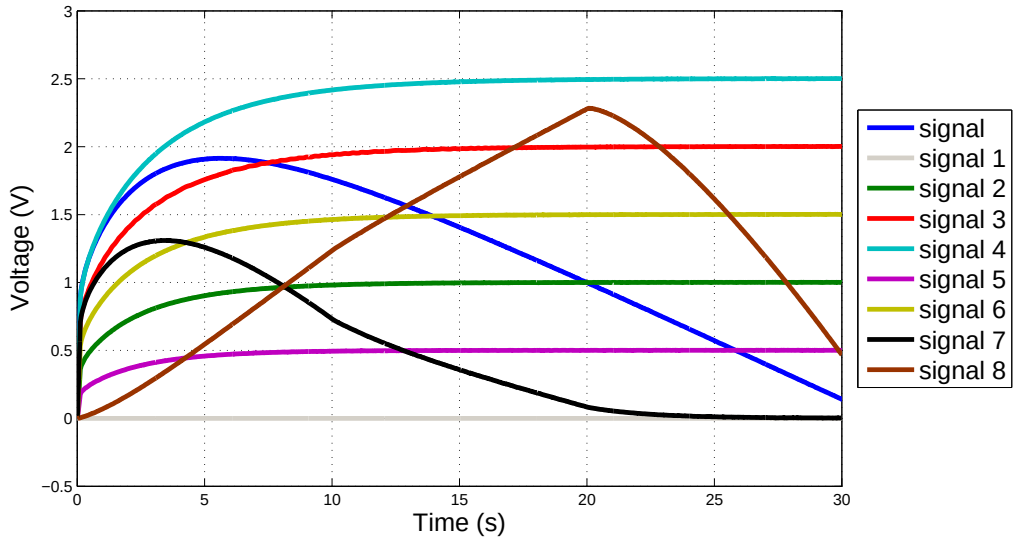

Fig. 5.9. Ultracapacitor response for input signals

At the beginning of the modelling process it was necessary to establish parameters of the neural network. As a result following configuration of the fractional order neural network for the ultracapacitor modelling were achieved:

- Seven inputs;
- Two layers;
- Five neurons in Hidden-layer;
- One neuron in Output-layer;
- Activation function: tansig function (hidden layer); linear function (output layer);
- Training algorithm: Levenberg-Marquardt;
- Epochs number: 35;
- $\alpha = 0.15$, $\beta = 0.3$.

Configuration of this parameters has been established empirically. It is worth to notice that the sum of α and β orders is approximately equal to the order of the ultracapacitor fractional order model presented in the Section 4.2. Another important result to highlight is a number of epoch enough for the network training. So adopted fractional order neural network configuration allows for very quick learning of the network.

As a result of neural network training the means of the Euclidean norm of an absolute error vector for all signals have been calculated. Obtained results are presented in the Table 5.1:

Table 5.1. Mean error of fractional order neural network model

Signals	**Error**	**Signals**	**Error**	**Signals**	**Error**
signal 1	$1.78e^{-4}$	signal 4	$2.42e^{-4}$	signal 7	$1.98e^{-4}$
signal 2	$3.57e^{-4}$	signal 5	$8.29e^{-5}$	signal 8	$2.98e^{-4}$
signal 3	$1.30e^{-4}$	signal 6	$9.45e^{-5}$	signal	$3.73e^{-4}$

Exemplary results achieved after neural network training process are presented in the Fig. 5.10 and 5.11.

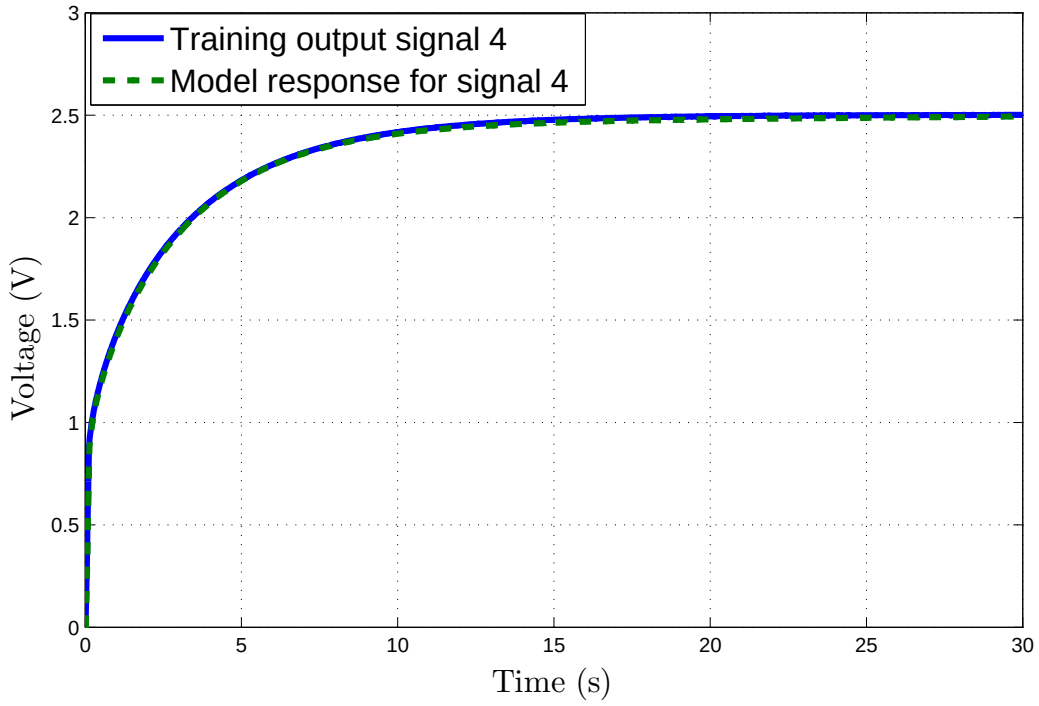

Fig. 5.10. Comparison of model and system responses for signal 4

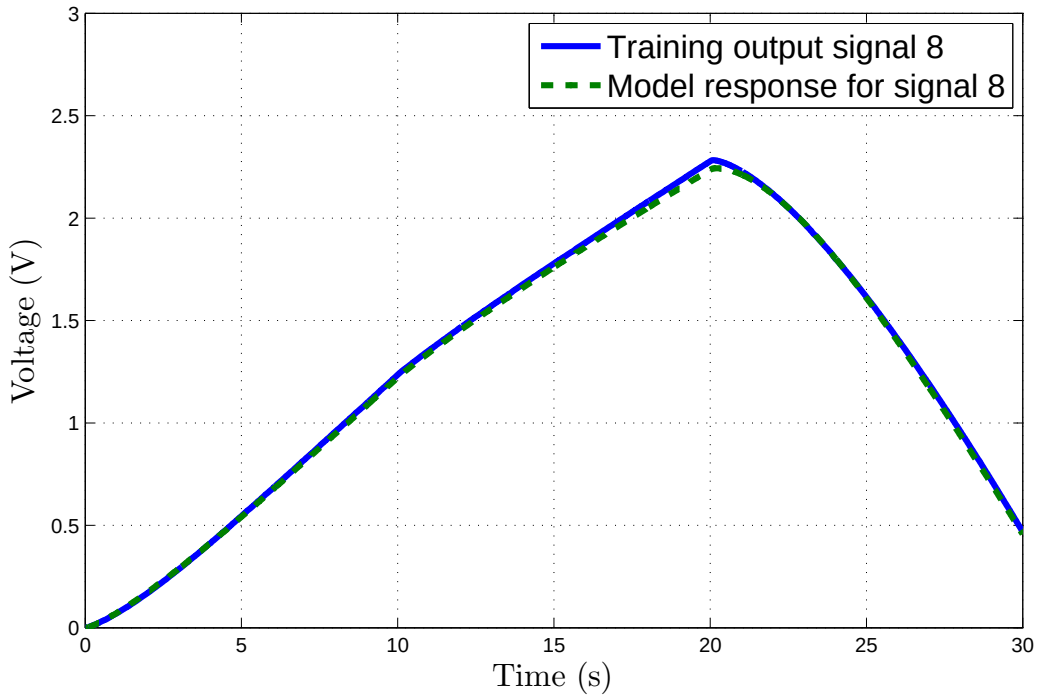

Fig. 5.11. Comparison of model and system responses for signal 8

The result of the model generalization for testing signal is presented in the Fig. 5.12. Presented results confirm the high level of convergence between the behaviour of modelled system and achieved model. In Fig. 5.12 we also see that the configuration of the used

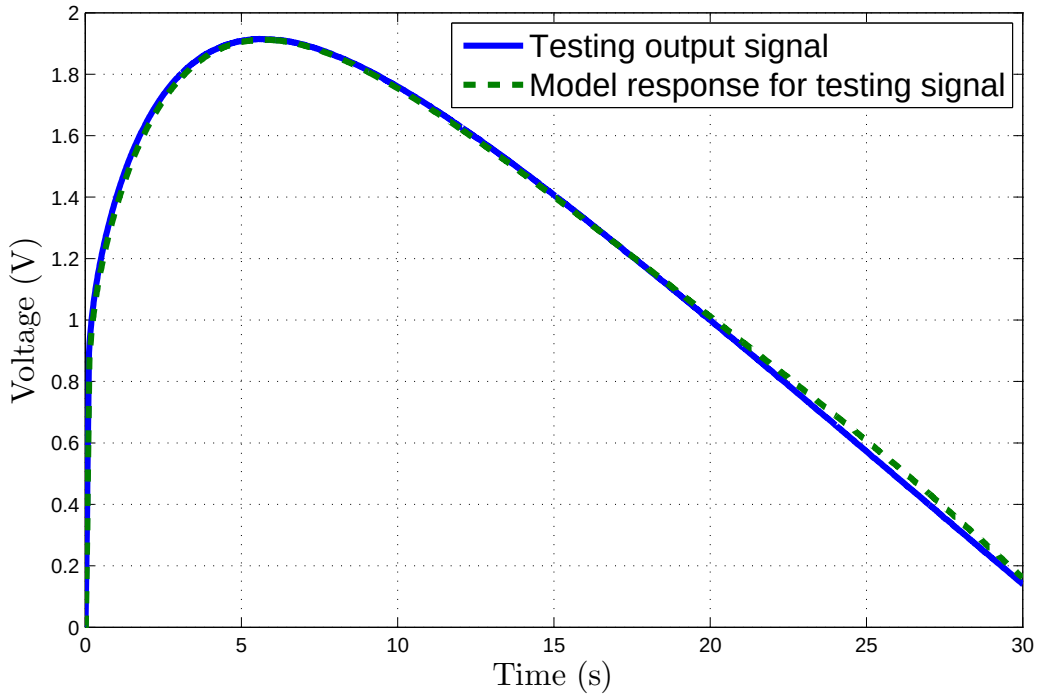

Fig. 5.12. Model response for testing signal

fractional order neural network has a property of generalization.

Possessing so accurate non–linear ultracapacitor model allowed for preparing a fractional order ultracapacitor controller. The idea of this controller is based on the neural network inverse controller. In our case the fractional order neural network presented in Fig. 5.4 and 5.5 was adopted. In order to train the network, training input signals and system responses have been were exchanged. System responses for training signals were used like input training signals and training input signals were used like system responses. In effect the fractional order neural network was learned like controller.

The mean error of controller training process in the Table 5.2 is presented.

Table 5.2. Mean error of achieved controller

Signals	**Error**	**Signals**	**Error**	**Signals**	**Error**
signal 1	$4.12e^{-5}$	signal 4	$4.73e^{-4}$	signal 7	$3.68e^{-4}$
signal 2	$2.38e^{-4}$	signal 5	$1.98e^{-4}$	signal 8	$2.43e^{-4}$
signal 3	$3.72e^{-4}$	signal 6	$2.79e^{-4}$	signal	$4.90e^{-4}$

Figure 5.13 presents the result of inverse controller training process. In Fig. 5.14 the ability of the neural network inverse controller generalization is shown. Both diagrams highlight great accuracy for all samples. These figures confirm the proper operation of the achieved controller.

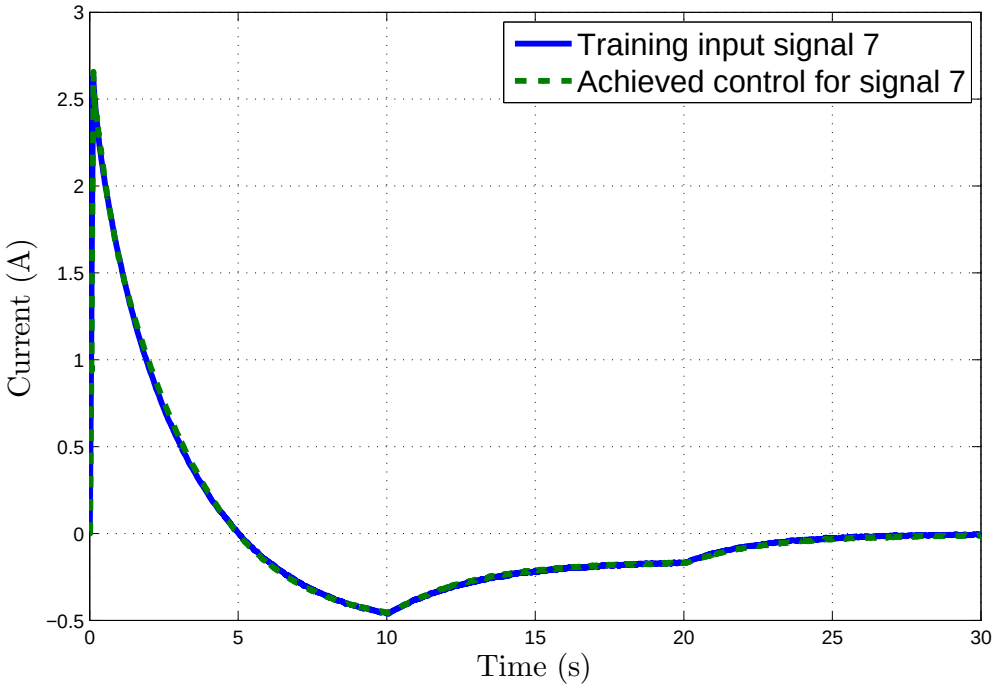

Fig. 5.13. Comparison of controller and system control signal for signal 7

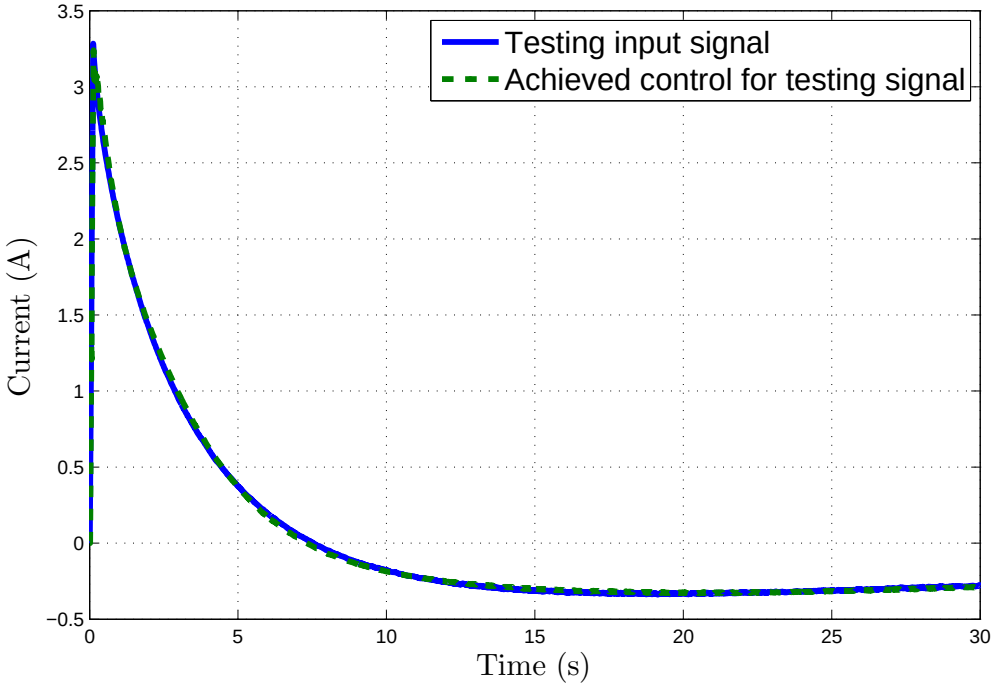

Fig. 5.14. Comparison of controller and system control signal for test signal

Possessing fractional order neural network model and controller it was necessary to test the ability of a signal reproduction. For this test the Simulink model presented in Fig. 5.15 was used.

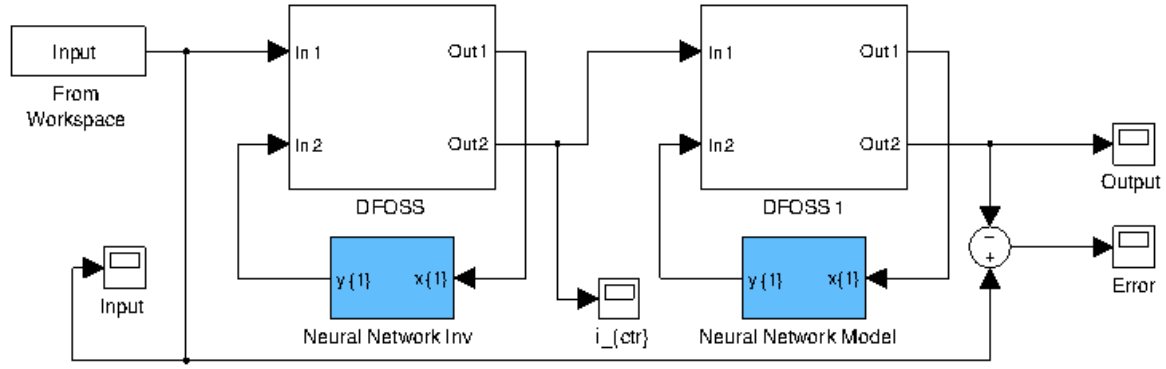

Fig. 5.15. Simulink schema for testing the signal reproducing

As a system input signal the response of the test signal was used. The result of signal reproducing is presented in Fig. 5.16. In this figure we can see that the voltage in the model output is quite close to the system input signal, which confirms the good preparation of the controller and allows to take them for the control of physical system with ultracapacitor.

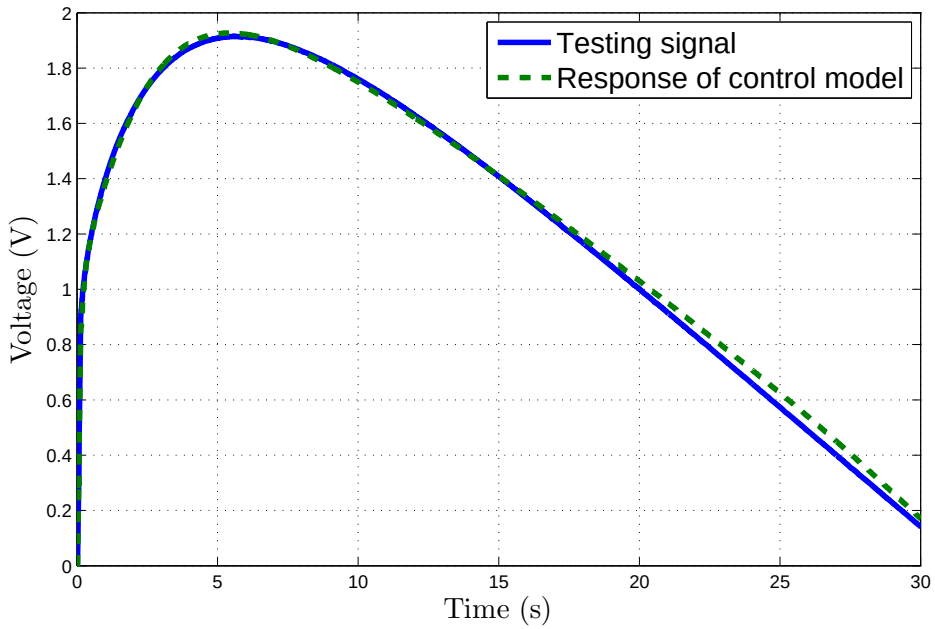

Fig. 5.16. Result of signal reproducing on the Simulink model

The experiment of ultracapacitor control based on the system input voltage signal reproducing at an ultracapacitor. The scheme of the system configuration used in this

case is presented in Fig. 5.17, where $u(t)$ is the input voltage which we would like to force on the ultracapacitor, $i_{ctr}(t)$ is the value of the control current, $i(t)$ is the value of system current and u_{uc} is the voltage on the controlled ultracapacitor. Using this configuration the input signal is changed with the inverse controller in the input control current $i_{ctr}(t)$. This current is amplified with the Power Interface which contains instrumental amplifier AD 620, implemented in DSpace DS1103 card, and Voltage–Current converter presented used for date acquisition.

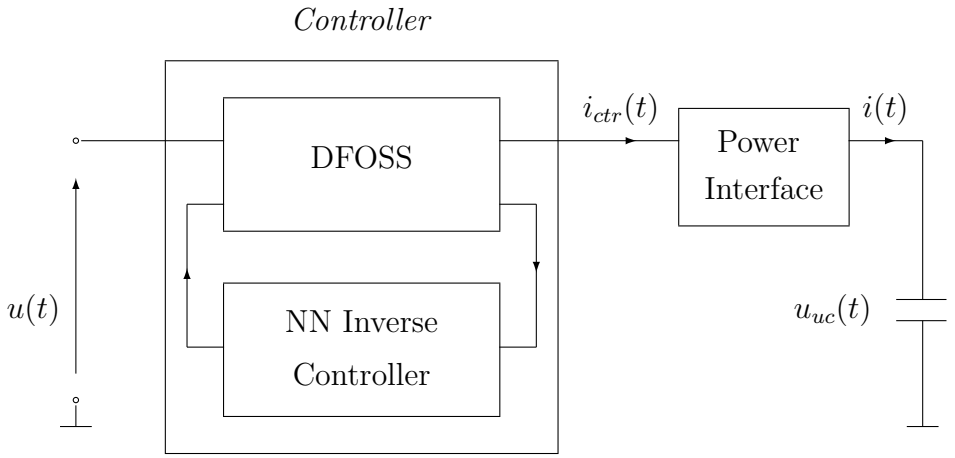

Fig. 5.17. Scheme of control system

Results of the ultracapacitor voltage control are presented in Fig. 5.18 and 5.19.

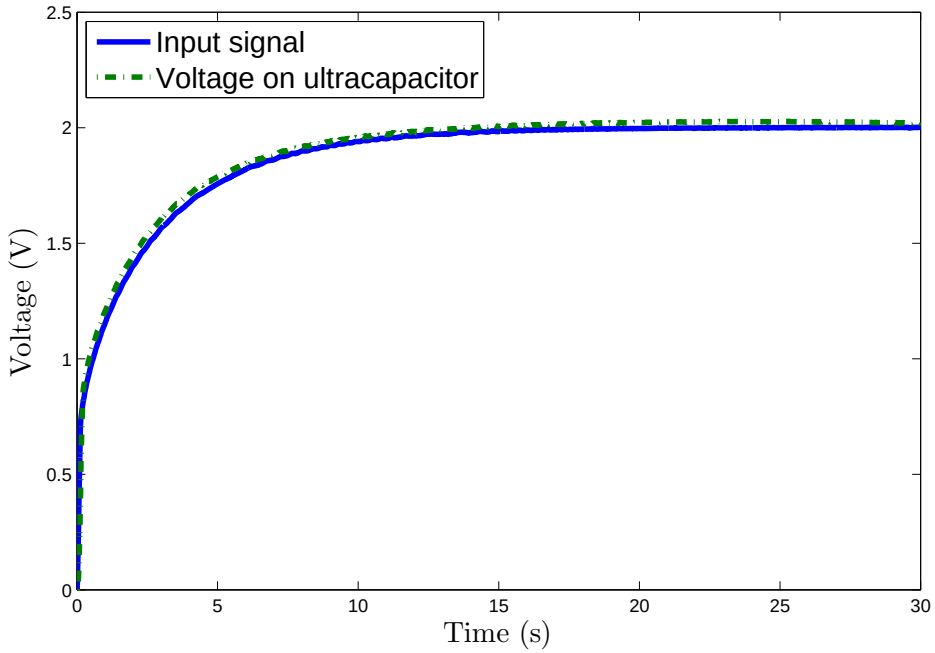

Fig. 5.18. Physical system control

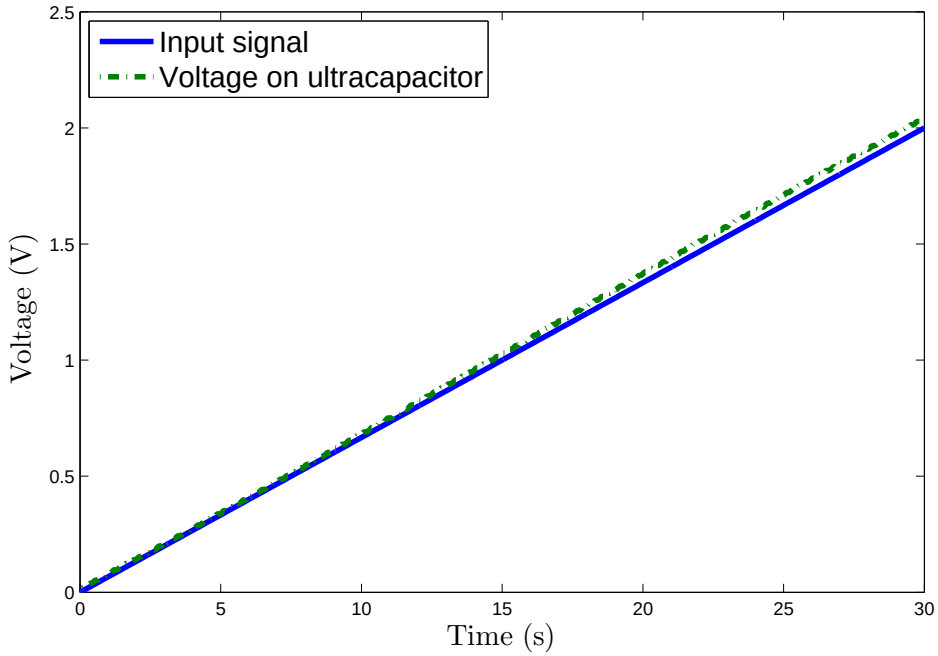

Fig. 5.19. Physical system control

Figures 5.18 and 5.19 confirm that the fractional order artificial neural network controller is very useful for control the charging and discharging ultracapacitor process. Small differences between input signals and theirs reproductions are the results of the measurement noise. Precise configuration of DFOSS blocks with orders sum equals the approximation of the ultracapacitor linear fractional model order allows using very simple neural network structure. This simple structure affects the training time, which is very short (35 epochs are enough). Also achieved fractional order artificial neural network model, which behaviours are presented in Fig. 5.10, 5.11 and 5.12, is very accurate and deals with the ultracapacitor non–linearity.

5.3 Summary

In this chapter the fractional order artificial neural network was presented. This network was used for ultracapacitor modelling and control charging and discharging process. Achieved results are very encouraging. Based on the experiments with ultracapacitors we can conclude that this type of system can be very useful for modelling and control fractional order nonlinear systems which is very complicated for solving in a traditional way. The ability of right combination of the fractional order discrete state space system with a traditional neural network can give very precise instrument applicable in many industrial applications.

Chapter 6

Conclusions

The work addressed the problem of modelling and control of ultracapacitors and systems with ultracapacitor using the fractional order calculus. First, based on the internal ultracapacitor structure the appropriateness of using fractional order calculus to ultracapacitors modelling are explained. Next, extending the assumptions, a new fractional order model of the ultracapacitor was derived. This model was based on the anomalous diffusion but it contains non physical parameters.

Further, the properties of existing and new derived model were analytically explained and discussed. In this part an important phenomenon known by the ultracapacitor producers was explained. This clarification also explains the validity of use of fractional calculus for description of the dynamics of whole system based on the diffusion equation.

As a main part of this work the ultracapacitors identification and the models validation are considered. Three different fractional order models were used for ultracapacitors identification. Achieved model parameters were compared with the parameters measured directly from the ultracapacitors. For this process equation the time domain step response of the ultracapacitors and the system with ultracapacitor for Davidson-Cole model were derived. Also two experimental setups were build. Moreover, for achieved parameters the characteristics of capacity decreasing as a function of frequency were discussed. During this research the ultracapacitors linearity was tested. As a result, it was shown that ultracapacitors possess nonlinear dynamics and even better results of modelling and control can be achieved using non–linear tools. To solve the problem of modelling and control of nonlinear fractional order object a new discrete fractional order neural network was proposed. This neural network was proposed like some combination of a traditional network with input signals being the noninteger order differences produced using discrete fractional order state space system (DFOSS). This new form of a neural network was adopted for ultracapacitor modelling and after achieving the positive results a new electrical circuit was built for control of charging and discharging process using fractional order neural network invert controller. Building this new type of neural network allows to omit the non–linearity of ultracapacitors in the process of ultracapacitor modelling and control.

As a result of presented experiments it can be concluded that fractional order calculus yields very powerful tool which can be very useful for modelling and control of devices and processes of which internal structure or mode of action are based on the normal or anomalous diffusion equations. Example of such devices are ultracapacitors used in the thesis. Use of somewhat more complicated equations can result in a simplified model of the device under consideration. Also application of the fractional order model can help to explain some phenomena difficult to explain in the traditional way.

In this thesis also a new structure of a neural network was proposed. Because this structure is a combination of fractional order prefiltering and traditional type of neural network in effect this combination can be widely used for modelling non–linear process. Utility of proper DFOSS can simplify neural network structure what can have great influence on its efficiency.

Using a fractional order calculus creates new problems. Proposed model is a linear model which can very precisely represent the dynamics of physical devices in the fairly wide range of frequencies but it is not ideal. It may turn out necessary to develop this model further especially on the nonlinear part, which will be more precise. Next problem is the form of equation obtained from this model in the attempt of calculation of the relation for the ultracapacitor step response. Existing relation is very difficult or even impossible to transform. Another problem was featured in the models which contains noninteger power of complex variable "s" in denominator. This type of models create new undefined parameters or parameters which are impossible for the physical understanding. In this case we cannot compare these parameters with parameters existing in the traditional models what can force us to define of a new description of systems. Also a problem of an LC resonance for the systems with ultracapacitors should be rediscussed. Having precise model it is necessary to focus on parameters changing in the function of temperature or ultracapacitor changing. Results of this kind of experiments can be very useful in all systems which work with the ultracapacitors cascade, what can help in system observation and can eliminate its damaging.

Bibliography

[1] G. A. Anastassiou. *Advances on Fractional Inequalities*. Springer, 2011.

[2] J. Audonet and J. M. Roquejoffre. An asymptotic fractional differential model of spherical flame. In *Fractional Differential Systems: Models, Methods and Aplications*, pages 15–27. ESAIM: Proceedings, December 1998.

[3] M. Axtell and E. M. Bise. Fractional calculus applications in control systems. In *Proceedings of the IEEE 1990 Nat. Aerospace and Electronics Conf.*, pages 563–566, New York, USA, 1990.

[4] D. Baleanu, J. A. T. Machado, and A. C. J. Luo. *Fractional Dynamics and Control*. Springer, 2011.

[5] J. L. Battaglia, O. Cois, J. C. Batsale, and A. Oustaloup. La dérivation non entière: Outil de modélisation en thermique. In *Les Sysémes á Dérivées Non Entières: Théorie et Applications*, volume 7. Alain Oustaloup and Michael Guglielmi, 2001.

[6] F. Belhachemi, S. Raël, and B. Davat. A physical based model of power electric double-layer supercapacitors. In *Proceedings of IEEE Industry Applications Conference*, volume 5, pages 3069 – 3076, October 2000.

[7] J. P. Bouchaud and A. Georges. Anomalous diffusion in disordered media: Statistical mechanisms, models and physical applications. *Physics Reports*, 195:127–293, November 1990.

[8] H. Brouji, J. M. Vinassa, O. Briat, N. Bertrand, and E. Woirgard. Ultracapacitors self discharge modelling using a physical description of porous electrode impedance. In *Proceedings of IEEE Vehicle Power and Propulsion Conference (VPPC)*, September 2008.

[9] S. Buller, E. Karden, D. Kok, and R.W. De Doncker. Modeling the dynamic behavior of supercapacitors using impedance spectroscopy. *IEEE Transactions on Industry Applications,*, 38(6):1622–1626, 2002.

[10] R. Caponetto, G. Dongola, L. Fortuna, and I. Petráš. *Fractional Order Systems: Modeling and Control Applications*. World Scientific, 2010.

[11] M. Caputo. Linear model of dissipation whose q is almost frequency independent. *II, Geophys. J. R. Astr. Soc.*, 13:529–539, 1967.

[12] M. Caputo. Elasticilà c dissipazione. *Zanichelli, Bologna*, 1969.

[13] G. E. Carlson and C. A. Halijak. Approximation of fractional capacitors (1/s)1/n by a regular newton process. *IEEE Transactions on Circuit Theory*, 7:210–213, Jun 1964.

[14] S. Chu-qi and Z. Du-que. Computer simulation study on ultracapacitor for electric vehicle. In *Intelligent Computing and Intelligent Systems, 2009. ICIS 2009. IEEE International Conference on*, volume 1, pages 199 –203, Nov 2009.

[15] ©Panasonic Corporation. Electric double layer capacitor(gold capacitor), series sd, catalogue. http://industrial.panasonic.com/www-data/pdf/ABC0000/ABC0000CE1.pdf, 2006.

[16] D. W. Davidson and R. H. Cole. Dielectric relaxation in glycerine. *J Chem Phys*, 18, 1951.

[17] D. W. Davidson and R. H. Cole. Dielectric relaxation in glycerine, propylene glycol, and n-propanol. *J Chem Phys*, 19:1484–90, 1951.

[18] H. D. Davis. *The theory of linear operators*. Principia Press, 1936.

[19] L. Dorčák, V. Lesko, and I. Koštial. Identification of fractional-order dynamical systems. In *Proceedings of 12th International Conference on Process Control and Simulation-ASRTP'96*, volume 1, pages 62–68, Kosice, Slovak Republic, September 1996.

[20] A. Dzieliński, G. Sarwas, and D. Sierociuk. Time domain validation of ultracapacitor fractional order model. In *Proceedings of the IEEE Conference on Decision and Control*, pages 3730–3735, 2010.

[21] A. Dzieliński, G. Sarwas, and D. Sierociuk. Comparison and validation of integer and fractional order ultracapacitor models. *Advances in Difference Equations*, 11, 2011.

[22] A. Dzieliński, G. Sarwas, D. Sierociuk, I. Petráš, I. Podlubny, and T. Škovránek. Identification of the fractional-order systems: A frequency domain approach. *Acta Montanistica Slovaca*, 16(1):26–33, 2011.

[23] A. Dzieliński, G. Sarwas, D. Sierociuk, and I. Petráš T. Škovránek. Frequency response based identification of fractional order dynamical systems. In *Carpathian Control Conference (ICCC), 2011 12th International*, pages 98 –102, May 2011.

[24] A. Dzieliński and D. Sierociuk. Adaptive feedback control of fractional order discrete state-space systems. In *Computational Intelligence for Modelling, Control and Automation, 2005 and International Conference on Intelligent Agents, Web Technologies and Internet Commerce, International Conference on*, volume 1, pages 804 –809, Nov 2005.

[25] A. Dzieliński and D. Sierociuk. Observer for discrete fractional order state-space systems. In *Proceedings of 2nd IFAC Workshop on Fractional Differentiation and its Applications, IFAC FDA'06*, pages 524–529. Porto, Portugal, 19-21 July, 2006.

[26] A. Dzieliński and D. Sierociuk. Stability of discrete fractional state-space systems. In *Proceedings of 2nd IFAC Workshop on Fractional Differentiation and its Applications, IFAC FDA'06*, pages 518–523. Porto, Portugal, 19-21 July, 2006.

[27] A. Dzieliński, D. Sierociuk, and G. Sarwas. Some applications of fractional order calculus. *Bulletin of The Polish Academy of Sciences - Technical Sciences*, 58(4):583–592, 2010.

[28] A. M. A. El-Sayed. Linear differential equations of fractional order. *Apll. Math. and Comput.*, 55:1–12, 1993.

[29] A. M. A. El-Sayed. Multivalued fractional differential equations. *Apll. Math. and Comput.*, 80:1–11, 1994.

[30] D. Elizarraraz and L. Verde-Star. Fractional Divided Differences and the Solution of Differential Equations of Fractional Order. *Advances in Applied Mathematics*, 24:260–283, 2000.

[31] R. Faranda, M. Gallina, and D.T. Son. A new simplified model os double-layer capacitors. In *Proceedings of International Conference on Clean Electrical Power, 2007. ICCEP '07.*, pages 706 – 710, 2007.

[32] R. Gorenflo. Fractional calculus: Some numerical methods. In A. Carpinteri and F. Mainardi, editors, *Scaling Laws and Fractality in Continuun Mechanics: A Survey of the Methods based on Renormalization Group and Fractional Calculus*. CISM, Udine, Sept. 1996.

[33] R. Gorenflo and F. Mainardi. Fractional calculus: Integral and differential equations of fractional order. In A. Carpintieri and F. Mainardi, editors, *Fractals and Fractional Calculus in Continuum Mechanics*, Viena-New York, 1997. Springer-Verlag.

[34] P. Górecki. 2700 faradów, czyli super(ultra)kondensatory. *Elektronika dla Wszystkich*, 6:21–24, 2001.

[35] A. K. Grünwald. Über "begrenzte" Derivationen und deren Anwendung. *Z. Angew. Math. Phys.*, 12:441–480, 1867.

[36] T. T. Hartley and C. F. Lorenzo. Dynamics and control of initialized fractional-order systems. *Nonlinear Dynamics*, 29(1-4):201–233, Jul 2002.

[37] J. W. Haus and K. W. Kehr. Diffusionnext term in previous termregular and disordered latticesnext term. *Physics Reports*, 150:263 – 406, June 1987.

[38] R. Hilfer, editor. *Application of fractional calculus in physics*. World Scientific, 2000.

[39] R. Hotzel and M. Fliess. On linear systems with a fractional derivation: Introductory theory and examples. *Mathematics and Computers in Simulation*, 45:385–395, 1998.

[40] W. Jifeng and L. Yuankai. Frequency domain analysis and applications for fractional-order control systems. *Journal of Physics: Conference Series*, 13:268–273, 2005.

[41] S.C. Jun. A note on fractional differences based on a linear combination between forward and backward differences. *Computers and Mathematics with Applications*, 41:373–378, 2001.

[42] T. Kaczorek. Practical stability of positive fractional discrete-time linear systems. *Technical Sciences*, 2008.

[43] T. Kaczorek. Reachability and controllability to zero tests for standard and positive fractional discrete-time systems. *Journal Europ'een des Syst'emes Automatis'es*, 2008.

[44] T. Kaczorek. Reachability of cone fractional continuous-time linear systems. *International Journal of Applied Mathematics and Computer Science*, 2009.

[45] T. Kaczorek. *Selected Problems of Fractional Systems Theory.* Springer, 2011.

[46] M. Klimek. *On Solutions of Linear Fractional Differential Equations of a Variational Type.* Częstochowa : University of Technology, 2009.

[47] T. Kosztołowicz. Subdiffusion in a system with a thick membrane. *Journal of Membrane Science*, 320:492–499, July 2008.

[48] J. S. Lai, S. Levy, and M. F. Rose. High energy density double-layer capacitors for energy storage applications. *IEEE Aerospace and Electronic Systems Magazine*, 7, April 1992.

[49] L. Lay, A. Oustaloup, J. C. Trigeassou, and F. Levron. Frequency domain identification by non integer model. In *Preprints of the IFAC Conference on System Structure and Control*, volume 2, pages 297–302, Nantes, France, Jul 1998. IRCN and LAG and IFAC, IFAC.

[50] J. Liouville. Mémoire sur quelques quéstions de géometrie et de mécanique, et sur un noveau genre pour résoudre ces quéstions. *J. École Polytech.*, 13:1–69, 1832.

[51] C. F. Lorenzo and T. T. Hartley. Initialization, conceptualization, and application in the generalized fractional calculus. TM 1998-208415, NASA, NASA Center for Aerospace Information, 7121 Stadard Drive, Hanover, MD 21076, USA, Dec. 1998.

[52] C. F. Lorenzo and T. T. Hartley. Initialized fractional calculus. *Int. J. of Applied Mathematics*, 3(3):249–265, 2000.

[53] C. H. Lubich. Discretized fractional calculus. *SIAM J. Math. Anal.*, 17(3):704–719, May 1986.

[54] L. L. Ludovic, A. Oustaloup, J. C. Trigeassou, and F. Levron. Frequency identification by non integer model. In *Proc. of IFAC Sumposium on System Structure and Control*, pages 297–302, Nantes, France, Jul 1998.

[55] J. A. T. Machado. Analysis and design of fractional-order digital control systems. *Journal of Systems Analysis-Modeling-Simulation*, 27:107–122, 1997.

[56] R. L. Magin. *Fractional calculus in bioengineering.* Begell House, Inc., 2004.

[57] J.N. Marie-Francoise, H. Gualous, and A. Berthon. Artificial neural network control and energy management in 42 v dc link. In *European Conference on Power Electronics and Applications*, pages 8 pp. –P.8, 0-0 2005.

[58] J.N. Marie-Francoise, H. Gualous, and A. Berthon. Supercapacitor thermal- and electrical-behaviour modelling using ANN. *Electric Power Applications, IEE Proceedings* -, 153(2):255 – 262, Mar 2006.

[59] D. Matignon. Stability properties for generalized fractional differential systems. In D. Matignon and G. Montseny, editors, *Proceedings of the Colloquium FDS'98: Fractional Differential Systems: Models, Methods and Applications*, volume 5, pages 145–158, Paris, Dec 1998.

[60] D. Matignon and B. D'Andréa-Novel. Some results on controllability and observability of finite-dimensional fractional differential systems. In *Computational Engineering in Systems Applications*, volume 2, pages 952–956. IMACS, IEEE-SMC, 1996.

[61] K. S. Miller and B. Ross. *An introduction to the fractional calculus and fractional differential equations*. John Wiley & Sons Inc., New York, 1993.

[62] C. A. Monje, Y-Q Chen, B. M. Vinagre, D. Xue, and V. Feliu. *Fractional-order systems and controls*. Springer, 2010.

[63] K. B. Oldham and J. Spanier. *The fractional calculus*. Academic Press, 1974.

[64] M. D. Ortigueira. Introduction to fractional linear systems I: Continuous-time case. *IEE Proceedings on Vision, Image and Signal Processing*, 147(1), 2000.

[65] M. D. Ortigueira. Introduction to fractional linear systems II: Discrete-time case. *IEE Proceedings on Vision, Image and Signal Processing*, 147(1), 2000.

[66] Manuel D. Ortigueira, Carlos J. C. Matos, and Moisés S. Piedade. Fractional Discrete-Time Signal Processing: Scale Conversion and Linear Prediction. *Nonlinear Dynamics*, 29(1-4):173–190, July 2002.

[67] P. Ostalczyk. The non-integer difference of the discrete-time function and its application to the control system synthesis. *International Journal of Systems Science*, 31(12):1551–1561, Dec 2000.

[68] P. Ostalczyk. A note on a relationship between a fractional-order continuous-time system pole configuration and its dynamics. *Journal européen des syst?mes automatisés*, 2008.

[69] I. Petráš. *Fractional Calculus in Control*. PhD thesis, Technical University of Kosice (Slovak Republic), 1999.

[70] I. Petráš, L. Dorčák, and I. Koštial. Methods for application of fractional-order controllers. *AT and P Journal (in Slovak)*, 4:59–60, 1998.

[71] I. Petráš, L. Dorčák, P. O'Leary, B. M. Vinagre, and I. Podlubny. The modelling and analysis of fractional-order control systems in frequency domain. In *Proceedings of ICCC'2000*, pages 261–264, High Tatras, Slovak Republic, May 23-26 2000.

[72] I. Podlubny. *Fractional differential equations*. Academic Press, 1999.

[73] I. Podlubny. Matrix approach to discrete fractional calculus. *Fractional Calculus and Applied Analysis*, 3(4):359–386, 2000.

[74] I. Podlubny, L. Dorčák, and J. Misanek. Application of fractional - order derivatives to calculation of heat load intensity change in blast furnace walls. *Transactions of Tech. Univ. of Kosice*, 5(5):137–144, 1995.

[75] I. Podlubny and Ahmed M. A. El-Sayed. On two definitions of fractional derivatives. Technical Report UEF-03-96, Slovak Academy of Sciences. Institute of Experimental Physics, Department of Contrlo Engineering. Faculty of Mining, University of Tecnology. Kosice, Jan 1996.

[76] J. J. Quintana, A. Ramos, and I. Nuez. Identification of the fractional impedance of ultracapacitors. In *Proceedings of the 2nd IFAC Workshop on Fractional Differentiation and its Applications*. IFAC FDA'06, Porto, Portugal, 19-21 July, 2006.

[77] D. Riu, N. Retière, and D. Linzen. Half-order modelling of supercapacitors. In *Proceedings of IEEE Industry Applications Conference, 39th IAS Annual Meeting*, volume 4, pages 2550 – 2554, 2004.

[78] B. Ross. Fractional calculus and its applications. In *International Conference on Fractional Calculus and Its Applications*, 1975.

[79] B. Ross. Fractional calculus: an historical apologia for development of a calculus using differentiation and antidifferentiation of non integral orders. *Mathematics Magazine*, 50(3):115 – 122, May 1977.

[80] S. G. Samko, A. A. Kilbas, and O. I. Maritchev. *Fractional integrals and derivatives. Theory and Applications*. Nauka i Tekhnika, Minsk, 1987.

[81] G. Sarwas. Modelowanie superkondensatorów przy użyciu rachunku różniczkowego ułamkowego rzędu. *Prace IEL*, 239, 2008.

[82] G. Sarwas, D. Sierociuk, and A. Dzieliński. Fractional order ultracapacitor model based on anomalous diffusion. In *Fractional Order Ultracapacitor Model Based On Anomalous Diffusion, 5th IFAC Workshop on Fractional Differentiation and its Applications*. Nanjing, China, 14-17 May, 2012.

[83] G. Sarwas, D. Sierociuk, and A. Dzieliński. Ultracapacitor modeling and control with discrete fractional order artificial neural network. In *Carpathian Control Conference (ICCC), 2012 13th International*, pages 617 – 622, May 2012.

[84] D. Sierociuk. Fractional order discrete state–space system Simulink Toolkit user guide. http://www.ee.pw.edu.pl/~dsieroci/fsst/fsst.htm.

[85] D. Sierociuk. *Estymacja i sterowanie dyskretnych układów dynamicznych ułamkowego rzędu opisanych w przestrzeni stanu*. PhD thesis, Warsaw University of Technology (Poland), 2007.

[86] D. Sierociuk and A. Dzieliński. Fractional Kalman filter algorithm for states, parameters and order of fractional system estimation. *International Journal of Applied Mathematics and Computer Science*, 16:129–140, 2006.

[87] D. Sierociuk and Ivo Petráš. Modeling of heat transfer process by using discrete fractional-order neural networks. In *Proceedings of 16th International Conference on Methods and Models in Automation and Robotics, MMAR'11 Międzyzdroje*, Aug 2011.

[88] D. Sierociuk, G. Sarwas, and A. Dzieliński. Discrete fractional order artificial neural network. *Acta Mechanica et Automatica*, 5(2):128–132, 2011.

[89] B. M. Vinagre, V. Feliú, and J. J. Feliú. Frequency domain identification of a flexible structure with piezoelectric actuators using irrational transfer function models. In *Proceedings of the 37th IEEE Conference on Decision and Control*, pages 1278–1280, Tampa,Florida,USA, Dec 1998.

[90] B.M. Vinagre. *Modelado y Control de Sistemas Dinámicos caracterizados por Ecuaciones Integro-Diferenciales de Orden Fraccional.* PhD thesis, Escuela Técnica Superior de Ingenieros Industriales, Universidad Nacional de Educación a Distancia, 2001.

[91] S. Westerlund and L. Ekstam. Capacitor theory. *IEEE Transactions on Dielectrics and Electrical Insulation*, 1, 1994.